University of Cape Town

Division of Biomedical Engineering, Department of Human Biology

Dissertation submitted in partial fulfilment of the requirements for the degree of MSc (Med) Biomedical Engineering

On the relationship between corticomuscular (EEG-EMG) phase coupling and muscular fatigue

Author: Jeff Joseph (JSPJEF001)

Supervisor: Dr Lester R. John

Co-supervisor: Dr Yumna Albertus-Kajee

April 2015

DECLARATION

I, Jeff Joseph, hereby declare that the work on which this dissertation is based is my original work (except where acknowledgements indicate otherwise) and that neither the whole work nor any part of it has been, is being, or is to be submitted for another degree in this or any other university.

I empower the university to reproduce for the purpose of research either the whole or any portion of the contents in any manner whatsoever.

Signed by candidate

Signature Removed

Signature: ……

Date: ……07/04/2015……..

ABSTRACT

Motivation: Contradictory results have been shown in studies measuring the effect of muscle fatigue on the level of synchrony between the oscillatory, cortical and muscular electrical activities (also known as corticomuscular coupling). In every study, the standard method (coherence) used to measure the level of synchrony takes into account both the amplitude and phase of the two signals. However, the use of the phase lock value (PLV) has been overlooked as a method for determining the level of synchrony. While the PLV is modulated purely by the phase between the two signals, it is unaffected by any amplitude variation. This study aims to determine whether amplitude variations in electroencephalography (EEG) and electromyography (EMG) could have caused the contradictory results when comparing pre-, during and post-fatigue measures of corticomuscular coupling, which consequently affected the conclusions drawn regarding the monitoring of fatigue by the central nervous system. A determination will be made regarding the contradictions by directly comparing the two methods (coherence and PLV) on the same dataset of simultaneously measured EEG and EMG signals throughout an isometric pre-, during and post-fatigue task.

Materials and Methods: Fifteen right-handed, healthy, male participants were tested during three stages of palmar abduction: Stage 1, pre-fatigue, was a 10% of maximal voluntary contraction (MVC) for 10s repeated 6 times; Stage 2, fatigue, was a 30% of MVC till task failure (when the % MVC dropped below 20% for more than 2 seconds); and Stage 3, post-fatigue, was a repeat of Stage 1. A 16-channel EEG cap was placed over the head and an 8-channel surface EMG electrode grid was placed over the abductor pollicis brevis (APB) muscle. Raw EEG, EMG and force signals throughout a voluntary APB muscle contraction pre-, during (which encompassed two stages one prior to transition to fatigue [first stage] and one after transition to fatigue [second stage]) and post-fatigue were recorded and analysed.

Results: Results from previous literature were replicated pre- and post-fatigue thereby validating the experimental protocol. The coefficient of variance of force significantly increased from pre-fatigue to post-fatigue (3.473 ± 2.269 to 7.873 ± 5.568%, $p = 0.001$), while the normalised beta force power spectral density significantly increased from pre-fatigue to post-fatigue (0.004 ± 0.001 to 0.005 ± 0.001, $p = 0.014$). The normalised EMG root mean squared significantly increased from pre-fatigue to post-fatigue (0.037 ± 0.022 to 0.051 ± 0.033, $p = 0.017$) while the EMG mean power frequency significantly decreased from pre-fatigue to post-fatigue (100.589 ± 17.366 to 86.948 ± 19.814Hz, $p = 0.001$). The normalised beta EEG root

mean squared significantly increased from pre-fatigue to post-fatigue (0.043 ± 0.017 to 0.048 ± 0.021, p = 0.025).

Novel results that appear to also resolve contradictions in the literature relating to the corticomuscular coupling methods, PLV and coherence, were observed pre-, during and post-fatigue. The beta EEG-EMG coherence peak amplitude significantly increased from pre-fatigue to post-fatigue (0.023 ± 0.007 to 0.034 ± 0.017, p = 0.008), and the beta EEG-EMG PLV peak amplitude also significantly increased from pre-fatigue to post-fatigue (0.102 ± 0.014 to 0.125 ± 0.029, p = 0.011).

However, due to amplitude co-variations during the fatigue stage, it was observed that the EEG-EMG coherence significantly decreased from the first part to the second part of the fatigue stage (0.059 ± 0016 to 0.042 ± 0.017, p = 0.001), whilst the EEG-EMG PLV did not (0.16 ± 0.04 vs. 0.154 ± 0.039, p = 1.000).

Conclusion: This study provides evidence that the corticomuscular phase coupling in the beta band between the sensorimotor cortex and the APB muscle increases significantly, without the confounding effect of the EEG and EMG amplitude, after muscle fatigue occurs during a sustained isometric submaximal contraction. These findings suggest that the amplitude co-variations from the EEG in the sensorimotor cortex and the EMG in the APB muscle support the previously published conclusions regarding the central nervous system monitoring pre- and post-fatigue. However, during an actual fatiguing contraction, as a result of the confounding effect of amplitude, the coherence and PLV measures of the corticomuscular coupling provide different results. In such experiments, PLV provides a more reliable measure, resulting in a physiological conclusion that there is no change in corticomuscular phase coupling during the fatiguing contraction.

ACKNOWLEDGEMENTS

I would like to thank Dr. L. R. John for his support and guidance throughout this study; Dr. Y. Albertus for her advice on the physiology aspects; N. Divekar for his help and support with his extensive knowledge of corticomuscular coupling, building the electromyography system and providing the basis for this study; S. Stoeckight for building the electroencephalography system; D. Williams for his statistical support; C. Harris (Mechanical Workshop, University of Cape Town) for construction of the custom isometric contraction device; A. Sayed for his help with the design of the custom isometric contraction device; and S. Anwarsha, M. Mushabe, J. Joseph, L. Johan, R. M. Alex and A. Thomas for proofreading my study.

I would also like thank my wife, Ann Thomas, my parents and my family for their love, care and encouragement throughout the duration of this study.

TABLE OF CONTENTS

LIST OF FIGURES

LIST OF TABLES

LIST OF ABBREVIATIONS

AIF	Average instantaneous frequency
APB	Abductor pollicis brevis
CL	Confidence level
CMRR	Common mode rejection ratio
CSD	Current source density
CV	Coefficient of variance
DAC	Digital to analogue convertor
DAQ	Data acquisition
DRL	Driven right leg
DV	Dependent variable
EEG	Electroencephalogram
EMG	Electromyogram
IV	Independent variable
IZ	Innervation zone
MEG	Magneto encephalography
MPF	Mean power frequency
MU	Motor unit
MVC	Maximum voluntary contraction
PLV	Phase lock value
PLS	Phase lock statistics
PSD	Power spectral density
REF	Reference
RMS	Root mean squared

1. INTRODUCTION

The general field of interest of the present study is on the level of synchrony between the oscillatory cortical and muscular electrical activities. This synchrony is commonly known as corticomuscular coherence or corticomuscular coupling (the preferred term used in the present study). By measuring the corticomuscular coupling, one can gain insight into the level of monitoring of a muscle by the central nervous system. However, current fatigue studies provide contradictory results for the level of corticomuscular coupling. Understanding the methods of determining levels of corticomuscular coupling will provide insight into the physiology of muscular fatigue and could potentially resolve contradictory results in the current studies.

1.1 Motivation

Fatigue is defined as 'both physical and mental exhaustion due to prolonged stimulation or exertion'. There are two types of physiological fatigue: peripheral and central. Peripheral fatigue is a metabolite-induced failure of the contractile function of the skeletal muscle, while central fatigue refers to the reduced activation of a skeletal muscle by efferent output from the motor cortex of the central nervous system (Noakes & St Clair Gibson, 2004).

While the origin of muscle fatigue is still in dispute, there are two main streams of thought. The more popular belief is that muscle fatigue, which occurs during most forms of exercise, is due to a peripheral fatigue and independent of central fatigue. Alternatively, as proposed by Noakes and St Clair Gibson (2004), 'fatigue in any form of exercise may form part of a regulated anticipatory response co-ordinated in the subconscious brain, the ultimate goal of which is to preserve homeostasis in all physiological systems during exercise' .

Interestingly, studies have found increasing evidence suggesting contributions from both the central and peripheral systems. Early studies identified muscle fatigue using electromyography (EMG) measures alone (González-Izal et al., 2003; Kumar et al., 2003), however, further development involved the addition of electroencephalography (EEG) recordings during muscle fatigue. For example, Abdul-latif et al. (2004) observed an increase in beta (15-35 Hz) EEG activity post-fatigue in the contra-lateral motor cortex. Similarly, van Duinen, et al. (2007) showed that activity in the cerebellum, pre-supplementary motor area and frontal area increased during fatigue.

Current studies use EEG and EMG recordings to determine the corticomuscular coupling during fatigue, which is typically calculated using EEG-EMG coherence (Ushiyama et al., 2011; Yang et al., 2009). However, these studies provide contradictory results.

One significant method for determining the level of corticomuscular coupling, the use of the phase lock value (PLV), has been overlooked. The PLV is modulated purely by the phase between the two signals and is unaffected by any amplitude variation (Lachaux, et al., 1999; Srinath & Ray, 2014). This is of particular importance in fatigue studies, because both the EMG and EEG amplitudes are known to change during fatigue (Yang et al., 2009; Ushiyama et al., 2011).

Therefore, the focus of this study is to investigate if the changes in the EEG and EMG amplitude confound the measures of corticomuscular coupling using coherence, thereby affecting the conclusions regarding the central nervous system's monitoring of muscular fatigue.

1.2 Literature Review

Section 1.2 describes the literature directly related to the present study.

1.2.1 Muscle fatigue

Muscle fatigue is typically quantified as the inability to sustain or reach a set level of maximal voluntary contraction (MVC) due to the nature of both the skeletal muscle tissue (peripheral fatigue) and the neuromuscular junction (central fatigue) (Gandevia, 2001; Enoka & Duchateau, 2008) .

Peripheral fatigue is related to the impairment of the muscle contraction, due the reduction of the metabolites and blood supply in the contracting muscle. While, central fatigue is related to a reduction in the nerve-based motor command to the muscle (Gandevia, 2001; Enoka & Duchateau, 2008).

The contributions of central and peripheral fatigue during muscle fatigue are still in dispute. The more popular model, known as the anaerobic/catastrophe/limitations model, suggests that fatigue is caused by a variety of cellular effects, which can alter muscle force production (Weir et al., 2006). While, Noakes et al. (2005) suggested that a central governing model manages muscle fatigue in order to preserve homeostasis in all physiological systems during exercise.

However, other studies suggest that when muscle fatigue occurs, it contains both central and peripheral components and is possibly task-dependent (Gandevia, 2001; Weir et al., 2006).

1.2.2 Muscle fatigue influence on force, EMG and EEG

Multiple studies have shown that muscle fatigue has an influence on force, EMG and EEG measures. These influences are explored in Section 1.2.2.

1.2.2.1 Muscle force changes due to muscle fatigue

As mentioned in Section 1.2.1 fatigue is usually quantified by the inability to sustain a set level force, however determining a fixed point of when a muscle cannot sustain a force is a difficult task and varies from study to study. Also, it has been argued that manifestation of fatigue doesn't instantaneously occur but rather develops over time (Roberto Merletti & Parker, 2004).

Nonetheless, there is a generally accepted protocol to fatigue a participant for a sustained contraction:

1. The participant's MVC is measured (usually with a force transducer).
2. After the participant is given sufficient time to rest their muscle, he/she is required to maintain a submaximal isometric contraction (usually below 50% of MVC).
3. Once the %MVC has dropped by more than 10% for a set time, the participant's muscle was considered fatigued. This set time varies between 2-5 seconds.

Accordingly it is generally accepted that fatigue has occurred once a participant cannot sustain a targeted %MVC for a set amount time (Yang et al., 2009; Kattla and Lowery, 2010; Ushiyama et al., 2011).

Yang et al. (2009) and Ushiyama et al. (2011) also observed that the force generated by the muscle becomes less steady during a fatiguing contraction. This was estimated by calculating the coefficient of variance of force ($force_{CV}$, i.e. the higher the $force_{CV}$, the less steady the force). Ushiyama et al. (2011) further observed that force within the beta (15–35 Hz) band (beta $force_{PSD}$) significantly increased after the onset of fatigue suggesting that the sensorimotor cortex reinforces the rhythmic grouped discharges in the EMG within the beta band possibly in an attempt to maintain a stable force output.

1.2.2.2 EMG changes due to muscle fatigue

Two well established EMG indices have been used to evaluate central fatigue during an isometric contraction. These indices can be calculated by measuring electric potentials of the muscle and observing the changes in the amplitude and frequency; such as the EMG root mean

squared, EMG_{RMS} and the EMG mean power frequency, EMG_{MPF}, respectively (Viitasalo & Komi, 1977; De Luca, 1983; Bigland-Ritchie & Woods, 1984).

Multiple studies have shown a significant increase in the EMG_{RMS} during a fatiguing contraction (Viitasalo & Komi, 1977; De Luca, 1983; Arendt-Nielsen et al., 1989; Esposito et al., 1998). This increase in EMG_{RMS} would be due to recruitment of additional motor units and/or an increase in motor unit firing frequency (Arendt-Nielsen et al., 1989; Dimitrova & Dimitrov, 2003).

During a fatigued isometric contraction, the EMG_{MPF} has been shown to shift to lower frequencies in both other muscles (De Luca, 1983; Bigland-Ritchie & Woods, 1984; Merletti et al., 1984; Esposito et al., 1998; Georgakis et al., 2003) and the abductor pollicis brevis (APB) muscle (Barandun et al., 2009). A decrease in EMG_{MPF} is compatible with a decrease in the firing rate of motor units. However, even though the EMG is associated with the central drive to the muscle, it has been argued that a decrease in the EMG_{MPF} could rather be linked to a decrease in conduction velocity and/or change of shape of the motor unit action potentials, therefore indicating mechanisms of peripheral fatigue (Eberstein & Beattie, 1985; Moritani et al., 1986; Arendt-Nielsen et al., 1989; Merletti & Lo Conte, 1997; Schillings et al., 2003). Therefore a decrease in EMG_{MPF} could be a measure of central and/or peripheral fatigue.

1.2.2.3 EEG change due to muscle fatigue

EEG measures have been observed to also change due to central fatigue. Liu et al. (2003) and van Duinen et al. (2007) observed an increase in brain activation levels as fatigue sets in. More specifically, Abdul-latif et al. (2004) observed an increase in the beta (15–35 Hz) EEG root mean squared (beta EEG_{RMS}; i.e. an amplitude measure in the contra-lateral motor cortex (specifically C3 and FC3; see Figure 2-9) after exercise-induced fatigue of the adductor pollicis muscle. This suggests that the motor cortex needs an increased descending command to recruit new motor units and/or increase the motor unit firing rate within the contracting muscle to compensate for the force reduction (Liu et al., 2003 ; van Duinen et al., 2007).

1.2.3 Corticomuscular coupling measures and muscle fatigue

Recent studies have implemented a measure of the synchrony between oscillatory cortical (usually measured using EEG) and muscular (usually measured using EMG) electrical activities in order to provide insight into central muscle fatigue (Tecchio et al., 2006; Ushiyama et al., 2011; Yang et al., 2009, 2010). This synchrony is known as corticomuscular coupling.

Additionally, corticomuscular coupling has been demonstrated to be a useful parameter in the central (i.e. the brain) assessment of the state of peripheral muscular contraction (Baker, 2007). According to Gwin & Ferris (2012), the corticomuscular coupling's phase lags are consistent with the conduction time between the motor cortex and the respective muscle. This is suggestive of a central-peripheral feedback loop. Consistent with this is the suggestion that the oscillations in the motor cortex originating in the beta-band (which are similar to the oscillations in the activity of contralateral contracting muscles) not only engage motor structures, but also sensory feedback from the muscle to the central nervous system via feedback afferent pathways, as shown in Figure 1-1 (Baker, 2007). Thus beta corticomuscular coupling is a useful measure in determining the relationship between the muscle and motor cortex during muscle fatigue.

Additionally, gamma band (35–50 Hz) corticomuscular coupling has been observed during strong (Brown, 2000) and dynamic contractions (Omlor et al. ,2007).

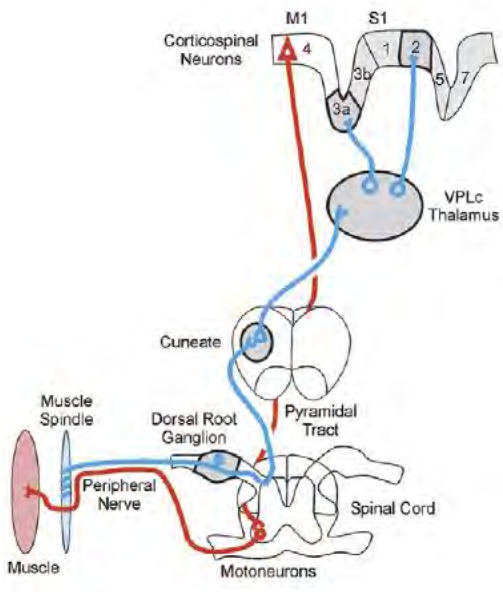

Figure 1-1: Pathways which could mediate corticomuscular coupling (Descending (red) and ascending (blue). The figure was adopted from Baker (2007).

1.2.3.1 Coherence

The standard measure of corticomuscular coupling is coherence. Coherence, by definition, is a spectral measurement of two signals *x(t)* and *y(t* calculated from the cross-spectral density

between the two waveforms and normalised by the power spectral density of each waveform. The equation used is shown below:

$$C_{xy}(f) = \frac{(\sum_{i=1}^{n} X_i(f) Y_i^*(f))^2}{\sum_{i=1}^{n} [X_i(f)]^2 \sum_{i=1}^{n} [Y_i(f)]^2} \qquad \textbf{Equation 1-1}$$

where $X_i(f)$ and $Y_i(f)$ are the Fourier transforms of the signals *x* and *y* for the *i*th data segment at frequency *f*, and * indicates the complex conjugate. Coherence values range from 0 (if the signals are incoherent) to 1 (if the signals are perfectly coherent).

EEG-EMG coherence, therefore, is the coherence between field potentials generated by the brain measured using EEG techniques and the muscle measured using EMG techniques. A typical EEG-EMG coherence graph is shown in Figure 1-2.

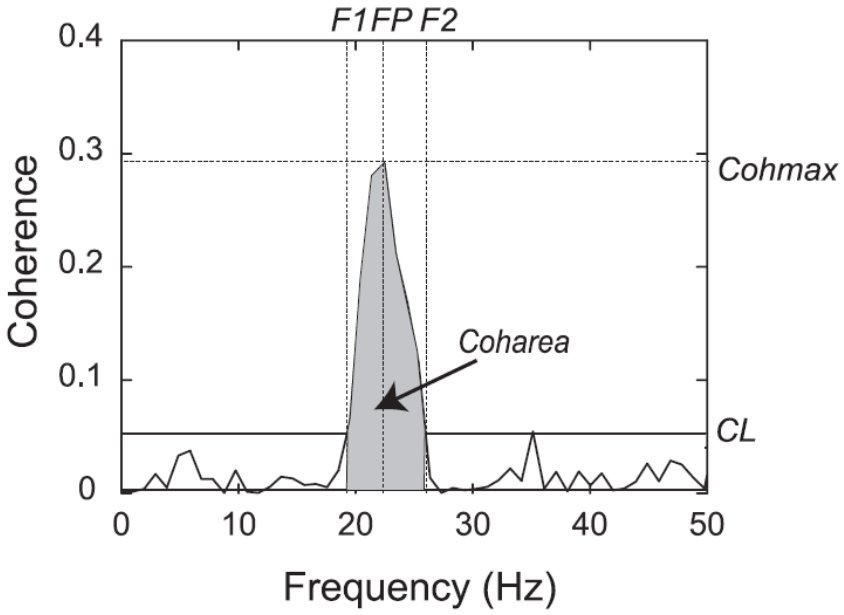

Figure 1-2: Typical EEG-EMG coherence spectrum for an isometric contraction task, adapted from Ushiyama et al. (2011). Coherence is considered significant if it falls above the confidence limit (CL). FP (known as EEG-EMG coherence$_{\text{PEAK FREQ}}$ in the present study) is the frequency at which coherence is at its peak indicated as Cohmax (known as EEG-EMG coherence$_{\text{PEAK AMP}}$ in the present study). F1 and F2 are the frequency points where coherence intersects with the confidence limit. Coharea is the area of coherence between F1 and F2.

1.2.3.1.1 Corticomuscular coupling research investigating muscle fatigue

The following section highlights literature from four studies that analyse the effect of muscle fatigue on corticomuscular coupling using EEG-EMG coherence. The results are summarised in Table 1-1.

Tecchio et al. (2006) investigated isometric contractions of the extensor communis digitorum muscle. The magnetoencephalography (MEG)-EMG coherence was compared pre- and post-fatigue. During the pre-fatigue stage, the participant maintains a force at 20–35% of MVC for 20 seconds and rests for 20 seconds thereafter. This exercise was repeated for 5 minutes. During the fatigue stage, the participant maintained MVC for as long as possible. The post-fatigue stage followed 2–10 minutes after the fatigue stage and was a repetition of actions during the pre-fatigue stage. When compared with the pre-fatigue stage, the MEG-EMG coherence in the beta band (15–35 Hz) increased significantly in the post-fatigue stage (see Figure 1-3).

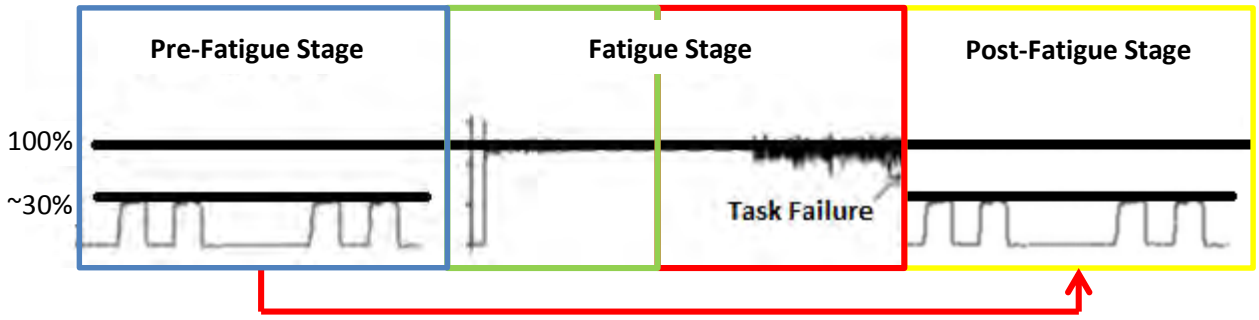

Figure 1-3: Tecchio et al.'s (2006) pre-fatigue (blue), fatigue (green and red) and post-fatigue (yellow) stages. The red arrow represents the two stages which were compared. This figure was adopted and edited from Kattla and Lowery (2010).

Following this, Yang et al. (2009) also quantified EEG-EMG coherence, but now at the beginning and end of a fatiguing contraction. Their experiments involved sustaining an isometric elbow flexion at 30% of MVC until the percentage of MVC dropped below 20% for longer than 3 seconds. The fatigue stage was consequently broken into two stages: minimal and severe fatigue (as shown in Figure 1-4). The EEG-EMG coherence decreased significantly in the severe fatigue stage, when compared with the minimal fatigue stage (Yang et al., 2009).

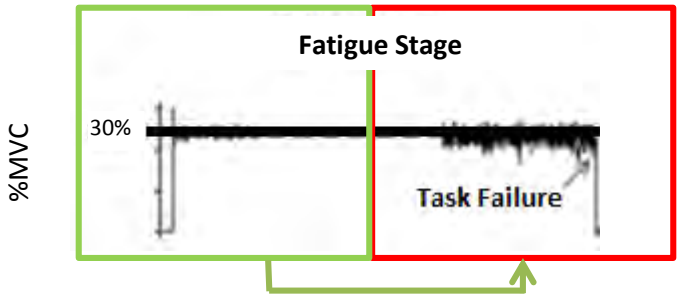

Figure 1-4: Yang et al.'s (2009) minimal fatigue (green block) stage was represented by the first half of the isometric fatiguing contraction, while the severe fatigue stage (red block) was represented by the second half. The green arrow represents the two stages that were compared. This figure was adopted and edited from Kattla and Lowery (2010). Compare this to the green and red fatigue stages in Figure 1-3.

Yang et al. (2010) on noting that the progressive nature of fatigue cannot be studied by simply comparing corticomuscular coupling pre- and post-fatigue or between two long-duration time blocks within a fatiguing contraction, proposed to address this issue by investigating the wavelet EEG-EMG coherence during the fatiguing stage with two or more sequential blocks (as shown in Figure 1-5). The experiment involved participants performing 200 maximal intermitted handgrip contractions in a single fatigue stage. Each trial was 2 seconds long, and the wavelet EEG-EMG coherence was completed.

The fatigue stage was broken into two-, five- and 10-blocks (see Figure 1-5) with wavelet EEG-EMG coherence measures generated for each block. For the 10-block fatigue stage, the wavelet EEG-EMG coherence measures in the beta band (15–35 Hz) showed an increase from the first to the fifth block followed by a decrease to the tenth block. Although using 10-blocks provided a more detailed time course of the coherence alteration, it lacked statistical significance. For the corresponding two-block fatigue stage grouping (similar to Figure 1-4), there however was a significant decrease between the wavelet EEG-EMG coherence from the first block to the second block i.e. identical results to their previous results (Yang et al, 2009).

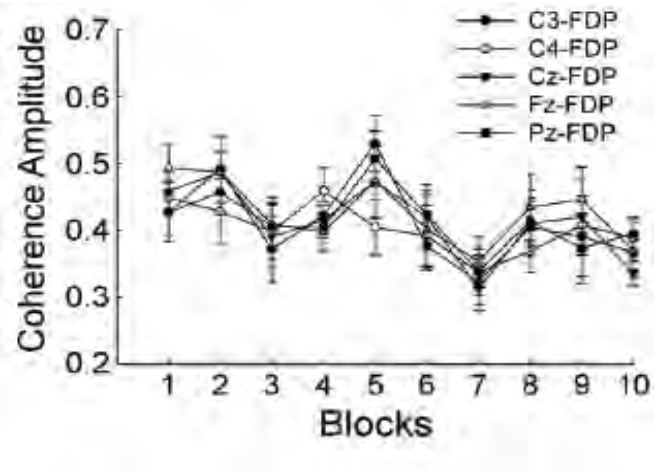

Figure 1-5: The wavelet EEG-EMG coherence in the beta band during the fatigue stage was separated into 10 blocks. A general increase from the first block to the fifth block and then a decrease to the tenth block can be noted. The figure was adopted from Yang et al. (2010).

Ushiyama et al. (2011) then presented a fatigue study of the tibialis anterior muscle in an attempt to explain the contradictory results found in the three previous studies (Tecchio et al., 2006; Yang et al., 2009; Yang et al., 2010) using a muscle shown to provide greater EEG-EMG coherence among various upper and lower limb muscles (Ushiyama et al., 2010). This study required three stages of movements:

1. pre-fatigue: dorsiflex the foot for 60 seconds at 30% of MVC;
2. fatigue: rest for 60 seconds, then dorsiflex the foot at 50% of MVC until force dropped below 40% of MVC for longer than 5 seconds;
3. post-fatigue: no rest, dorsiflex the foot again for 60 seconds at 30% of MVC.

Ushiyama et al. (2011) then observed similar result as Tecchio et al. (2006) which was an increase in EEG-EMG coherence from pre-fatigue to post-fatigue. The study also observed an increase during the fatigue stage, although significance was not observed for the fatigue stage.

Ushiyama et al. (2011) suggested that differences between their study and Yang et al. (2009) study, was that Yang et al. (2009) recorded from biceps brachii, brachioradialis and triceps but not brachialis, which is the major agonist muscle for elbow flexion. Thus compensatory brachialis activities that may have been induced (see Table 1-1) were not accounted for by Yang et al. (2009) after muscle fatigue developed. Ushiyama et al. (2011) further suggested that differences between their study and Yang et al. (2010) study, was that the respective study did a repetitive dynamic contraction which commonly associated with peripheral fatigue compared to isometric contraction which commonly associated with central fatigue (Søgaard et al, 2006).

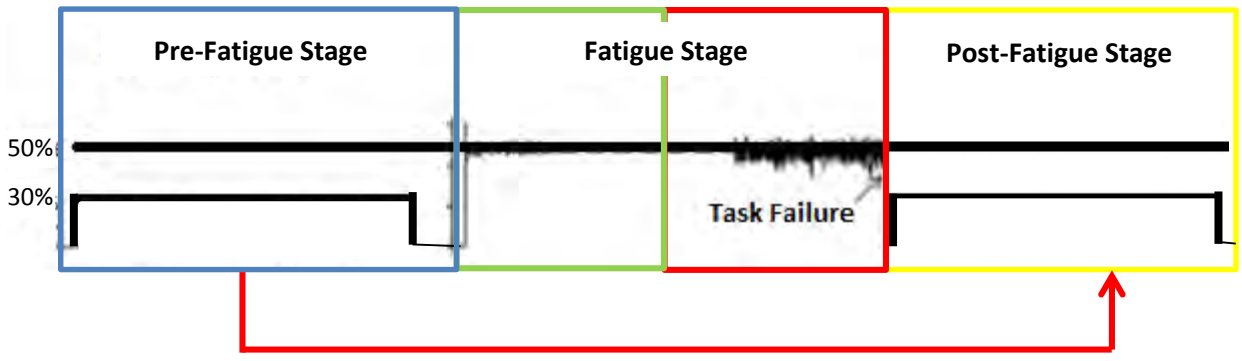

Figure 1-6: Ushiyama et al.'s (2011) pre-fatigue stage (blue block), fatigue stage (green and red block) and post-fatigue stage (yellow block) . The red arrow represents the two stages that were compared. This figure was adopted and edited from Kattla and Lowery (2010).

A summary of the studies mentioned is shown in Table 1-1.

Table 1-1: Summary of studies, investigating the effect muscle fatigue has on corticomuscular coupling. See Figure 1-7 for colour key of stages that were compared in each study.

Study	Movement or Contraction	Muscle	Stage 1	Stage 2	EEG-EMG coherence in the beta band**	EMG amplitude **	EEG amplitude **	N*
Tecchio et al. (2006)	Isometric	Extensor Communis Digitorum	blue	yellow	⬆	No significant change	⬆	14
Yang et al. (2009)	Isometric	Biceps Brachii, Brachioradialis, Triceps Brachii	green	red	⬇	⬆	⬆	9
Yang et al. (2010)	Dynamic	Flexor Digitorum Profundus, Flexor Digitorum Superficialis	green	red	⬇	⬇	⬇	8
Ushiyama et al. (2011)	Isometric	Tibialis Anterior	blue	yellow	⬆	⬆	⬆	7

*N= number of participants

** ⬆ increased, ⬇ decreased

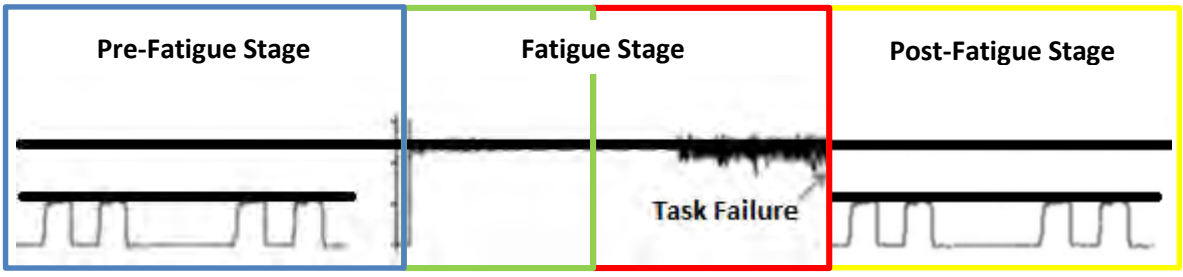

Figure 1-7: The stages represented by the colour blocks of the experimental procedure in Table 1-1. This figure was adopted and edited from Kattla and Lowery (2010).

From the literature summary of Table 1-1, it can be noted that the EEG (aside from Tecchio et al, 2006) and EMG amplitude varies significantly with the effect of fatigue. As a result it is possible that using coherence to measure the level of corticomuscular coupling could provide misleading results for the phase synchrony between the EMG and EEG, as prior literature (Srinath & Ray, 2014) demonstrated that coherence is dependent on both phase and amplitude. Thus the use of phase lock value (PLV) had been proposed to single out the role of phase consistency (Lachaux et al., 1999; Srinath & Ray, 2014) and exclude the effect of amplitude. However PLV has not been previously implemented in a muscle fatigue study where changes in amplitude occur.

In addition the studies (i.e. Table 1-1) differed in the muscles as well as the in the stages of fatigue that were investigated.

1.2.3.2 Phase lock value (PLV)

PLV is a measure of phase synchrony between two signals commonly used in EEG studies instead of coherence, since coherence is influenced by amplitude co-variations (Lachaux et al., 1999; Srinath & Ray, 2014). PLV, also known as phase coherence, 'is a measure of phase consistency of phase differences between electrodes across trials. This is calculated by forcing the amplitudes of the signals at frequency to 1, so as to remove any effects of co-variations in amplitude' (Srinath & Ray, 2014). See Appendix A for a comparison between coherence and PLV using simulated data generated by the author and sampled data from Divekar and John (2012).

The phase-locking value between signals *x(t)* and *y(t)* is defined as:

$$PLV = \frac{1}{N}\sum_{i=1}^{n} e^{-j\theta(t,i)} \qquad \textbf{Equation 1-2}$$

where $\theta(t,i) = \varphi_X(t,i) - \varphi_Y(t,i)$ is the phase difference between the two signals at time t in the ith segment/trial. PLV ranges from 0 (no synchronisation) to 1 (perfect synchronisation).

EEG-EMG PLV would therefore represent the phase relationship between field potentials generated by the brain measured using EEG techniques and the muscle measured using EMG techniques

1.2.3.3 EMG Electrode location could influence corticomuscular coupling measures

Masuda et al. (1999) observed that the EMG electrode location, relative to the muscle innervation zone (IZ), could influence the spectral estimates. For the Abductor Pollicis Brevis (APB) muscle, Keenan et al. (2012) observed that the electrode pair furthest from the IZ provided a greater EMG-EMG coherence amplitude peak. Thus to remove the effect of electrode location the IZ should first be detected and avoided. This would require the use of a linear electrode array (i.e. a linear adjacent series of bipolar electrodes) instead of a single bipolar electrode set.

The method used by Keenan et al. (2012) to identify the IZ was shown in Figure 1-8. The EMG bipolar differences between the series of adjacent electrodes were used to identify the IZ. The IZ was then identified as the mid-point of the closest two EMG signals with motor unit action potentials propagating in opposite directions i.e. where a clear change in the polarity of the phases of the potential was present.

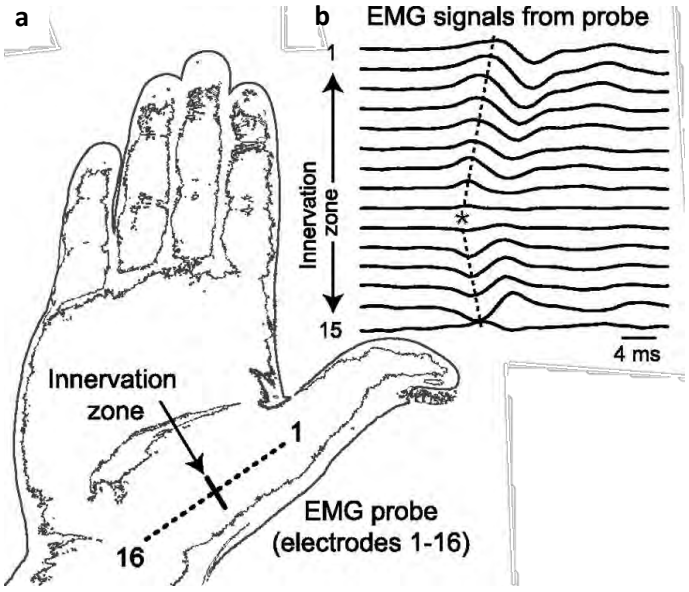

Figure 1-8: Explanation of Keenan et al.'s (2012) method of identifying the IZ for the APB muscle: a) a linear EMG array with 16 electrodes was placed over the APB muscle. b) this resulted in 15 sequential bipolar signals (i.e. between adjacent electrodes). The IZ was then estimated as the location of the interpolated EMG signal that would be closest to the location where motor unit action potentials started to propagate in both directions i.e. a clear change in the polarity of the phases of the potential was present (identified with an asterisk, *). The dashed line is provided as reference to identify the propagation of the muscle fibre action potentials. This figure was adopted from Keenan et al. (2012).

1.2.3.4 EEG Electrode location could influence corticomuscular coupling measures

It has long been established that the sensorimotor region of the brain is involved with muscle movements. The greatest change in corticomuscular coupling during fatigue studies was observed in the contra-lateral sensorimotor regions (Tecchio et al., 2006; Ushiyama, et al., 2011; Yang et al., 2009; Yang et al.,2010).

This is also true for the execution of complex finger movements (Shibasakiet et al, 1993).

1.2.3.5 Transition point during the fatigue stage

Measuring the corticomuscular coupling between two, five or 10 blocks (see Yang et al.'s, 2010 study in Section 1.2.3.1.1) during the fatigue stage can be misleading as the onset of fatigue could differ amongst participants (Al-Mulla and Sepulveda ,2010).

Additionally, Srinath and Ray (2014) observed that coherence and phase lock value measures are sensitive to the number of trials. Since the time span of the fatigue stage varies amongst participants, the number of trials for the corticomuscular coupling measures will vary. Thus, separating the fatigue stage into two, five or 10 blocks, could result in a misleading conclusion.

Al-Mulla and Sepulveda (2010) therefore suggested a method of identifying the time point of transition to fatigue using the EMG total band power (EMG_{POWER}) and EMG median frequency (EMG_{MDF}). EMG_{MDF} is subtracted from EMG_{POWER} to calculate the output '1D spectro' (see Figure 1-9). The transition to fatigue point is then found when 1D spectro increases (see Figure 2-15). Therefore observing parameters (such as corticomuscular coupling measures) before and after this transition point could provide a more reliable measure than using 2 fixed time blocks.

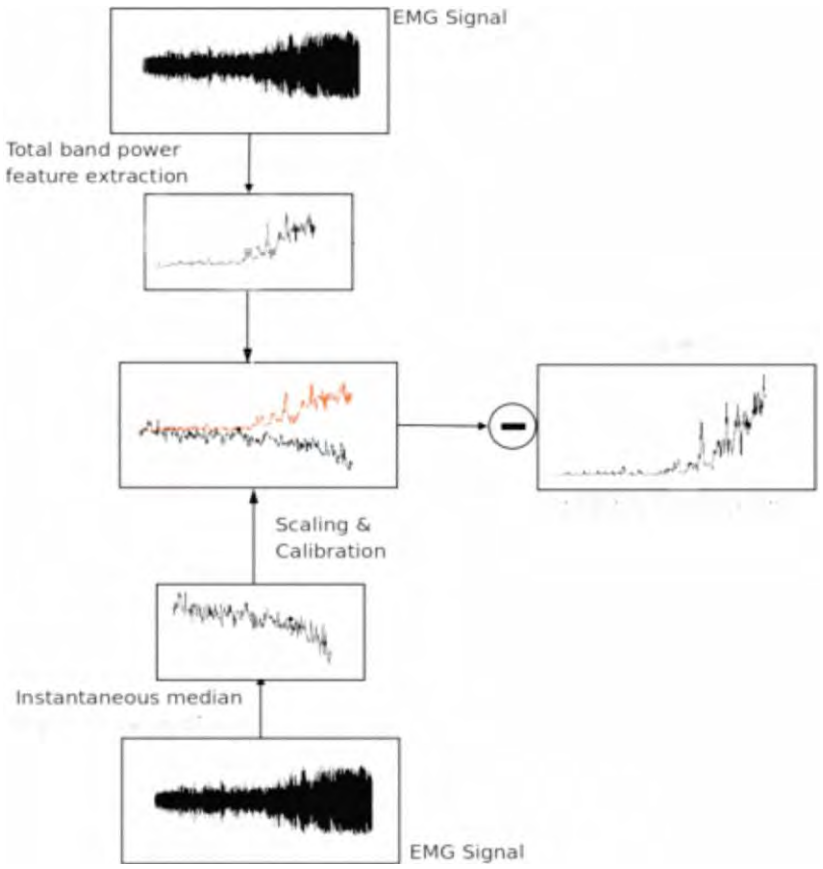

Figure 1-9: 1D spectro is calculated by subtracting EMG_{MDF} from EMG_{POWER}. This figure was adopted from Al-Mulla and Sepulveda (2010).

1.2.4 Summary

Corticomuscular coupling using coherence has been observed to both increase (Ushiyama et al., 2011) and decrease (Yang et al., 2009) significantly in the beta band due to fatigue. Both studies also showed a change in EEG and EMG amplitude due to fatigue. In a non-fatigue study, PLV has been recommended over coherence by Srinath and Ray (2014). This is because the change in coherence between EEG and EMG can be evaluated as a change in amplitude, phase shift or both. Therefore, to single out the role of phase consistency in corticomuscular coupling, a PLV analysis would be preferable.

1.3 Hypothesis

The hypothesis of the study is that the EEG-EMG PLV would provide a more accurate measure of EEG-EMG phase coupling than EEG-EMG coherence, which is confounded by amplitude variation. Hence the novel use of EEG-EMG PLV in muscular fatigue studies may resolve apparent contradictions in the literature.

1.4 Aim

The main aim of the present study is to investigate if the corresponding EMG and EEG amplitude changes confound coherence measures pre-, during and post-fatigue measures of corticomuscular coupling by comparison to PLV measures. This may ultimately influence the physiological conclusions regarding central nervous system monitoring of muscular fatigue.

1.5 Sub aims and corresponding experimental outcome variables

Sub aims and objectives were derived. The objectives related to force, EMG, EEG and the corticomuscular coupling, which were measured pre-, during and post-fatigue. The objectives were then grouped according to sub aims, and each objective is listed below with the actual variable names given in brackets.

1.5.1 Sub Aim 1: Carry out an experimental protocol which predominantly gives rise to central fatigue (hence the corresponding outcome measures listed below)

1. Raw electromyography (EMG_{RAW})
2. Raw electroencephalography (EEG_{RAW})
3. Force as % of maximal voluntary contraction (%MVC)
4. Electromyography power spectral density (EMG_{PSD})
5. Electroencephalography power spectral density (EEG_{PSD})
6. Force as % of maximal voluntary contraction power spectral density ($force_{PSD}$)

1.5.2 Sub Aim 2: Determine the influence muscle fatigue has on force, EMG and EEG (hence the corresponding outcome measures listed below)

1. Co-efficient of variance of force ($force_{CV}$)
2. Normalised beta force as % of maximal voluntary contraction power spectral density (beta $force_{PSD}$)
3. Electromyography root mean squared (EMG_{RMS})
4. Electromyography mean power frequency (EMG_{MPF})
5. Beta electroencephalography root mean squared (beta EEG_{RMS})

1.5.3 Sub Aim 3: Determine corticomuscular coupling as measured by EEG-EMG coherence (with EMG and EEG amplitude confounds) compared to EEG-EMG PLV (no amplitude confounds) (hence the corresponding outcome measures listed below)

1. Electroencephalography channel selected (EEG_{SELECT})
2. Electromyography channel selected (EMG_{SELECT})
3. Electromyography band power (EMG_{POWER})
4. Electromyography median frequency (EMG_{MDF})
5. 1D spectro ($1D_{SPECTRO}$)
6. Beta electroencephalography–electromyography coherence peak amplitude (beta EEG-EMG $coherence_{PEAK\ AMP}$), pre- and post-fatigue
7. Beta electroencephalography–electromyography coherence peak frequency (beta EEG-EMG $coherence_{PEAK\ FREQ}$), pre- and post-fatigue
8. Beta electroencephalography–electromyography phase lock value peak amplitude (beta EEG-EMG $PLV_{PEAK\ AMP}$), pre- and post-fatigue
9. Beta electroencephalography–electromyography phase lock value peak frequency (beta EEG-EMG $PLV_{PEAK\ FREQ}$), pre- and post-fatigue
10. Beta electromyography root mean squared (beta EMG_{RMS}) before and after transition to fatigue (first and second part of the fatigue stage)
11. Beta electroencephalography root mean squared (beta EEG_{RMS}) before and after transition to fatigue (first and second part of the fatigue stage)
12. Beta electroencephalography–electromyography coherence peak amplitude (beta EEG-EMG $coherence_{PEAK\ AMP}$), before and after transition to fatigue (first and second part of the fatigue stage)
13. Beta electroencephalography–electromyography phase lock value peak amplitude (beta EEG-EMG $PLV_{PEAK\ AMP}$), before and after transition to fatigue (first and second part of the fatigue stage).

1.6 Scope of the study

The present study is a pilot with 15 right-handed human participants, using EEG and EMG measurement techniques. Only neurologically-normal, healthy participants were used in this study. Fatigue was assumed if the participant could not hold 10% below a targeted %MVC for longer than 2 seconds. The muscle analysed was limited to the APB muscle (see section 2.1.1.2).

1.7 Plan of development

Section 2 (METHODOLOGY) describes the participants, experimental protocol, data recording, data analysis and statistical analysis carried out to test objectives of the present study.

Section 3 (RESULTS) contains the results of the comparisons of the variables (listed under the objectives) between pre- and post-fatigue in both qualitative and quantitative form.

Section 4 (DISCUSSION) discusses the results obtained and explores possible reasons for the outcomes.

Section 5 (CONCLUSIONS) discusses the outcome from the study and possible further research.

A detailed view of methodology and results for each sub aim in Section 1.5 is provided in Figure 1-10.

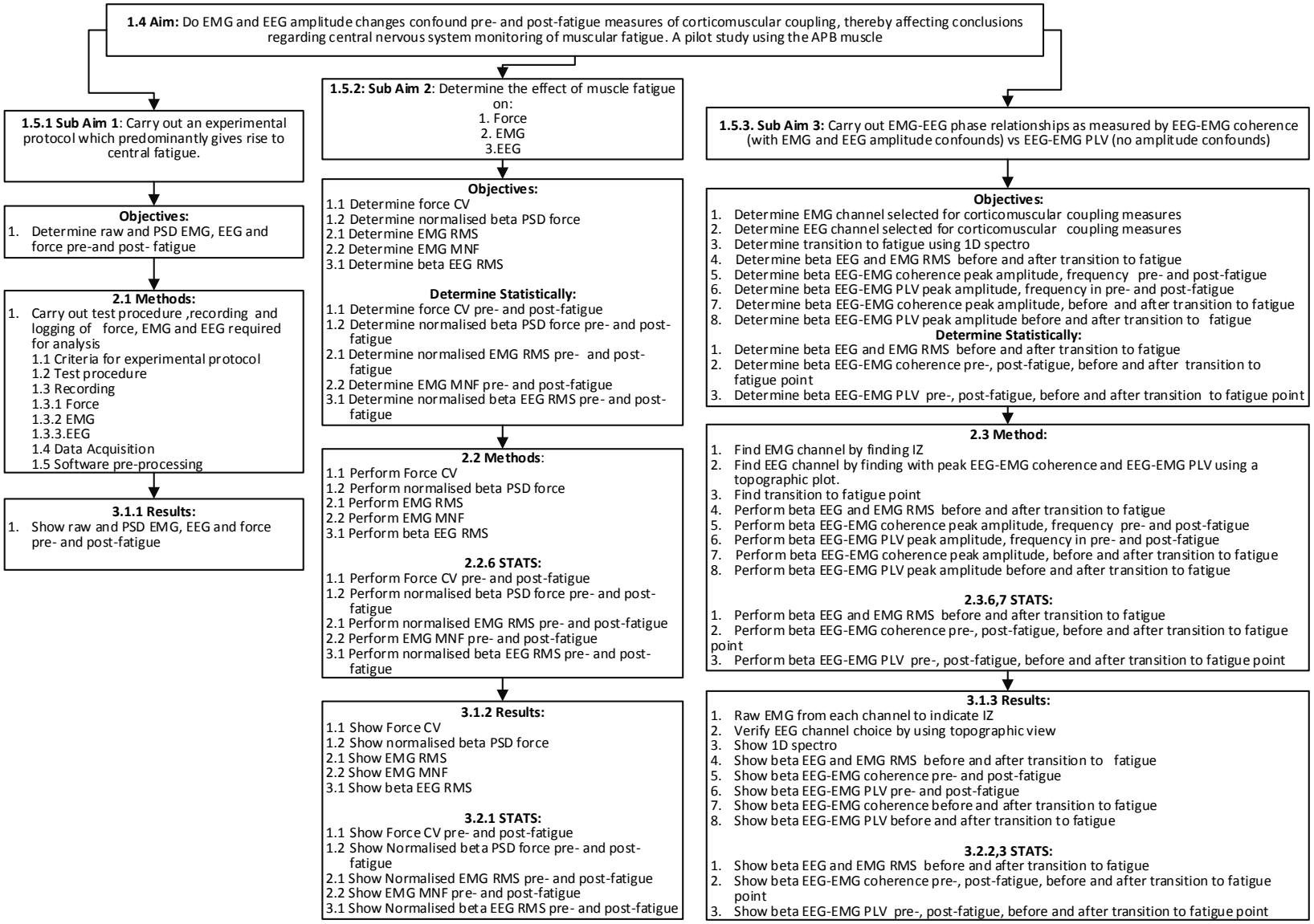

Figure 1-10: The relationship between the aim, sub-aims, objectives, methods and results. The number next to each heading represents the section number.

[This page is intentionally left blank]

2. METHODOLOGY

Section 2 describes the methodology corresponding to the objectives mentioned in Section 1.5.

2.1 Experimental protocol methodology

Section 2.1 deals with the how the experiment was carried out and how signals for force, EMG and EEG were acquired during the experiment.

2.1.1 Criteria for experimental protocol

The present study follows on the theory purposed by Weir et al. (2006) that, during muscle fatigue, the contributions of central and peripheral fatigue are task-dependent; therefore, an appropriate experimental protocol was derived.

Section 1.2.2 describes:

- Types of contraction
- Selection procedure of the muscle
- Test protocol used in a fatigue study
- Criteria for each participant

2.1.1.1 Type of contraction selection

Studies have indicated that, as opposed to a repetitive MVC task, central fatigue forms a greater proportion of the attenuated force during a submaximal isometric contraction (Søgaard et al, 2006; Taylor & Gandevia, 2008).

For this study, a submaximal isometric concentration was selected to focus on central fatigue (for more detail on %MVC selected, see Section 2.1.1.3).

2.1.1.2 Muscle selection

Phillips and Porter (1964) observed that the cortico-motoneuronal connections to distal muscles are stronger than those to proximal muscles. Additionally, in order to prevent movement artefacts and excessive muscle activity interfering with the EEG (as this is a muscle fatigue study), a small muscle distal from the head and neck region would be ideal.

Barandun et al. (2009) argued that since the abductor pollicis brevis (APB) muscle has one motor point, that there would be a high probability that any observed innervation zone (IZ) will

not extend into the measuring region. Additionally, the APB muscle is close to the surface under a thin layer of fat allowing for low impedances between the muscle fibre and electrode (Merletti & Parker, 2004).

Therefore, for the present study, the APB, a distal muscle, was selected. Thus, as a result, the cortico-motoneuronal connections would be stronger and would prevent artefacts and excessive muscle activity interfering with the EEG signals. Additionally, the IZ in the APB muscle may be experimentally avoided, and the impedance between the muscle fibre and electrode would be small.

2.1.1.3 Testing procedure from a fatigue study

In order to allow for testing of pre-, during and post-fatigue, an experimental protocol was adopted from Kattla and Lowery (2010), who conducted a fatigue study that recorded EMG and force, in three:

Stage 1: An initial non-fatiguing contraction at a 10% of MVC, allowing for a control-observed parameter for each participant

Stage 2: Required the participant to fatigue the specific muscle at 30% of MVC. A participant was considered fatigued if the targeted %MVC dropped by 10% for longer than 2 seconds.

Stage 3: Performed the same task as in Stage 1, with no rest between Stage 2 and 3.

Through these stages, a direct comparison of an observed parameter between Stage 1 and 3 can be conducted. In addition the time course changes within Stage 2 may be observed.

2.1.1.4 Participant inclusion and exclusion criteria

In order to remove external factors that could influence the outcome, participants had to satisfy certain criteria to be selected. These external factors included:

- neurological diseases or pre-existing neurological conditions; and
- the consumption of cigarettes, caffeine or alcohol before the experiment.

Performance of muscle groups significantly differ with age and gender, for example. Dedrick et al. (2008) found that ‘female recreational athletes utilise a different neuromuscular control pattern for performing a drop jump sequence when estrogen levels are high compared to when they are low’. Thus, only male participants were selected, because it is uncertain to what

extent neuromuscular signals are affected by hormones, such as oestrogen and progesterone. In contrast, adult male testosterone levels remain relatively unchanged.

2.1.1.5 Summary for criteria of experimental protocol

- Participants selected for this study were healthy males from the same age group with no prior neurological disorders and no consumption of cigarettes, caffeine or alcohol before the experiment.
- The muscle selected was the APB muscle.
- A submaximal isometric contraction was used to fatigue the muscle.
- The testing procedure would have three stages: pre-fatigue, fatigue and post-fatigue.

2.1.2 Test protocol

The Human Research Ethics Committee approved the ethics for testing before the experiments were carried out (HREC REF: 157/2011).

Fifteen participants (see Appendix B for sample size estimation) were recruited from amongst the adult UCT student population (age: 25 ± 2 years). All participants were right-handed males with no history of neurological or muscular disorders, nor any epilepsy of any kind (refer to Section 2.1.1.4).

Prior to testing, the detail of the study was thoroughly explained to each participant. Each participant received a consent form (see Appendix C) explaining all the testing procedures, risks and benefits. The study was performed in accordance with the principles of the Declaration of Helsinki (October, 2008), ICH Good Clinical Practice (GCP) and the laws of South Africa. Participants had the right to withdraw from the experiment at any stage without stating a reason and without prejudice. The investigators, who were working under the mandate of the University of Cape Town, were responsible for treating any adverse or untoward events arising from participation in this research study.

In the present study, testing involved a three-step procedure. First, the participants were familiarised with the custom-designed isometric contraction device (refer to Section 2.1.3.1), and the details of the study were thoroughly explained to them. Second, each participant's peak isometric force was assessed on the APB muscle using a custom designed and built isometric contraction device (see Section 2.1.3.1). The participant was seated with his right arm and hand strapped down. All isometric tests were conducted with the elbow flexed at approximately 90° (see Figure 2-10). When measuring the force output, the thumb would push

against the isometric contraction device at approximately 30° from the hand. A standardised warm-up included isometric contractions at 30%, 50% and 70%, followed by MVC of the participant's perceived output. The test included three MVCs of 5 seconds, each separated by 60-second intervals. Participants were verbally motivated to encourage them to achieve their maximum contraction. The maximum MVC value from these tests was selected as their MVC. Third, participants were prepared for the placement of the EMG and EEG electrodes and a prolonged resting period was given in order to prevent the onset of fatigue. Thereafter, the participant performed six isometric contractions at 10% of MVC for 10 seconds for the pre-fatigue stage. After a 2-minute rest period, the participant performed an isometric contraction at 30% of MVC until task failure (when the % MVC dropped by 10%, in this case to below 20% of MVC for more than 2 seconds) for the fatigue stage. Following this, the participants repeated the six initial sub-maximal movements for the post-fatigue stage (see Figure 2-1).

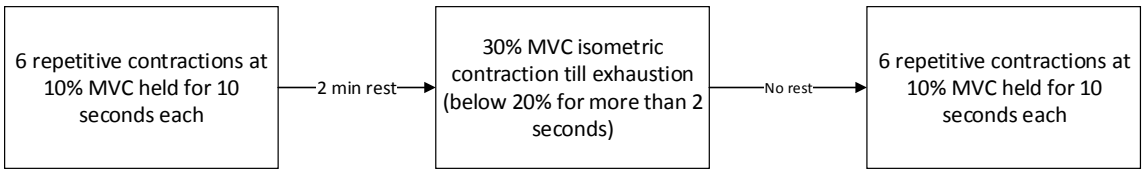

Figure 2-1: Protocol for a single trial for a single participant.

2.1.3 Recording

Section 2.1.3 explains the recording of force, EMG and EEG signals during the experiment.

2.1.3.1 Force recordings

The experiment required an isometric contraction device with the following requirements:

1. force output to be provided,
2. APB muscle to be the primary mover for the movement required by the participant throughout the experiment, and
3. adjustable for any right-handed person.

The resulting design was conceptualised and developed in SOLIDWORKS Student version 2011. The device was made to attach to a Manipulandum design by Divekar and John (2012). Figure 2-2 is a picture of the assembly in SOLIDWORKS.

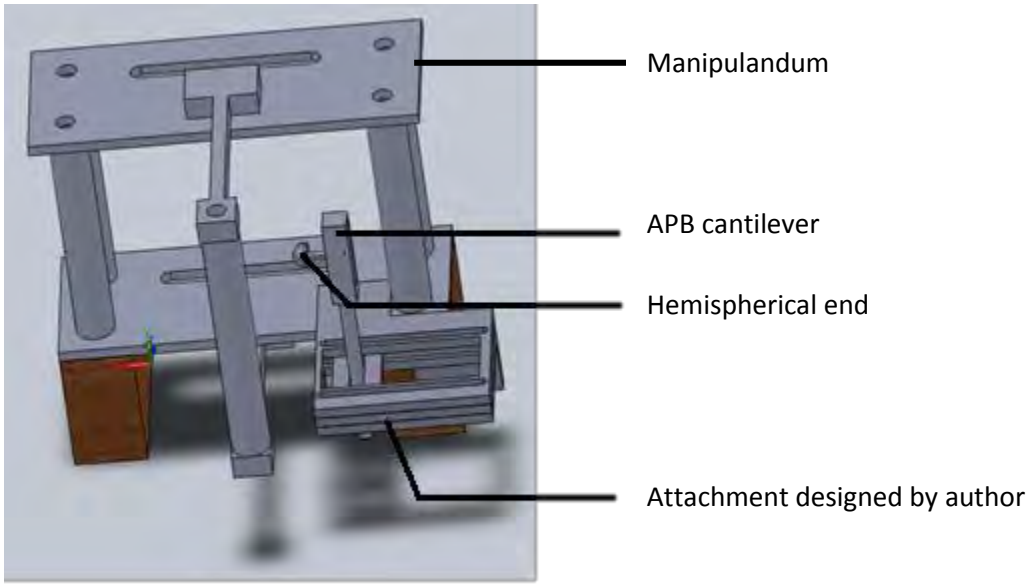

Figure 2-2: SOLIDWORKS design of the isometric contraction device.

2.1.3.1.1 Output force measurement for the isometric contraction device

The force applied by the APB muscle was determined with the use of mild steel, 2mm strain gauges (purchased from RS Components, South Africa,), which were placed on the APB cantilever shown in Figure 2-3.

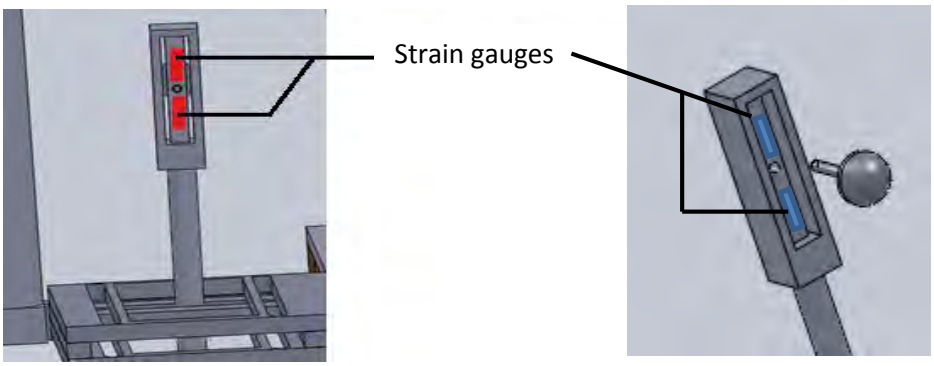

Figure 2-3: Positioning of strain gauges: Strain gauges were placed behind and in front of the APB cantilever (see Figure 2-2) as shown by the red blocks and blue blocks, respectively.

The four strain gauges formed a full-bridge strain gauge setup. This was electrically connected to a commercial strain gauge amplifier (RS Components, Stock no. 435-692; refer to Appendix J)

with a high common mode ratio (CMRR) (> 120 dB), low voltage offset w.r.t. temperature (0.5µV/°C for input voltage and 20µV/°C for bridge supply voltage) and high-precision resistors (1% tolerance and 50ppm/°C temperature coefficient) (see Figure 2-4). The bridge voltage supply was set to 9.0V. The strain gauge amplifier applied a gain, shown by the following equation:

$$Gain = \frac{R_1}{R_2} + 1 \qquad \textbf{Equation 2-1}$$

$$where\ R_1 = 270\ k\Omega\ and\ R_2 = 100\ \Omega$$

$$Gain = 2701$$

The output voltages from the strain gauge amplifier were digitally converted at 1 KHz and visually displayed to the participant and invigilator (refer to Section 2.1.4).

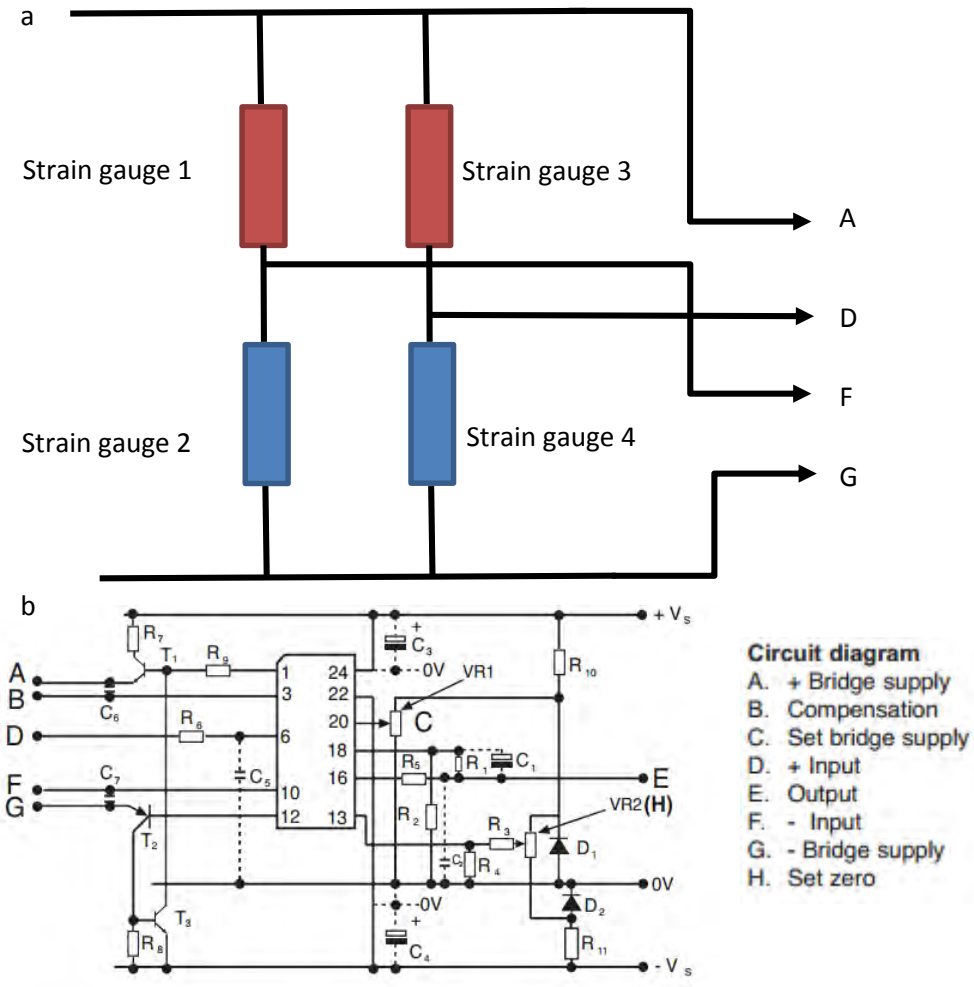

Figure 2-4: a) the connection of the full-bridge strain gauge (see Figure 2-3) circuit to the b) commercial strain gauge amplifier (schematic adopted from RS Components Stock No. 435-692 Datasheet). The A, D, F and G outputs of the full-bridge stain gauges were connected to the

inputs of the commercial gauge amplifier. Output (E), the force applied by the participant in volts, was presented back to the participant on a monitor (see Section 2.1.4).

2.1.3.1.2 Palmar abduction performed on the isometric contraction device

The APB muscle was found to be most active during palmar abduction (van Oudenaarde and Oostendorp, 1995). Palmar abduction is defined as the movement of the thumb anteriorly, a direction perpendicular to the palm. In order to perform this movement, the hand and forearm are constrained in their neutral positions, while the thumb abducts against the APB cantilever (see Figure 2-5), thus performing a palmar abduction, while the hand remains in a neutral position.

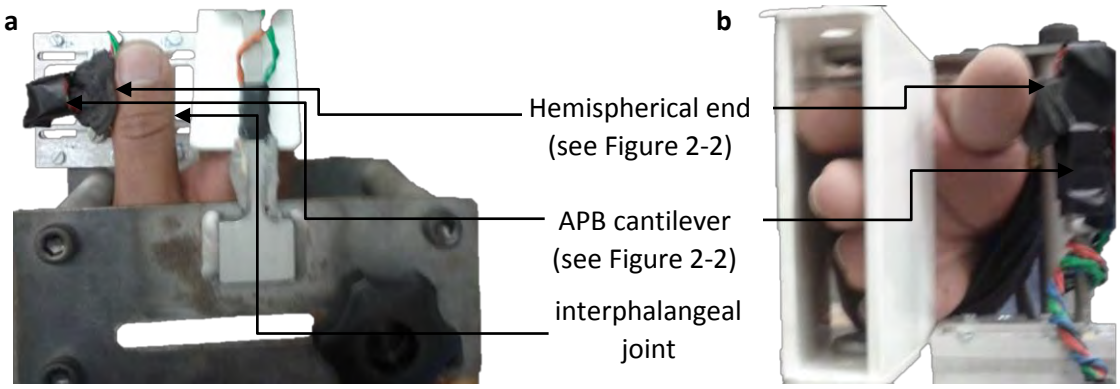

Figure 2-5: Top view (a) and front view (b) of a thumb performing a palmar abduction against the isometric device. The black padding around the hemispherical end (see Figure 2-2) was to provide cushioning for the thumb to make it more comfortable for the participant.

2.1.3.1.3 Adjustable positioning of the isometric contraction device

The hemispherical end (shown in Figure 2-2) was designed to be spherical in order to maintain consistency regarding the location of where the participants transferred their force to the cantilever.

The APB cantilever was designed to be adjustable (i.e., move up or down, closer or further from the thumb and toward or away from the body). This was achieved by loosening the bolts shown in Figure 2-6 and adjusting the position of the APB cantilever, which allowed for a consistent angle between the thumb and index finger as well as keeping the interphalangeal joint of the thumb firm against the centre of the hemispherical end.

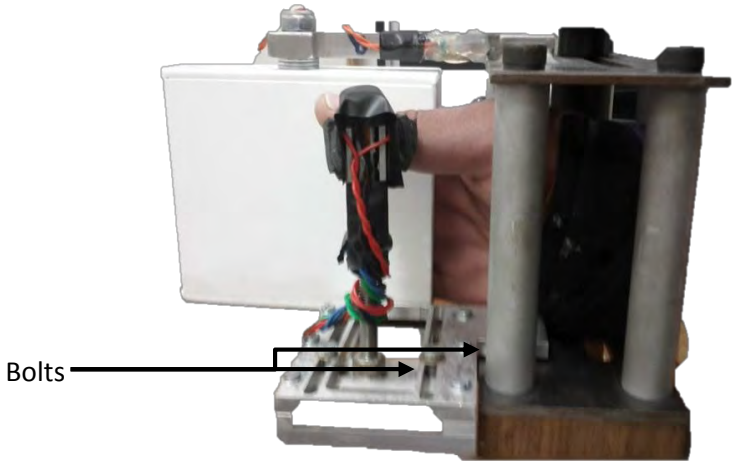

Figure 2-6: Side view of thumb pressing against the isometric contraction device.

2.1.3.2 EMG recordings

Keenan, Collins, Massey, Walters, and Gruszka (2011) observed that the EMG-EMG coherence can be altered if the distance from the IZ is not taken into account. Therefore, for this study, an electrode grid was used to first determine the IZ in the APB muscle.

This design was based on an electrode grid by Nawab, Chang, and De Luca (2010) (see Figure 2-7). Nawab et al. (2010) implemented a five-pin electrode grid, with each electrode being 0.5mm in diameter: four-pin electrodes were placed in a square, 3.6mm apart from one another, and one pin in the centre of the square. This electrode grid was used for motor unit detection and IZ detection for a small hand muscle (the first dorsal interosseous muscle).

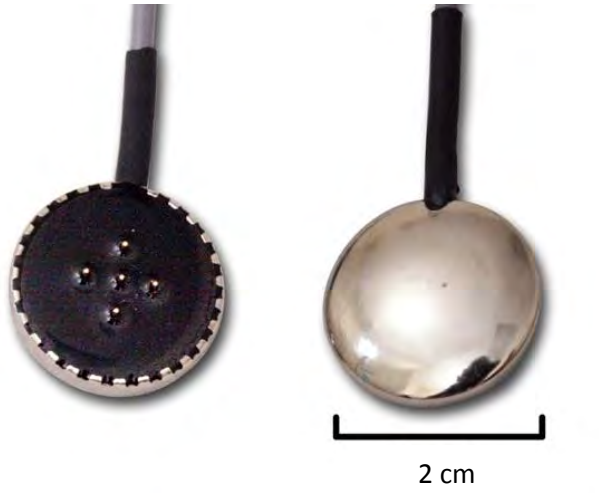

Figure 2-7: Electrode grid developed by Nawab et al. (2010).

The design for the present study used eight bipolar channels to form an electrode grid. Each electrode was made from silver, 1mm in diameter, and the centres were 2.5mm apart from one

another (see Figure 2-8a). The common reference for each bipolar channel was the 'REF' electrode (see Figure 2-8a). The grid was held down by Micropore™ (see Figure 2-8b).

The active ground electrode was a cup-type silver electrode (Nihon Kohden, Japan, diameter = 10mm) and was placed over the ulnar styloid process. The active ground electrode, which is called the driven right leg (DRL), is used for noise cancelation presented on the EMG amplifier boards.

Abrasion and cleaning (with ethanol) of the skin over the muscle was done prior to placing the electrodes. The electrode tips were lightly dipped in Elefix electrode paste (Nihon Kohden, Japan) to further reduce contact impedance. The electrode grid was placed on the belly of the muscle, and the electrode ends were smoothed out, so they only indented and did not pierce the skin. The impedance of the EMG electrode pair were kept below 10 kΩ during the recording.

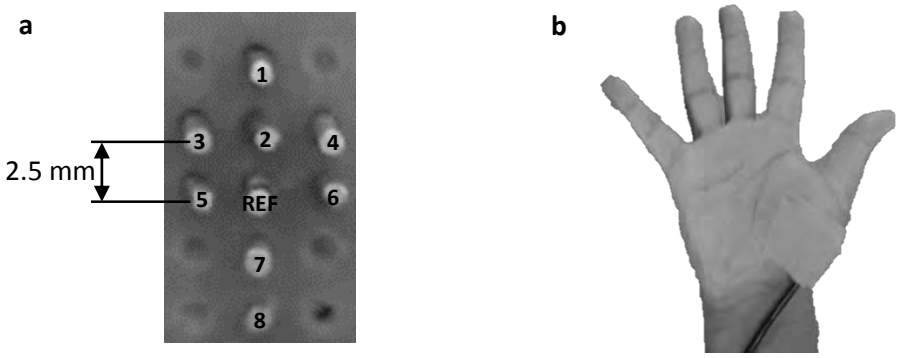

Figure 2-8: a) Electrode grid showing the EMG channels. Each electrode was 1mm in diameter and the centres were 2.5mm from one another. The numbers represent the channel number of each electrode. b) Electrode grid was placed against the participant's palm and covered by Micropore™ to detect the APB EMG.

The EMG data were recorded using bio-amplifiers with gains of 1800. The EMG data was filtered in the range of 5–200 Hz. The original bio-amplifiers had been developed and used in the study by Divekar and John (2012).

2.1.3.3 EEG recordings

Sixteen tin electrodes on a commercial electrode cap (electro-cap) were modified from Divekar and John's (2012) study and were used in this study. The 16 electrodes placed on the cap are shown in Figure 2-9. Electrolyte gel was placed in each electrode to allow contact between the

electrode and scalp. Impedance of the EEG electrodes was kept below 5 kΩ during the recording. The ground electrode was Pz and the DRL was on FPz.

The final setup of the experiment is shown in Figure 2-10.

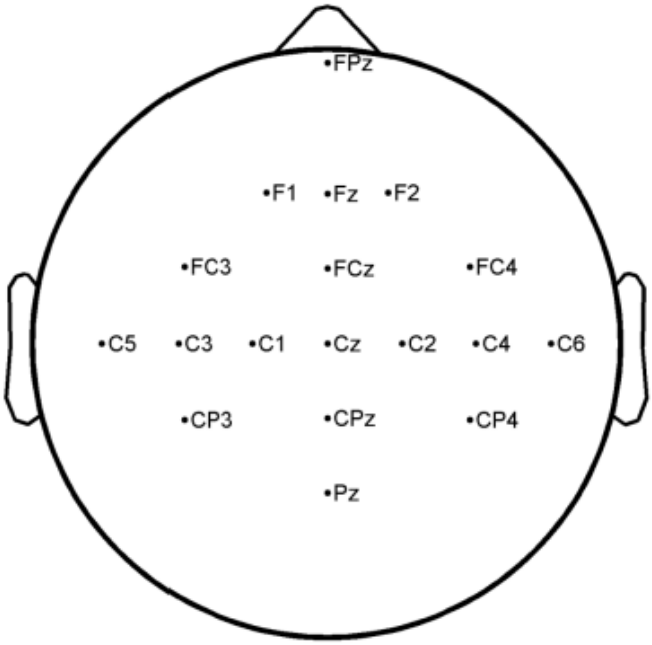

Figure 2-9: Selected 16-channel EEG montage following international 10-10 system spacing for EEG detection with the ground at Pz and the DRL at FPz. Note that the view is of the top of the head, with a schematic of the nose identifying the anterior part (Divekar & John, 2012).

EEG data were recorded using bio-amplifiers with gains of ≈ 5000. The data was off-line filtered in the range of 0.1–200 Hz. The bio-amplifiers had been developed and used in the study of Divekar and John (2012).

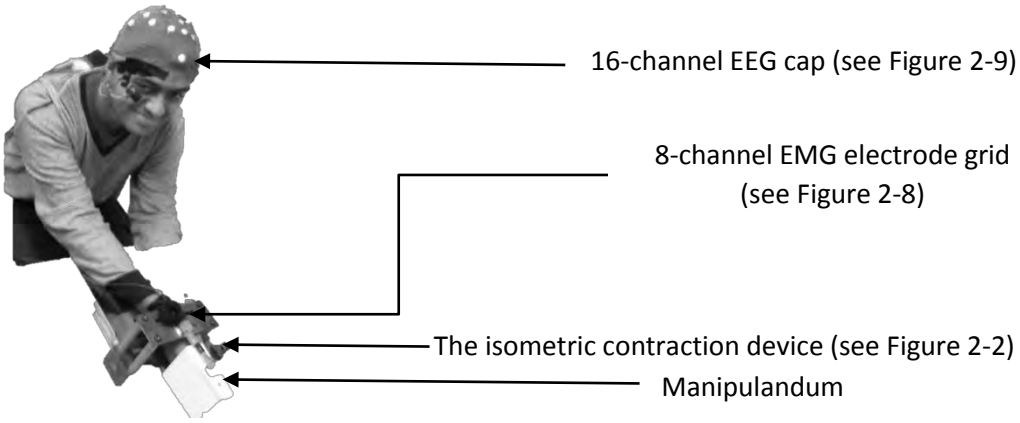

Figure 2-10: Final setup of a participant before the experiment began**.**

2.1.4 Data acquisition of force, EMG and EEG

After pre-processing and sensor amplification (see Section 2.1.3), the data were digitally sampled and acquired using a 16-channel NI DAQ (National Instruments Data Acquisition 6210) for the EEG, which was synchronised with a second 16-channel NI DAQ for EMG and force, as shown in Figure 2-11. All of the data was digitalised at 1 kHz with a 16-bit resolution (Divekar & John, 2012).

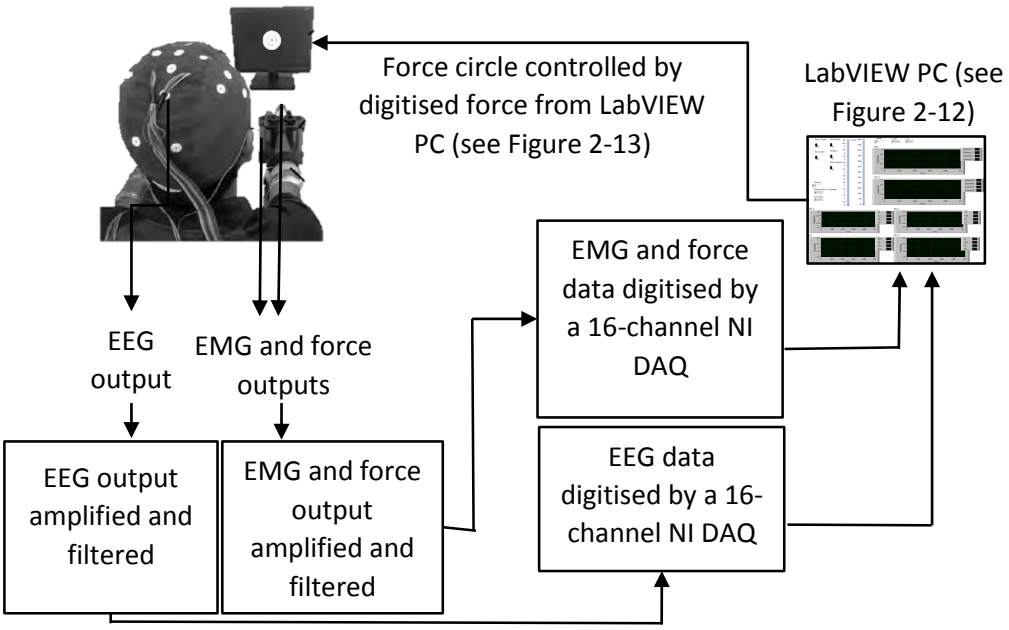

Figure 2-11: Block diagram of the overall system used during the experiment, which includes the %MVC visual feedback, EEG, EMG and force recordings.

The user interface application between the recording device and invigilator (i.e. the author) was developed by the author using National Instruments LabVIEW 2010. This application contained two user interface screens, one for the participant and one for the invigilator.

The invigilator, who controls the experiment, has a screen which shows raw EEG and EMG signals, force in volts, time elapsed for single experimental stage and switches to select which experimental stage should be performed (see Figure 2-12).

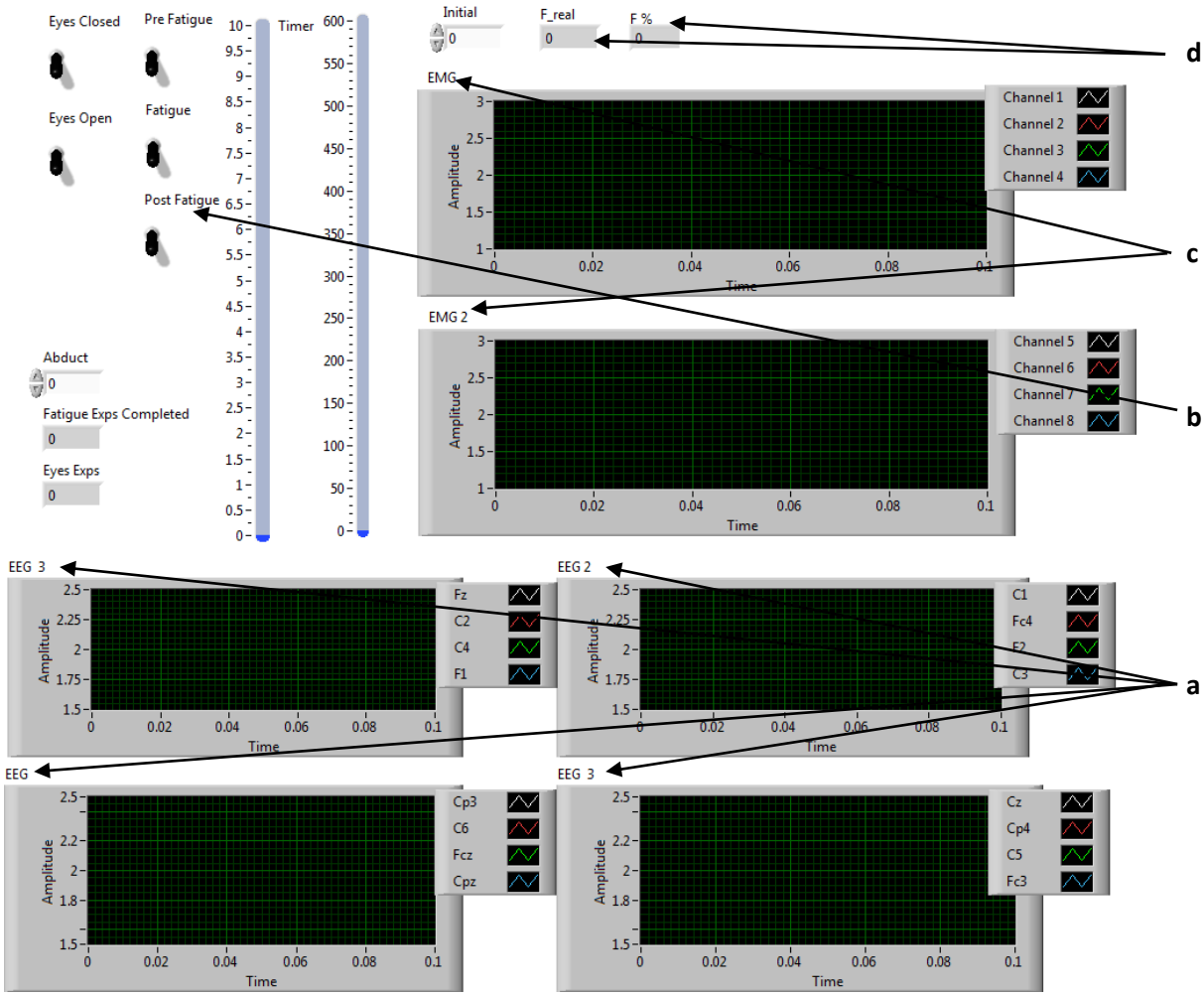

Figure 2-12: Invigilator's testing screen during an experiment. The graphs, a) EEG and c) EMG, show raw EMG and EEG signals from the participants. d) 'F_real' and 'F%' show the strain gauge output in voltage and the percentage of the MVC of the participant respectively (refer to Figure E-5). b) The switches allowed the invigilator to select which stage of the experiment should be performed.

The participants' screen (see Figure 2-13) provides visual feedback of the %MVC applied by the participant. The screen was turned off during the MVC tests and only turned on during the pre-fatigue, fatigue and post-fatigue stage. The screen shows a black dot and a circle within a larger circle. When force is applied to the hemispherical end of the isometric contraction device (see Figure 2-5), the black dot slides from right to left (lower %MVC to higher %MVC), with the midpoint being the targeted %MVC. The inner circle indicates a range of 2% of the targeted %MVC and the outer circle indicates a range of 4% of the targeted %MVC.

Force out is < 4% of the targeted MVC	Force out is 2% smaller than the targeted MVC	Force out is equal to targeted MVC	Force out is 2% greater than the targeted MVC	Force out is > 4% of the targeted MVC

Figure 2-13: Five examples of screens shown to the participants during the experiment. The black dot within the circle slides from right to left (lower %MVC to higher %MVC). The midpoint is the targeted %MVC percentage (i.e., 10% or 30%, depending on the experimental stage) for the participant. The inner circle indicates the range within 2% of the targeted MVC and the outer circle indicates the range within 4% of the targeted MVC. The visual angle of the circle was small in order to minimise the participant's eye movement.

A summary of the steps undertaken by the invigilator is described in Figure 2-14. The data was then saved into a text file for offline analysis, which was conducted later using MATLAB R2011 (see Sections 2.1.5, 2.2 and 2.3). A single stage per participant contains two files: one encompassing EMG and force recordings and the other EEG recordings.

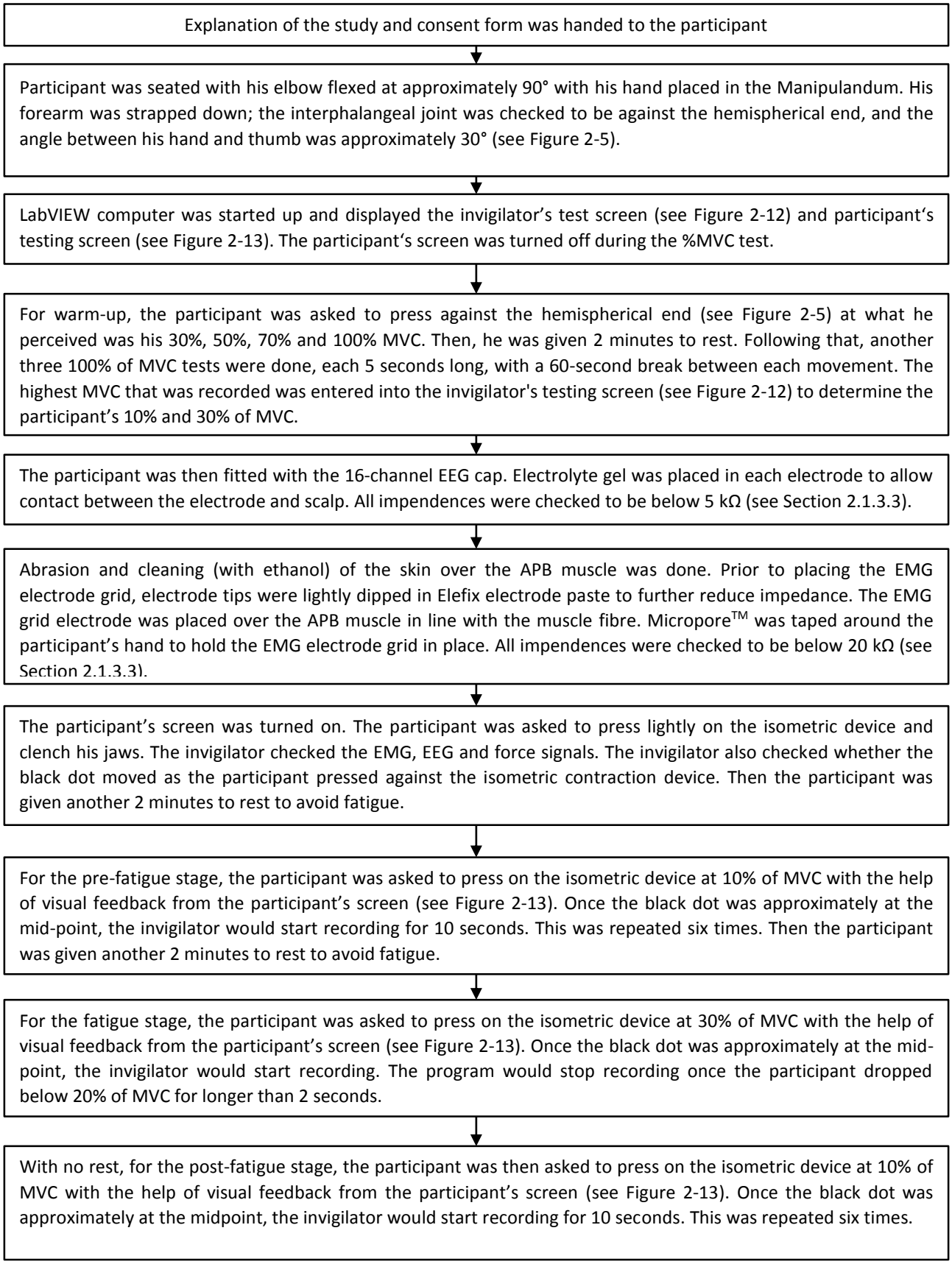

Figure 2-14: Description of the invigilator's test protocol.

2.1.5 Software pre-processing of raw EMG, EEG and force signals

Section 2.1.5 deals with the software pre-processing of force, EMG and EEG signals acquired during the experiment.

2.1.5.1 Extraction of participant data

Data files containing the recordings were first separated according to their respective names. Each stage per participant contained two files (one file from each of the two DAQs used). One file contained 16-channel EEGs, while the other contained 8-channel EMGs and a single force channel. The files were loaded into MATLAB as a matrix, where each column represented a different EMG, EEG or force channel (see Code G-1).

2.1.5.2 Software pre-processing of data

The data was pre-processed to remove noise from the signal and then filtered to remove low frequencies caused by movement and high frequencies to avoid signal aliasing (Gerdle et al., 1999). The EMG, EEG and force data were filtered with a fourth-order zero-phase-shift Butterworth filter between 0.5–100 Hz, 10–200 Hz and a low pass filter of 200 Hz, respectively (see Code G-2).

The gains by the bio-amplifier boards to the EEG and EMG signals (see Section 2.1.3.2 and 2.1.3.3) were corrected for to determine the actual EEG and EMG voltages i.e. EEG data was divided by 5000 and EMG data was divided by 1800 (see Code G-3).

The EEG voltage signals were converted to current source density estimates using the spherical splines algorithm (Kayser, 2001).

Once a bipolar EMG channel was selected based on the muscle IZ (refer to Section 2.3.1), the data was rectified to boost the progressive pattern of grouped firing motor units (Halliday & Farmer, 2010) (see Code G-4).

Section 3.1 illustrates the raw EMG, EEG and force waveforms with their respective PSDs, pre- and post-fatigue, for a typical participant.

2.2 Muscle fatigue influence on force, EMG and EEG

Section 2.2 deals with data analysis for measuring the influence of muscle fatigue on force, EMG and EEG, as shown in previous studies mentioned in Section 1.2.2. This was done to validate the experimental protocol.

2.2.1 Power spectral density (PSD)

The power spectrum of a signal can be used to determine the dominant frequencies within that signal. For this study, the Welch method was used to determine the power spectral to provide information on the predominant frequencies (see Code G-5).

$$EMG_{PSD} = P_{EMG}(f) \qquad \textbf{Equation 2-2}$$

2.2.2 Coefficient of variance of force ($force_{CV}$)

The $force_{cv}$ was the ratio of the standard deviation to the mean of the force acquired, which was then multiplied by 100 to determine the percentage of the coefficient of variance:

$$force_{CV}(\%) = \frac{\sigma}{\mu} * 100 \qquad \textbf{Equation 2-3}$$

where $\sigma$is the standard deviation of the force acquired and μ is the mean of the force acquired (see Code G-6).

2.2.3 Normalised beta force power spectral density (beta $force_{PSD}$)

The normalised beta (15-35 Hz) $force_{PSD}$ was calculated using the power spectral density derived from the Welch method, and then the following equation was used:

$$normalised\ beta\ force_{PSD} = \frac{\int_{15}^{35} P_{Force}}{\int_{1}^{500} P_{Force}} \qquad \textbf{Equation 2-4}$$

where P_{Force} is the PSD of the actual force in %MVC (see Code G-10).

2.2.4 EMG root mean squared (EMG_{RMS})

The EMG_{RMS} was applied using the following formula (see Code G-7):

$$EMG_{RMS} = \sqrt[2]{\frac{1}{n}\sum_{i=1}^{n}(EMG_i\ (t))^2}\ \ n = length\ of\ the\ signal \qquad \textbf{Equation 2-5}$$

2.2.5 EMG mean power frequency (EMG_{MPF})

The mean power frequency was calculated as the sum of the product of the power spectrum and the frequency, divided by the total sum of the power spectrum (an alternative method for measuring the mean frequency, not trial-dependent, is shown in Appendix F). The power spectrum was determined using the Welch method (see Code G-8).

$$EMG_{MPF} = \frac{\sum_{i=0}^{n} P_{EMG_i} * f_i}{\sum_{i=0}^{n} P_{EMG_i}}$$ **Equation 2-6**

2.2.6 Beta EEG root mean squared (beta EEG_{RMS})

The EEG data were first filtered between 15Hz–35 Hz (beta band) using a fourth-order zero-phase-shift Butterworth filter. The beta EEG_{RMS} was found using the following formula (see Code G-11):

$$EEG_{RMS} = \sqrt[2]{\frac{1}{n}\sum_{i=1}^{n}(EEG_i\,(t))^2} \quad n = length\ of\ the\ signal$$ **Equation 2-7**

2.2.7 Statistical analysis for muscle fatigue influence on force, EMG and EEG

Statistical analysis of the data was carried out using SPSS v19.

The experiment contained 3 stages: pre-fatigue, fatigue and post-fatigue. The fatigue stage was designed to fatigue the participant's APB muscle, while the pre-fatigue stage determined a control value for each participant. Finally, the post-fatigue stage was compared to the pre-fatigue stage to determine the change in the observed parameters, due to the effect of muscle fatigue (see Section 2.1.1).

The six repetitions of 10 seconds within the pre-fatigue stage were grouped to form one 60-second stage; similarly, the six repetitions of 10 seconds within the post-fatigue stage were grouped to form one 60-second stage. $Force_{CV}$, normalised beta $force_{PSD}$, EMG_{RMS}, $EMG_{MPF,}$ and beta EEG_{RMS} was then applied to the 60-second block for pre-fatigue and post-fatigue.

Thereafter, a paired *t*-test was carried out for all 15 participants in order to test the effect of the independent variables (IVs, pre- and post-fatigue) on the dependent variables (DVs, $force_{CV}$, normalised beta $force_{PSD}$, EMG_{RMS}, $EMG_{MPF,}$ and beta EEG_{RMS}).

The following assumptions were considered when preparing for the paired *t*-test:

1. The DV should be measured on a continuous scale. In this study, the DVs are observed to be on a continuous scale.
2. The IV should consist of related groups. In this study, the participants' pre- and post-fatigue remained the same; thus, the groups are related.
3. There are no significant outliers in the differences between the two related groups. This was verified by plotting a box plot for each observed parameter, shown in Appendix J below each measure.
4. The distribution of the differences in the dependent variable between the two related groups should be approximately normally distributed. This was verified by doing a Shapiro-Wilk test of normality, as shown in Appendix J below each measure.

Section 3.1.2 validates the fatigue stage by plotting the time course changes in $force_{CV}$, normalised beta $force_{PSD}$, EMG_{RMS}, EMG_{MPF} and beta EEG_{RMS} for a typical participant, while Section 3.2.1 shows the statistical results of $force_{CV}$, normalised beta $force_{PSD}$, EMG_{RMS}, EMG_{MPF} and beta EEG_{RMS} in regards to the effect of muscle fatigue.

However, it should be noted that, in order to remove any outliers for the statistical results between participants, the EMG amplitudes and EEG amplitudes for each participant were normalised with their peak EMG and peak EEG amplitudes (found within each participant throughout the experiment) respectively (Halaki and Ginn, 2012).

2.3 Corticomuscular coupling measures

Section 2.3 deals with determining a suitable EEG and EMG electrode pair for the corticomuscular coupling measures as well as determining the transition to fatigue during the fatigue stage. Finally, this section denotes the data analysis for corticomuscular coupling measures. Section 1.2.3 forms the literature background for this section.

2.3.1 Selection of EMG channel for corticomuscular coupling measures

The method of determining the IZ was adopted from the study published by Keenan et al. (2012) (see Section 1.2.3.3). Each participant's IZ was selected visually by checking the waveforms, similar to Figure 3-3.

In this study, the eight-channel electrode grid was placed parallel to the motor fibres (shown in Figure 2-8b). The bipolar differences between the two adjacent electrodes (i.e., electrode 1–2, 2-ref, ref-7 and 7–8 shown in Section 3.1.3.1) were observed to identify the IZ zone, which was estimated to be between two bipolar channels with a clear polarity change.

Since the bipolar channel furthest from the innervation has been shown to provide greater EMG-EMG coherence amplitude peaks (Keenan et al., 2012), the electrode channel furthest from the IZ was selected. The selected EMG electrode is called EMG_{SELECT} and may vary between participants.

2.3.2 Selection of EEG channel for corticomuscular coupling measures

As mentioned in Section 1.2.3.4, the electrodes in the contra-lateral sensorimotor region were selected (C1, C3, C5, FC3 and CP3).

To verify that these electrodes were indeed the most relevant ones, an EEG topographical plot for pre- and post-fatigue beta EEG-EMG coherence and beta EEG-EMG PLV peak amplitudes (see Figure 3-4) was generated using a topographical plotting function from an open source toolbox in MATLAB, known as EEGLAB (Delorme & Makeig, 2004). The selected EEG electrode was the contralateral one with maximal coherence or PLV (respectively) to the selected EMG channel, and is called EEG_{SELECT}.

2.3.3 Transition to fatigue

As mentioned in Section 1.2.3.5, the transition to fatigue time point was determined in order to examine the corticomuscular coupling during the fatigue stage. The transition to fatigue time point is found when 1D spectro increases (see Figure 2-15).

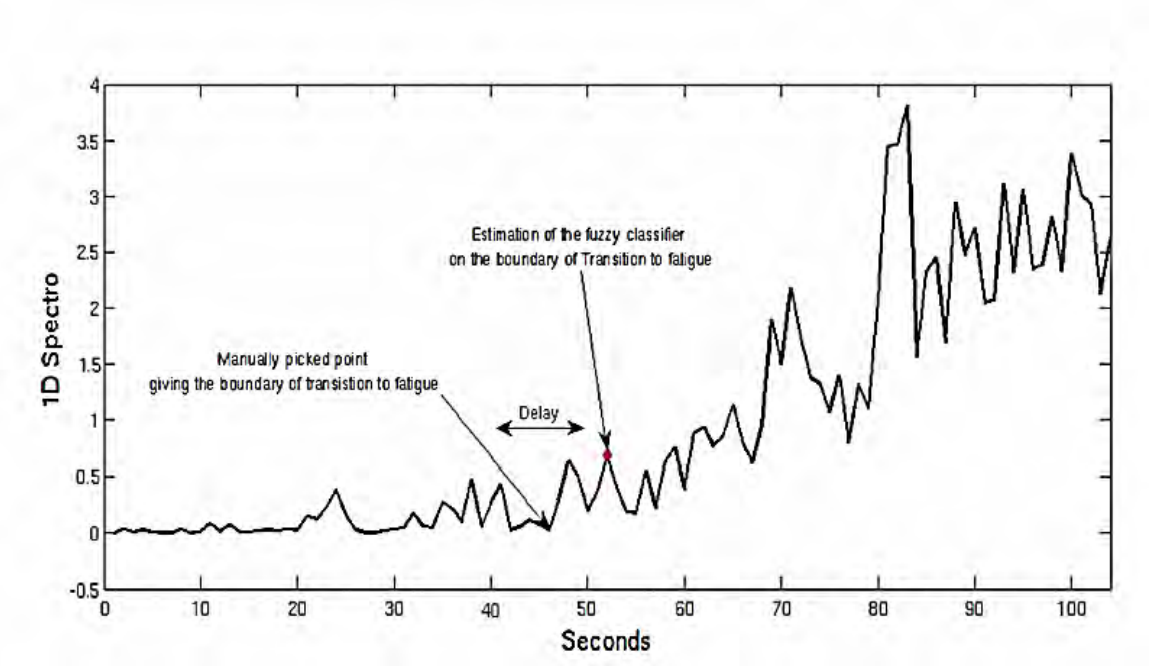

Figure 2-15: Determination of the transition to fatigue point using a 1D spectro waveform**.** The figure adopted from Al-Mulla and Sepulveda (2010).

Since it was unclear from Al-Mulla and Sepulveda's (2010) study on how the EMG_{POWER} and EMG_{MDF} were scaled before subtracting, the present study assumed it was normalised. Thus, for the present study, the transition to fatigue time point is manually identified by visually selecting the time point when 1D spectro increases (i.e. when 'normalised EMG_{POWER}' subtracted from the 'normalised EMG_{MDF}' increases)

1. EMG_{POWER} in the 5-200 Hz band was determined using the following equation:

$$EMG_{POWER} = \int_{5}^{200} P(f)df \qquad \textbf{Equation 2-8}$$

2. EMG_{MDF} was determined using the following equation:

$$EMG_{MDF} = \int_{5}^{EMG_{MDF}} P(f)df = \int_{EMG_{MDF}}^{200} P(f)df \quad \textbf{Equation 2-9}$$

3. Normalise EMG_{POWER} and EMG_{MDF} using the following equations:

$$Normalised\ EMG_{POWER} = EMG_{POWER} / \max(EMG_{POWER}) \quad \textbf{Equation 2-10}$$

$$Normalised\ EMG_{MDF} = EMG_{MDF} / \max(EMG_{MDF}) \quad \textbf{Equation 2-11}$$

4. 1D spectro was estimated using the following formula (see Code G-15):

$$1D\ spectro = Normalised\ EMG_{POWER} - Normalised\ EMG_{MDF} \quad \textbf{Equation 2-12}$$

The EMG_{POWER}, EMG_{MDF} and 1D spectro of a typical participant during the fatigue stage were illustrated by sliding a 30-second window along the signal in 1-second increments (see Figure 3-6).

2.3.4 EEG-EMG coherence

As discussed in Section 1.2.3.1, EEG-EMG coherence is one of the measures of corticomuscular coupling. In this study, electrodes EMG_{SELECT} and EEG_{SELECT} (refer to Section 2.3.1 and 2.3.2) were provided as the inputs to measure EEG-EMG coherence using a function in MATLAB, called *'mscohere'* (Magnitude squared coherence; refer to Code G-12).

The magnitude squared coherence estimate, C_{xy}, of the input signals *x* and *y* using Welch's averaged, modified periodogram method. C_{xy} a function of frequency with values between 0 and 1 that indicates how well *x* corresponds to *y* at each frequency, 0 (if the signals are incoherent) and 1 (if the signals are perfectly coherent). C_{xy} was calculated with the following equation:

$$C_{xy} = \frac{|P_{xy}(f)|^2}{P_{xx}(f)P_{yy}(f)} \quad \textbf{Equation 2-13}$$

where $P_{xx}(f)$ and $P_{yy}(f)$ are the power spectral densities of *x* and *y*, respectively, and $P_{xy}(f)$ is the cross power spectral density of *x* and *y*.

The coherence estimate was considered significant where $C_{xy} > Confidence\ Level\ (CL)$.

$$CL = 1 - \alpha^{\frac{1}{L-1}}$$ **Equation 2-14**

where L is the total number of disjointed segments used to calculate the coherence and α = 0.05 (i.e., above the 95% confidence interval) (Rosenberg, Amjad, Breeze, Brillinger, & Halliday, 1989).

The window size used for the '*mscohere'* was 256 samples (i.e., 256 ms since the sample rate was 1 Khz), which can capture frequencies as low as 4 Hz. Since the study was related to the EEG-EMG coherence in the beta band (15–35 Hz), this window size proved to be adequate.

The 6 repetitions of 10 seconds within the pre-fatigue stage were grouped to form a 60-second stage; similarly, the six repetitions of 10 seconds within the post-fatigue stage were grouped to form one 60-second stage. Thereafter, the EEG-EMG coherence waveforms were generated for both pre- and post-fatigue stages. Thus, in this study, L for Equation 2-14 is approximately 234 and CL is 0.0128.

2.3.5 EEG- EMG phase lock value (EEG-EMG PLV)

As discussed in Section 1.2.3.2, the EEG-EMG PLV is another one of the measures of corticomuscular coupling. Figure 2-16 help illustrate the method of determining the PLV and PLS (Phase Lock Statistics) waveforms in this study.

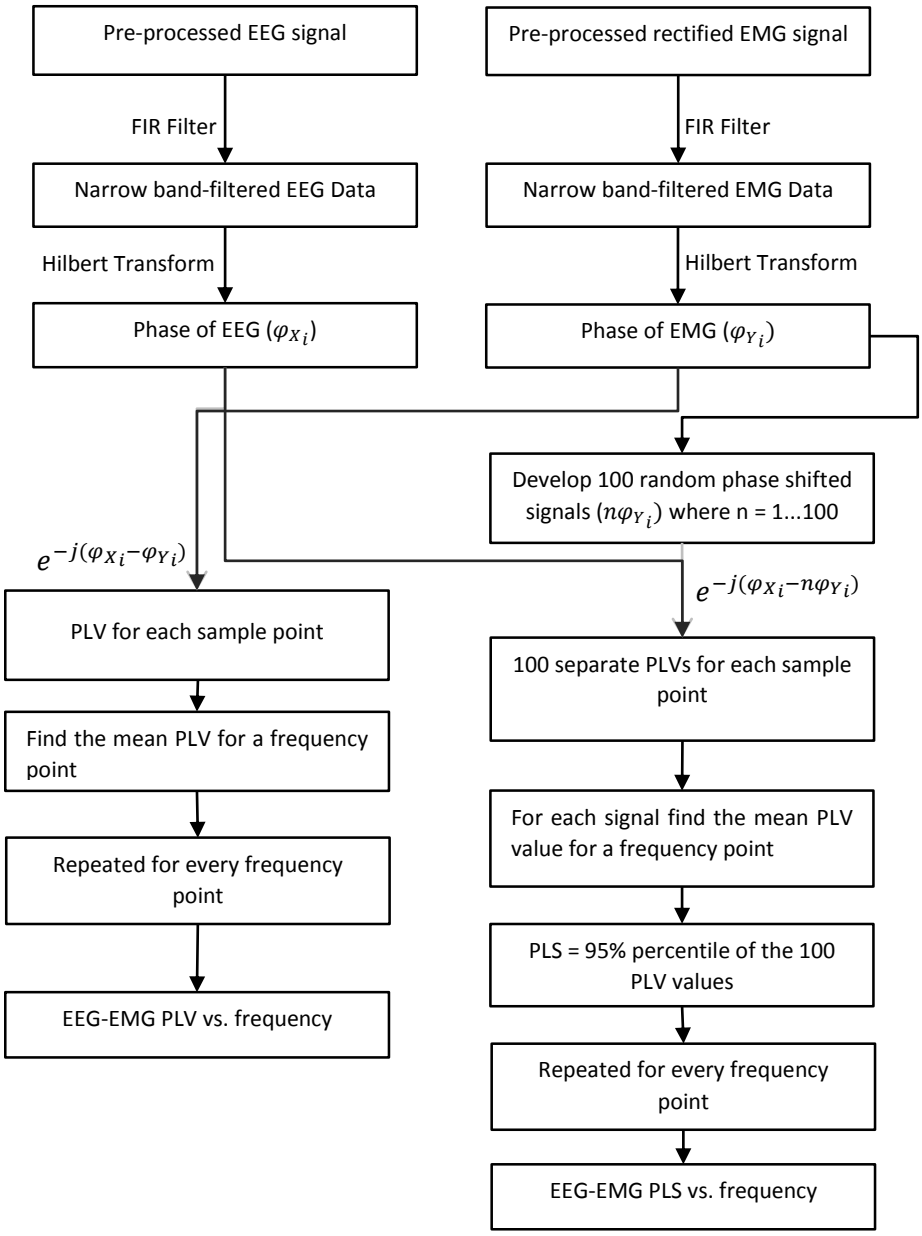

Figure 2-16: Illustration of the method of determining PLV and PLS waveforms in the present study.

To determine EEG-EMG PLV, EEG and EMG data were first narrow-band filtered ($f_c \pm 0.5Hz$), using finite impulse response (FIR) filter for each frequency point (f_c).

EEG-EMG PLV for f_c was calculated using the following equation (adopted from Lachaux et al., 1999):

$$EEG - EMG\ PLV(f_c) = \frac{1}{n}\sum_{i=1}^{n} e^{-j\theta_i} \qquad \textbf{Equation 2-15}$$

where i is a sample point; $\theta_i = \varphi_{X_i} - \varphi_{Y_i}$ is the phase difference between the two signals and n is the length of the signal.

In this study, electrodes EMG_{SELECT} and EEG_{SELECT} (refer to Section 2.3.1 and 2.3.2) were used to measure the EEG-EMG PLV using a MATLAB function developed by the author (see Code G-13).

The instantaneous phase was found for each signal using the Hilbert transform, which was chosen because there were minor differences found between using the wavelet and Hilbert transforms for neurological signals (Le Van Quyen et al., 2001) and the Hilbert transform was preferred as it requires less computational time.

The EEG-EMG PLVs were calculated using a bootstrap technique on 100 'shift surrogates'. These 'shift surrogates' were generated by time shifting one series relative to the other by random lags. By using the 'shift surrogates' as opposed to 'shuffled surrogates' (which are generated by shuffling the samples within one time series), the timing structure of the signal was maintained. Additionally, it was shown to preserve the inherent autocorrelations of the signals and only remove the cross-correlations. This method was adopted from Gupta and James (2007).

Therefore, the EEG-EMG PLV was deemed significant if it fell above the 95th percentile (EEG-EMG PLS) of the 100 shifted surrogates (refer to Code G-14).

Since phase difference was determined between two different neurological systems, the phase locking ratio, ($\theta_i = n\varphi_{X_i} - m\varphi_{Y_i}$) where n:m=2:1(EMG phase: EEG phase), should be used. However, by rectifying the EMG signals, the phase lock ratio was implicitly derived.

2.3.6 Statistical analysis for corticomuscular coupling measures pre- and post-fatigue

As discussed in Section 2.2.7 pre- and post-fatigue were grouped to form two 60-second stage blocks. Thereafter, the EEG-EMG coherence waveforms and the EEG-EMG PLV waveforms were generated for both pre- and post-fatigue (see Section 3.1.3.3). For each participant, the maximum beta EEG-EMG coherence and beta EEG-EMG PLV amplitude (beta EEG-EMG coherence$_{PEAK\ AMP}$ and beta EEG-EMG PLV$_{PEAK\ AMP}$) with their respective frequencies (beta EEG-EMG coherence $_{PEAK\ FREQ}$ and beta EEG-EMG PLV$_{PEAK\ FREQ}$) were found in the beta band for the pre-fatigue stage and post-fatigue stage (see Figure 3-5).

A paired *t*-test was carried out to test the effect of the IVs (pre- and post-fatigue) on the DVs (beta EEG-EMG coherence $_{PEAK\ AMP}$ and beta PLV$_{PEAK\ AMP}$) for all 15 participants. The same assumptions shown in Section 2.2.7 for the paired *t*-test were considered.

Section 3.1.3.3 illustrates an example of a typical participant's EEG-EMG coherence and EEG-EMG PLV waveforms pre- and post-fatigue, while Section 3.2.2 shows the statistical results for beta EEG-EMG coherence $_{PEAK\ AMP}$ and beta EEG-EMG PLV$_{PEAK\ AMP}$ pre- and post-fatigue.

2.3.7 Statistical analysis for corticomuscular coupling measures before and after transition to fatigue

A non-parametric signed test was carried out in order to examine the corticomuscular coupling during the fatigue stage (as paired *t*-test failed the assumption of no outliers even after the application of the arc hyperbolic tangent transformation, Rosenberg et al., 1989).

Two blocks of 30 seconds before and after the transition to fatigue point (see Section 2.3.3) were segmented from the fatigue stage and defined as the *first part of the fatigue stage* and *second part of the fatigue stage*. Thereafter, the EEG-EMG coherence waveforms and the EEG-EMG PLV waveforms were generated for both the first part of the fatigue stage and second part of the fatigue stage (see Section 3.1.3.3). For each participant, the maximum beta EEG-EMG coherence and beta EEG-EMG PLV amplitude (beta EEG-EMG coherence$_{PEAK\ AMP}$ and beta EEG-EMG PLV$_{PEAK\ AMP}$) with their respective frequencies (beta EEG-EMG coherence $_{PEAK\ FREQ}$ and beta EEG-EMG PLV$_{PEAK\ FREQ}$) were found in the beta band for the before and after the transition to fatigue (see Figure 3-7). The non-parametric signed test measured the effect of the IVs (first part of the fatigue stage and second part of the fatigue stage) on the DVs (beta EEG-EMG coherence$_{PEAK\ AMP}$ and beta EEG-EMG PLV$_{PEAK\ AMP}$) for all 15 participants.

In order to perform a non-parametric signed test, the following assumptions were considered:

1. The differences are independent from one other, as the one participant cannot affect another participant's values.
2. The populations before and after are related.
3. The dependent variables are from a continuous scale.

Also, since the aim of the study is to determine the confounding effects of both the EEG and EMG amplitudes on the beta EEG-EMG coherence $_{PEAK\ AMP,}$ a paired *t*-test was carried out on both the EEG_{RMS} and EMG_{RMS}. The paired *t*-test assessed the effect of the IVs (30 seconds before and 30 seconds after the transition to fatigue point) on the DVs (beta EEG_{RMS} and normalised beta EMG_{RMS}) for all 15 participants. The same assumptions shown in Section 2.2.7 for the paired *t*-test were considered.

Section 3.1.3.5 illustrates an example of a typical participant's EEG-EMG coherence and EEG-EMG PLV waveforms before and after the transition to fatigue, while Section 3.1.3.4 shows the time course changes for EMG_{POWER}, EMG_{MDF}, 1D spectro, beta EMG_{RMS}, beta EEG_{RMS}, EEG-EMG coherence and EEG-EMG PLV.

Section 3.2.3 shows the statistical results for beta EMG_{RMS}, beta EEG_{RMS}, beta EEG-EMG $coherence_{PEAK\ AMP}$ and beta EEG-EMG $PLV_{PEAK\ AMP}$ before and after the transition to fatigue.

However, notably, EMG amplitudes and EEG amplitudes for each participant was normalised with the peak EMG and peak EEG amplitudes (found within each participant throughout the experiment) respectively, in order to remove any outliers for the statistical results between participants (Halaki and Ginn, 2012).

[This page is intentionally left blank]

3. RESULTS

Section 3 presents the results of the experiments that were carried out in order to test the present study's objectives. Section 3.1 presents the qualitative results, while Section 3.2 presents the quantitative results.

3.1 Qualitative results

Section 3.1 presents the qualitative results obtained from the experiments carried out in Section 2.

3.1.1 Experimental protocol results

This section deals with results obtained from the experiments carried out in Section 2.1.

Figure 3-1 illustrates typical examples of one second EEG_{RAW}, EMG_{RAW}, force, EMG_{PSD}, EEG_{PSD} and $force_{PSD}$ pre- and post-fatigue.

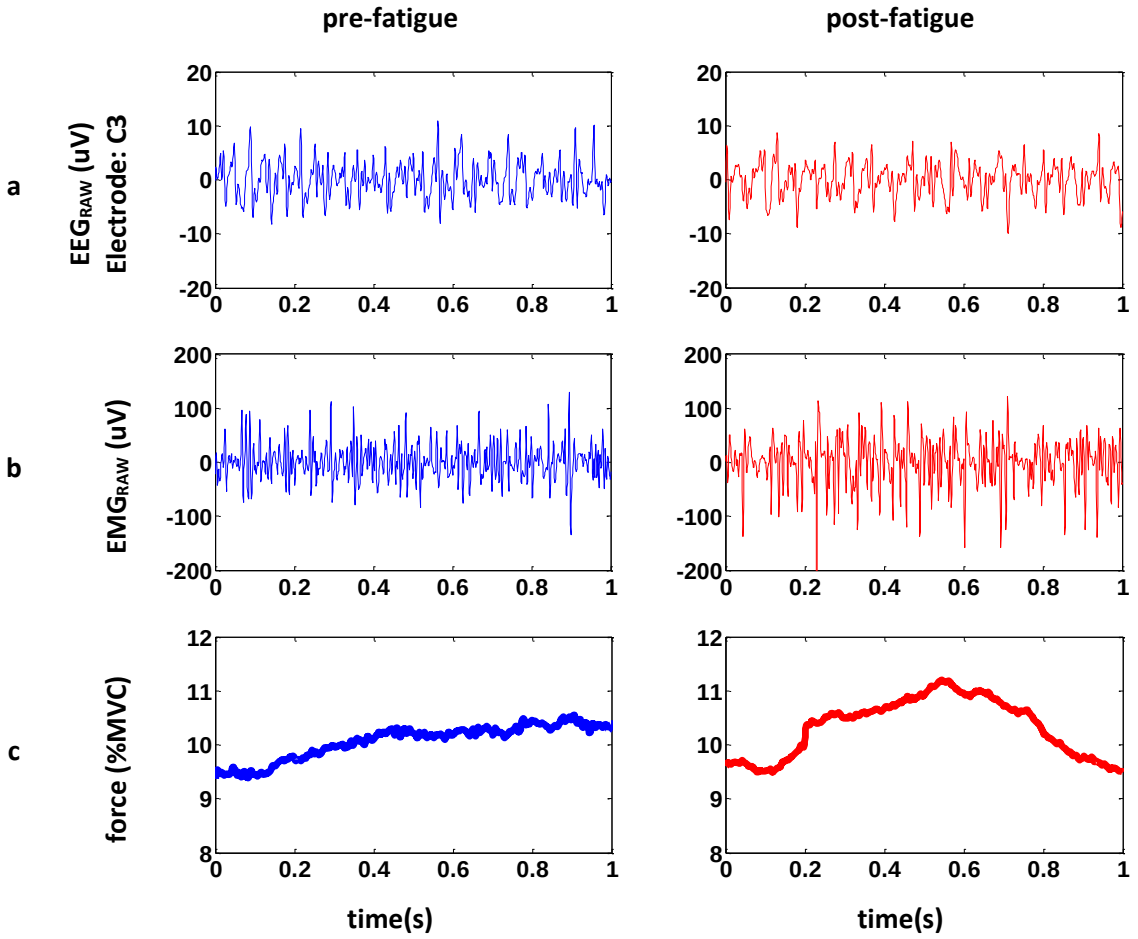

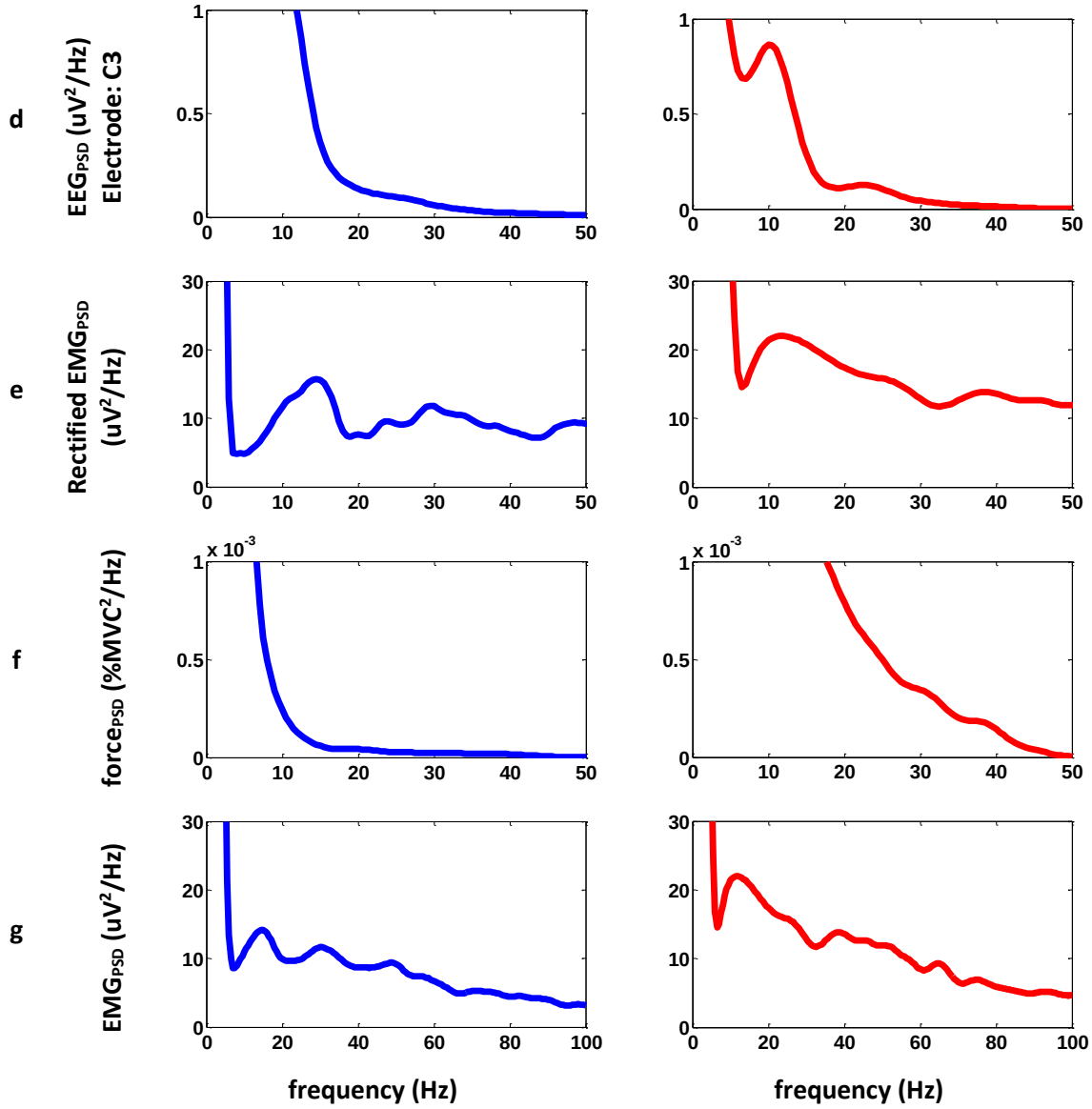

Figure 3-1: Pre- and post-fatigue comparisons between typical (a) EEG_{RAW}, (b) EMG_{RAW} and (c) force and (e, f, and g) their respective PSDs during a sustained isometric contraction at 10% MVC.

The EEG_{PSD} shown in Figure 3-1d is the power spectrum of EEG_{RAW}, shown in Figure 3-1a. It can be observed that EEG_{PSD} peaks in the beta band were clearer and more distinct post-fatigue compared to the pre-fatigue. Additionally, the EEG_{PSD} for both the pre-fatigue and post-fatigue stages, was predominated by alpha oscillatory activity.

The rectified EMG_{PSD} shown in Figure 3-1e, is the power spectrum of rectified EMG_{RAW} shown in Figure 3-1b. The rectified EMG_{PSD} waveforms showed an increase in the beta band post-fatigue as compared to pre-fatigue.

The $force_{PSD}$ shown in Figure 3-1f, is the power spectrum of the force shown in Figure 3-1c. It can be observed that the fluctuations were greater post-fatigue compared to pre-fatigue. This difference is more apparent in the beta band.

3.1.2 Muscle fatigue influence on force, EMG and EEG

This section deals with results obtained from the data analysis carried out in Section 2.2.

Figure 3-2 illustrates the force, EMG_{RAW}, $EEG_{RAW,}$ $force_{CV}$, normalised beta $force_{PSD}$, EMG_{RMS}, EMG_{MPF} and beta EEG_{RMS} during sustained isometric contraction of the APB muscle at 30% of MVC until task failure. $Force_{CV,}$ normalised beta $force_{PSD}$, EMG_{RMS}, EMG_{MPF} and beta EEG_{RMS} were calculated by sliding a 30-second window along the signal in 1-second increments.

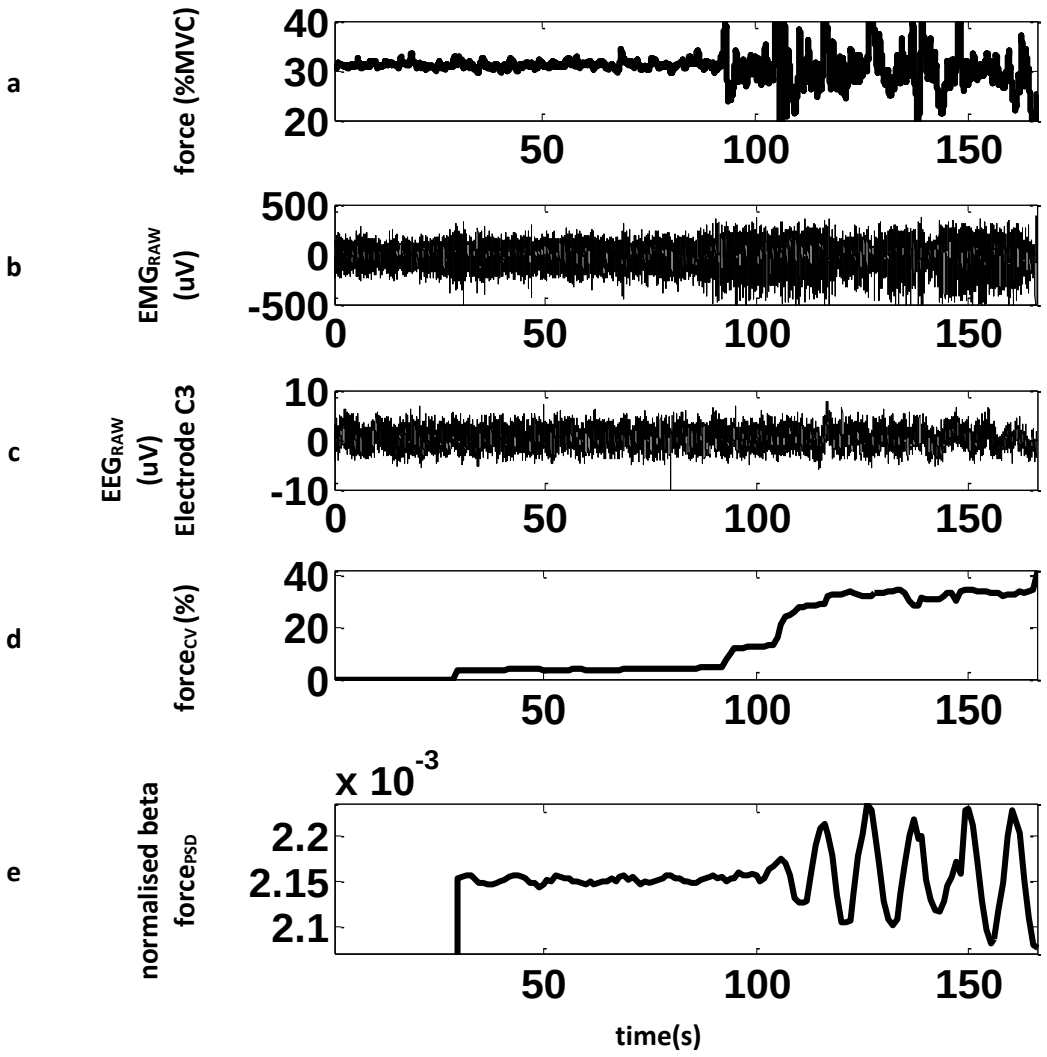

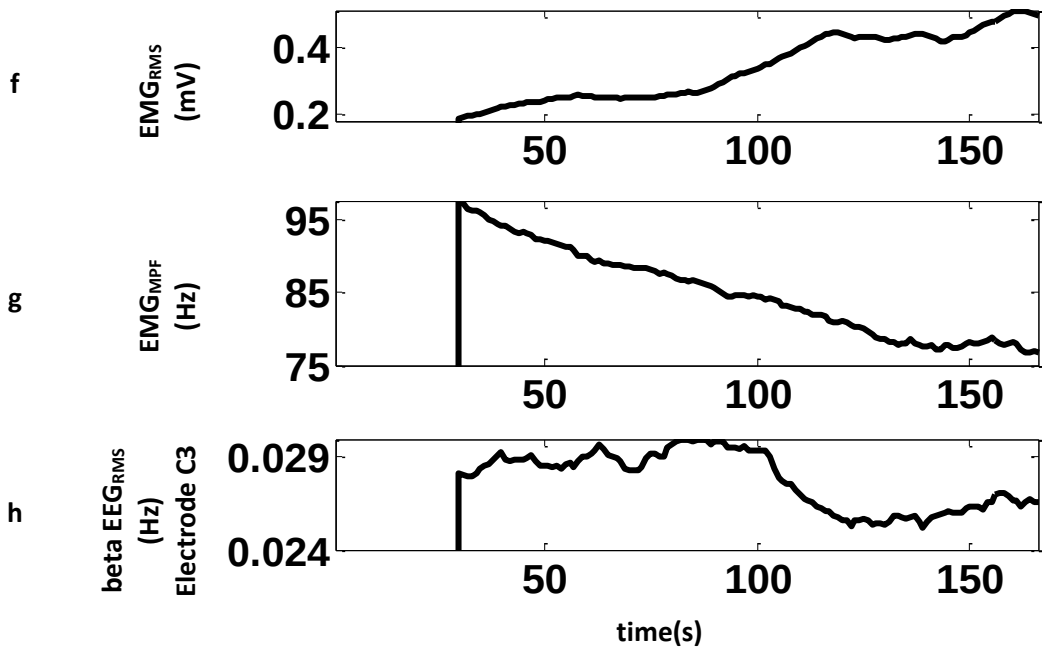

Figure 3-2: Typical example of a participant showing progressive changes in (a) force, (b) EMG_{RAW}, (c) EEG_{RAW}, (d) $force_{CV}$, (e) normalised beta $force_{PSD}$, (f) EMG_{RMS}, (g) EMG_{MPF} and (h) beta EEG_{RMS} during a sustained isometric contraction of the APB muscle at 30% of MVC until task failure. $Force_{CV}$, normalised beta $force_{PSD}$, EMG_{RMS}, EMG_{MPF} and beta EEG_{RMS} were calculated by sliding a 30-second window along the signal in 1-second increments.

From Figure 3-2a, Figure 3-2d and Figure 3-2e, it can be noted that the force, $force_{CV}$ and normalised beta $force_{PSD}$ during the fatigue stage were initially steady, but toward the last third of the fatigue stage, the normalised beta $force_{PSD}$ began to fluctuate and $force_{CV}$ started to increase.

From Figure 3-2b and Figure 3-2f, it can be noted that EMG_{RAW} and EMG_{RMS} during the fatigue stage, were initially steady but toward the last third of the fatigue stage it began to gradually increased toward the end of the fatigue stage.

From, Figure 3-2g it can be observed that EMG_{MPF} during the fatigue stage decreased gradually and then levelled off toward the last sixth of the fatigue stage.

From Figure 3-2c, it can be observed that EEG_{RAW}, and Figure 3-2h, beta EEG_{RMS} during the fatigue stage were initially steady, but just after the last third of the fatigue stage, the beta EEG_{RMS} decreased and finally levelled off toward the end of the fatigue stage.

3.1.3 Corticomuscular coupling results

This section discuss the results obtained from the data analysis carried out in Section 2.3.

3.1.3.1 Electromyogram channel selection (EMG_{SELECT})

Figure 3-3 illustrates a typical example of the raw EMG waveforms from the electrode grid during the fatigue stage.

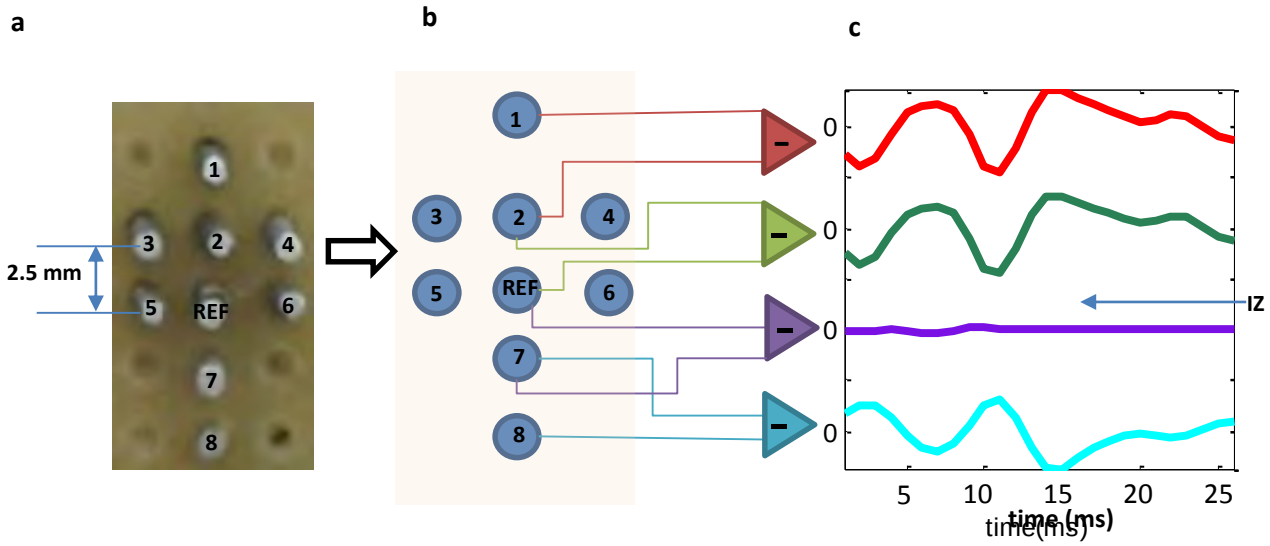

Figure 3-3: Detection of the IZ of a participant: a) Photo of the electrode grid that was placed on the APB muscle, with the longitudinal electrodes parallel to the muscle fibre. The numbers in black on each electrode indicate the electrode numbers. b) Provides a visual representation for the extraction of raw EMG signals between adjacent electrodes. c) Illustrates a section of raw EMG signals obtained from the difference of adjacent electrodes. This was used in determining the location of IZ as explained in Section 2.3.1.

From Figure 3-3c, which shows the EMG_{RAW} signals, it can be observed that there was a polarity change between the bipolar channels '8'-'7' and 'REF'-'2'. Therefore, the IZ was determined to approximately be somewhere between these channels, as explained in Section 2.3.1. Subsequently, the EMG_{SELECT} for this participant was the pair furthest from the IZ (i.e., bipolar channel 2-1).

The electrode grid was smaller than the length of APB muscle. As a result, for 4 out the 15 participants, the IZ could not be detected post-processing. However, from Section 1.2.3.3 it can be observed that EMG signals further from the IZ have greater amplitudes. Thus, the EMG_{SELECT} for these participants were the EMG pairs with the highest amplitudes.

3.1.3.2 Electroencephalography channel selection (EEG_{SELECT})

Figure 3-4 illustrates the topographic view of the values, both pre- and post-fatigue, for the beta EEG-EMG coherence $_{PEAK\ AMP}$ and the beta EEG-EMG PLV $_{PEAK\ AMP}$.

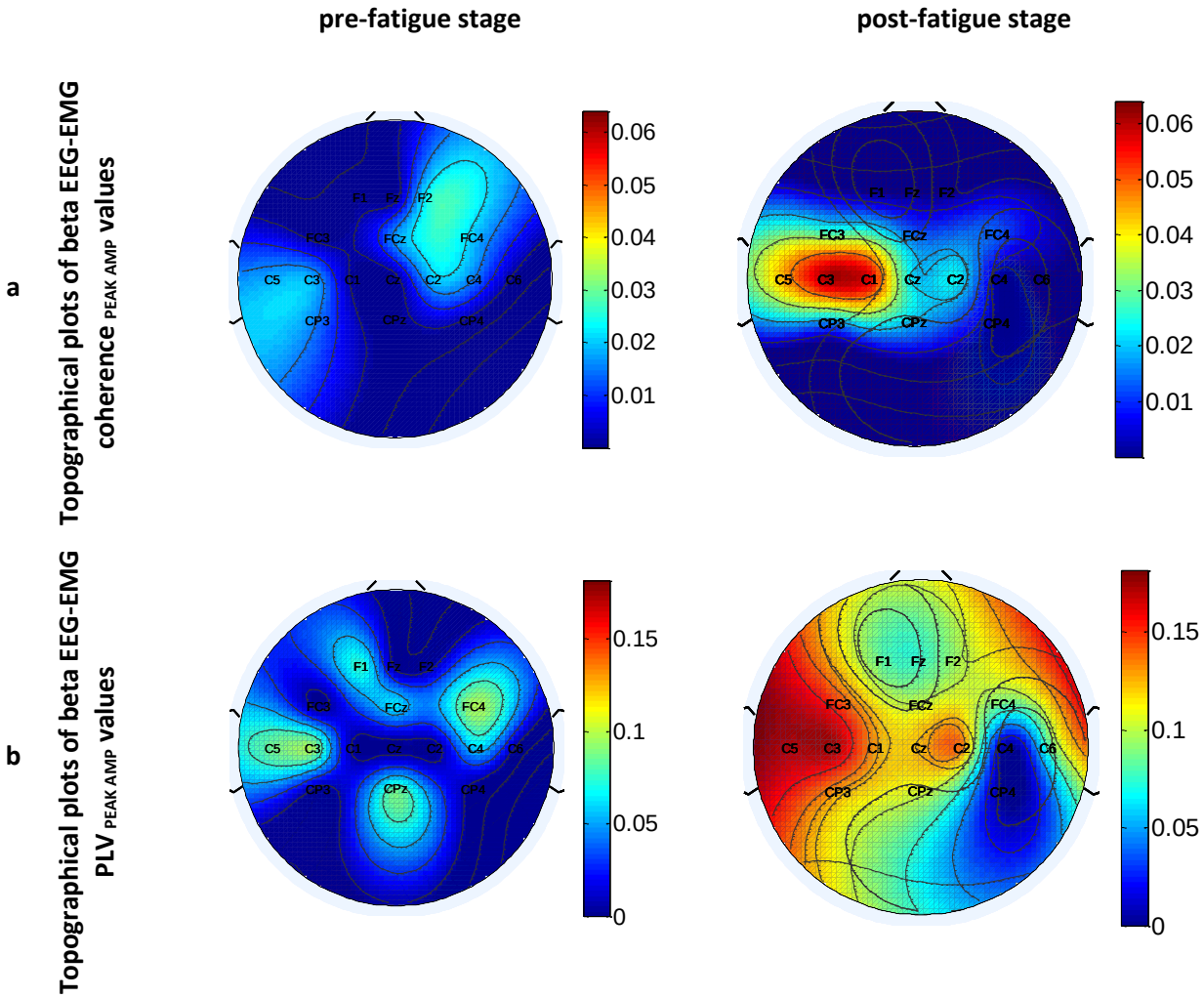

Figure 3-4: Topographical plots for (a) the beta EEG-EMG coherence $_{PEAK\ AMP}$ and (b)the beta EEG-EMG PLV $_{PEAK\ AMP}$ values pre-and post-fatigue during a sustained 10% of MVC isometric contraction of the APB muscle for a participant. Note that the view is of the top of the head, with a schematic of the nose identifying the anterior. The electrode labels are based on the international 10-10 system spacing.

From Figure 3-4, it can be observed that the EEG channels with the beta EEG-EMG PLV $_{PEAK\ AMP}$ and the beta EEG-EMG coherence $_{PEAK\ AMP}$ values were found in the contra-lateral (i.e., left side of the head) sensorimotor area post-fatigue.

Subsequently, the EEG_{SELECT} for the beta EEG-EMG $coherence_{PEAK\ AMP}$ analysis had the peak EEG-EMG coherence amplitude in the beta band (15–35 Hz) from C1, C3, C5, CP3 or FC3. The EEG_{SELECT} for the beta EEG-EMG $PLV_{PEAK\ AMP}$ analysis had the peak EEG-EMG PLV amplitude in the beta band (15–35 Hz) from C1, C3, C5, CP3 or FC3 (refer to Figure 2-9).

3.1.3.3 Corticomuscular coupling waveforms pre- and post-fatigue

Figure 3-5 illustrates the EEG-EMG coherence and the EEG-EMG PLV, pre- and post-fatigue.

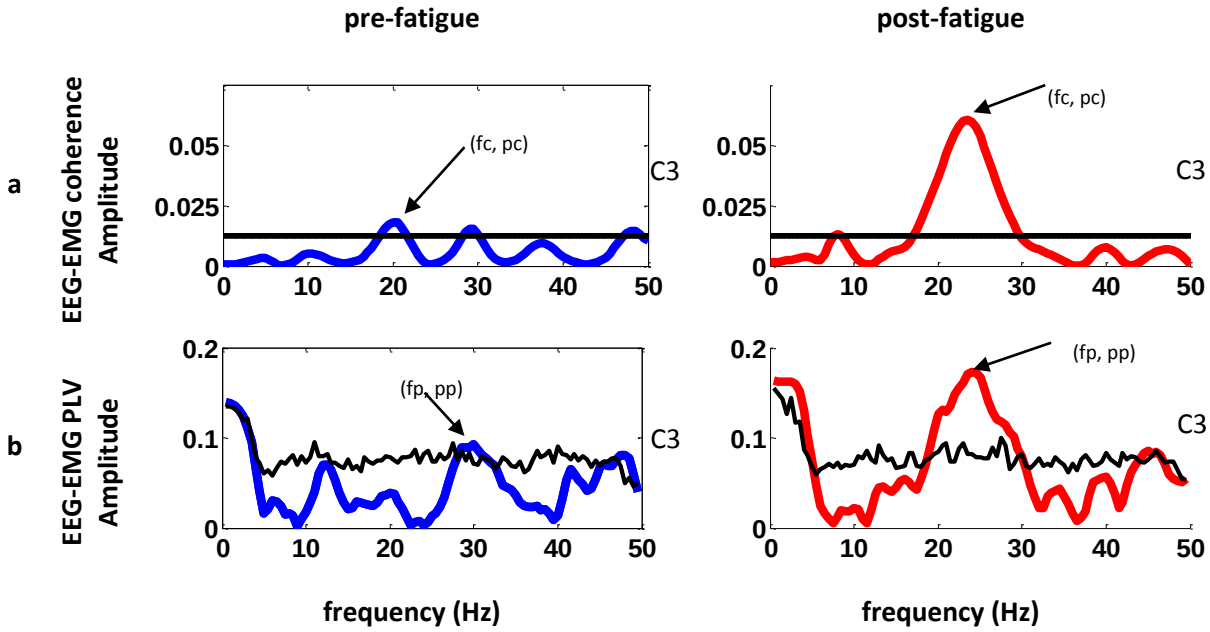

Figure 3-5: Pre- and post-fatigue comparisons of (a) EEG-EMG coherence and (b) EEG-EMG PLV while performing a sustained isometric contraction at 10% of MVC where pp = beta EEG-EMG $PLV_{PEAK\ AMP}$, pc = beta EEG-EMG $coherence_{PEAK\ AMP}$, fc = beta EEG-EMG $coherence_{PEAK\ FREQ}$ and fp = beta EEG-EMG $PLV_{PEAK\ FREQ}$. The estimated PLS and CL for the EEG-EMG PLV and the EEG-EMG coherence, respectively, is shown by the black lines within their respective graph. The EEG electrode used to determine the waveforms is displayed on the right side of each graph, and the corresponding EMG electrode was selected according to the procedure discussed in Section 3.1.3.1.

From Figure 3-5, the EEG-EMG coherence and EEG-EMG PLV waveforms have a greater peak post-fatigue as compared to pre-fatigue. For both stages (pre- and post-fatigue), the peaks were constrained to the beta band for the EEG-EMG coherence and the EEG-EMG PLV. (See Appendix H3 for the EEG-EMG coherence and EEG-EMG PLV waveforms for all 15 participants).

3.1.3.4 Transition to fatigue

Figure 3-6 illustrates the EMG_{POWER}, EMG_{MDF}, 1D spectro, beta EMG_{RMS} (mV), beta EEG_{RMS} (mV), EEG-EMG coherence and EEG-EMG PLV of a typical participant during the fatigue stage, which was calculated by sliding a 30-second window along the signal in 1-second increments.

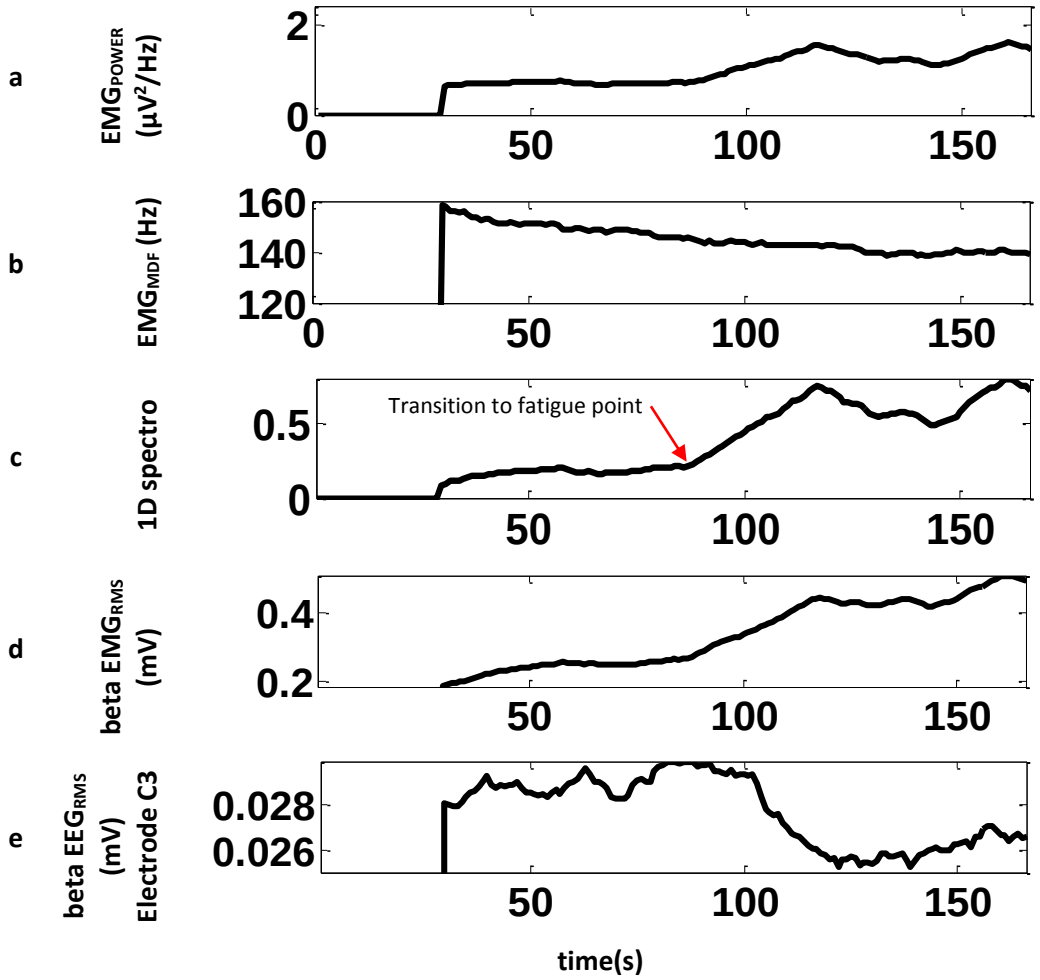

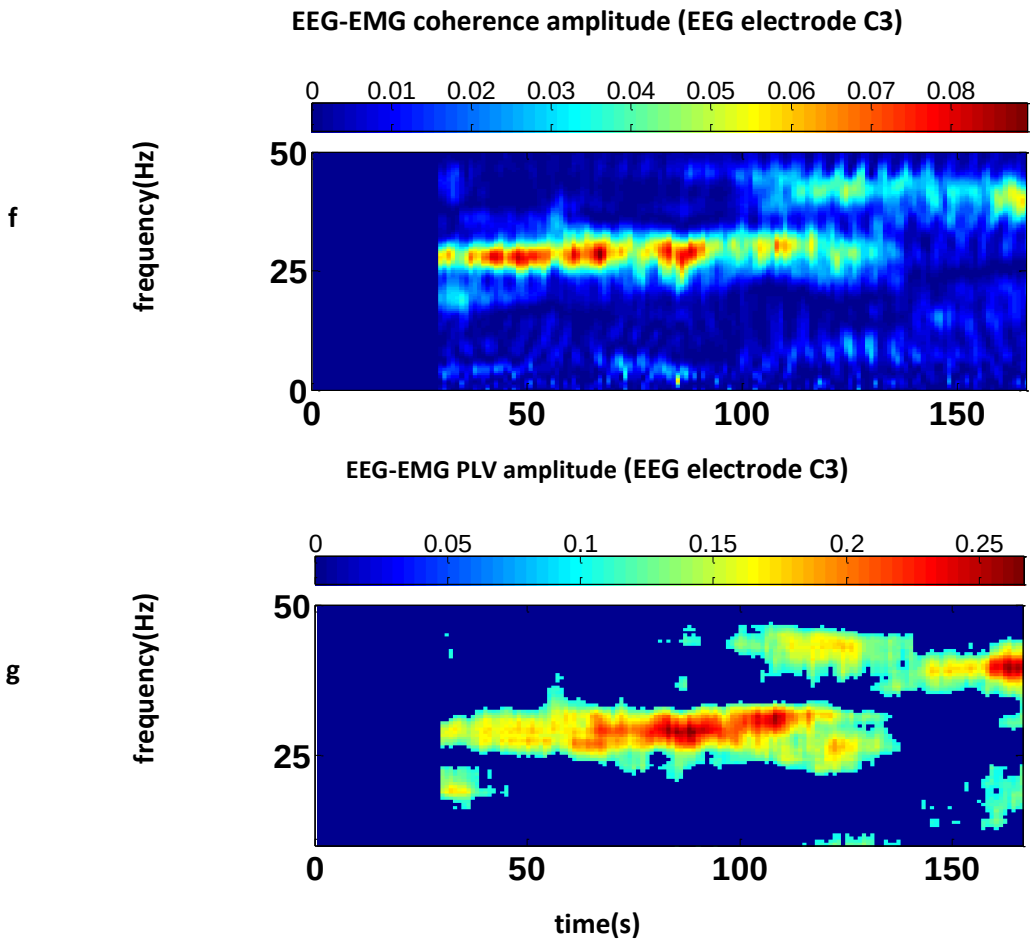

Figure 3-6: The a) EMG_{POWER}, b) EMG_{MDF}, c) 1D spectro, d) beta EMG_{RMS}, e) beta EEG_{RMS}, f) EEG-EMG coherence and g) EEG-EMG PLV of a typical participant during the fatigue stage was calculated by sliding a 30-second window along the signal in 1-second increments. The coloured bar above graph f and g represents the EEG-EMG coherence amplitudes and the EEG-EMG PLV amplitudes respectively. Graph c denotes the transition to the fatigue time point at approximately 90 seconds.

Figure 3-6a and Figure 3-6d observed that the EMG_{POWER} and beta EMG_{RMS} were initially constant, then gradually increased after the transition to fatigue point and then levelled off toward the end of the fatigue stage.

Figure 3-6b shows that the EMG_{MDF} gradually decreased and then levelled off as EMG_{POWER} levelled off toward the end of the fatigue stage.

In Figure 3-6c, it can be observed that the 1D spectro was initially constant, then gradually increased when the EMG_{POWER} increased, but finally slightly fluctuated toward the end of the fatigue stage. The transition to fatigue point was selected when the 1D spectro increased, which was approximately 90 seconds for this participant.

Figure 3-6e was mentioned in Section 3.1.2.

From Figure 3-6f and Figure 3-6g, greater peaks for both the EEG-EMG coherence and the EEG-EMG PLV in the beta band can be observed before the transition to fatigue. Gamma band peaks for both the EEG-EMG coherence and the EEG-EMG PLV occurred toward the end of the fatigue stage, but this was not the case for all participants. However, notably, the EEG-EMG coherence and EEG-EMG PLV seem to follow the same peak amplitude values, except after the transition to fatigue, in which case the EEG-EMG coherence drops, as EMG and EEG amplitudes vary.

3.1.3.5 Corticomuscular coupling waveforms for the first and second part of the fatigue stage

Figure 3-7 illustrates the EEG-EMG coherence and the EEG-EMG phase lock value (PLV) during the first and second part of the fatigue stage.

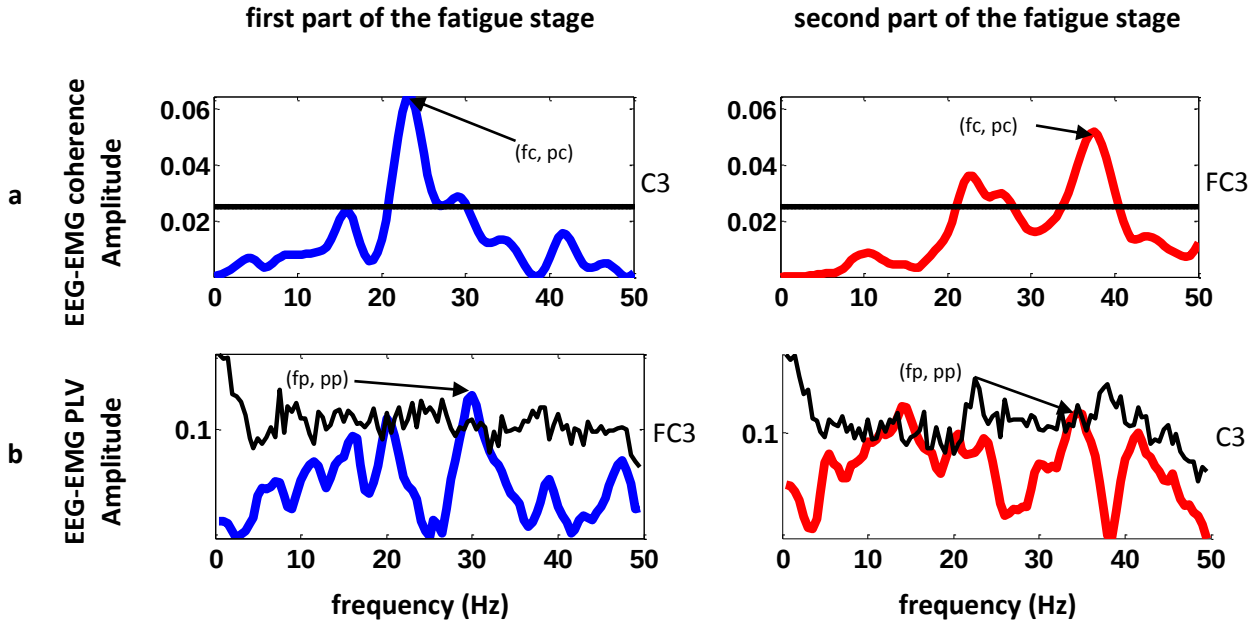

Figure 3-7: First part and the second part of the fatigue stage comparisons of (a) EEG-EMG coherence and (b) EEG-EMG PLV while performing a sustained isometric contraction at 30% of MVC where pp = beta $PLV_{PEAK\ AMP}$, pc = beta EEG-EMG $coherence_{PEAK\ \ AMP}$, fc = beta EEG-EMG $coherence_{PEAK\ FREQ}$ and fp = beta $PLV_{PEAK\ FREQ}$. The estimated PLS and CL for the EEG-EMG PLV and EEG-EMG coherence, respectively, is shown by the black lines within their respective graph. The EEG electrode used to determine the waveforms is displayed on the right side of each graph, and the corresponding EMG electrode was selected according to the procedure discussed in Section 3.1.3.1.

Figure 3-7a shows that the EEG-EMG coherence waveform had a greater peak during the first part of the fatigue stage compared to the second part of the fatigue stage.

In Figure 3-7b, it is observed that the EEG-EMG PLV waveform had a greater peak during the first compared to the second part of the fatigue stage. However, this varied between participants (see Appendix I3 for EEG-EMG PLV and EEG-EMG coherence waveforms for all 15 participants)

3.2 Quantitative results

Section 3.2 contains the results of the statistical comparisons of the neurophysiological variables, which were noted in Section 3.1. All data are represented as (means (M) ± standard deviation (SD)), and significance of a factor conforms to $p < 0.05$.

3.2.1 Muscle fatigue influence on force, EMG and EEG pre- and post-fatigue

Section 3.2.1 follows from Section 3.1.2 and provides the quantitative statistics as mentioned in Section 2.2.7 for all 15 participants in Table 3-1 (see Appendix J.1 for box plots and normality tests).

Table 3-1 : Group data for muscle fatigue influences on force, EMG and EEG measurements pre- and post-fatigue

Measurement	Comparison from pre-fatigue to post-fatigue.	pre-fatigue (Mean ± SD)	post-fatigue (Mean ± SD)	p value
$force_{CV}$	increased	3.473 ± 2.269 %	7.873 ± 5.568 %	p = 0.001
normalised beta $force_{PSD}$	increased	0.004 ± 0.001	0.005 ± 0.001	p = 0.014
normalised EMG_{RMS}	increased	0.037 ± 0.022	0.051 ± 0.033	p = 0.017
EMG_{MPF}	decreased	100.589 ± 17.366 Hz	86.948 ± 19.814 Hz	p = 0.001
normalised beta EEG_{RMS}	increased	0.043 ± 0.017	0.048 ± 0.021	p = 0.025

3.2.2 Corticomuscular coupling measures pre- and post-fatigue

Section 3.2.2 follows Section 3.1.3.3 and provides the quantitative statistics as mentioned in Section 2.3.6 for all 15 participants in Table 3-2 (see Appendix J.2 for box plots and normality tests).

Table 3-2: Group data for corticomuscular coupling measurements pre- and post-fatigue

Measurement	Comparison from pre-fatigue to post-fatigue.	pre-fatigue (M ± SD)	post-fatigue (M ± SD)	p value
beta EEG-EMG $coherence_{PEAK\ AMP}$	increased	0.023 ± 0.007	0.034 ± 0.017	p = 0.008
beta EEG-EMG $coherence_{PEAK\ FREQ}$	no change	26.967± 6.399	24.33 ± 7.459 Hz	p = 0.195
beta EEG-EMG $PLV_{PEAK\ AMP}$	increased	0.102 ± 0.014	0.125 ± 0.029	p = 0.011
beta EEG-EMG $PLV_{PEAK\ FREQ}$	no change	23.967± 5.835 Hz	24.8 ± 5.64 Hz	p = 0.686

3.2.3 Measures during the first and second part of the fatigue stage

Section 3.2.3 follows from Section 3.1.3.4 and provides the quantitative statistics, as mentioned in Section 2.3.7, for all 15 participants in Table 3-3 (see Appendix J.3 for box plots and normality tests).

Table 3-3: Group data for measurements during the first and second part of the fatigue stage

Measurement	Comparison from first to second part of the fatigue stage	first part of the fatigue stage (Mean ± SD)	second part of the fatigue stage (Mean ± SD)	p value
normalised beta EMG_{RMS}	increased	0.096 ± 0.081	0.122 ± 0.081	p = 0.004
normalised beta EEG_{RMS}	no change	0.089 ± 0.061	0.095 ± 0.055	p = 0.135
beta EEG-EMG coherence $_{PEAK\ AMP}$	decreased	0.059 ± 0.016	0.042 ± 0.017	p = 0.001
beta EEG-EMG $PLV_{PEAK\ AMP}$	no change	0.16 ± 0.04	0.154 ± 0.039	p = 1.000

3.3 Summary of results presented

Table 3-4 and Table 3-5 presents a summary of results shown in Section 3.

Table 3-4: Summary of results presented for the present study compared to previous studies for pre- and post-fatigue.

Measurement	Comparisons between pre- and post-fatigue		p value
	Present Study	Previous Literature	Present Study
$force_{CV}$	increased	Increased (Ushiyama et al., 2011)	p = 0.001
Normalised beta $force_{PSD}$	increased	Increased (Ushiyama et al., 2011)	p = 0.014
Normalised EMG_{RMS}	increased	Increased (Esposito et al., 1998; Tecchio et al., 2006; Yang et al., 2009; Ushiyama et al., 2011)	p = 0.017
EMG_{MPF}	decreased	Decreased (Esposito et al., 1998; Georgakis et al., 2003; Barandun et al., 2009; Ushiyama et al., 2011)	p = 0.001
Normalised beta EEG_{RMS}	increased	Increased (Abdul-latif et al., 2004; Tecchio et al, 2006)	p = 0.025
Beta EEG-EMG $coherence_{PEAK\ AMP}$	increased	Contradictory (Tecchio et al., 2006; Yang et al., 2009, 2010; Ushiyama et al., 2011)	p = 0.008
Beta EEG-EMG $coherence_{PEAK\ FREQ}$	no change	Does not significantly differ (Tecchio et al., 2006; Yang et al.,2009, 2010; Ushiyama et al., 2011)	p = 0.195
Beta EEG-EMG $PLV_{PEAK\ AMP}$	increased	Unknown	p = 0.011
Beta EEG-EMG $coherence_{PEAK\ FREQ}$	no change	Unknown	p = 0.686

Table 3-5: Summary of results presented for the present study compared to previous studies for the first part compared to the second part of the fatigue stage.

Measurement	Comparisons between the first and the second part of the fatigue stage		p value
	Present Study	Previous Literature	Present Study
Normalised beta EMG_{RMS}	increased	Increase (Al-Mulla & Sepulveda, 2010)	p = 0.004
Normalised beta EEG_{RMS}	no change	Unknown	p = 0.135
Beta EEG-EMG coherence $_{PEAK\ AMP}$	decreased	Contradictory (Ushiyama et al., 2011; Yang et al., 2009, 2010)	p = 0.001
Beta EEG-EMG $PLV_{PEAK\ AMP}$	no change	Unknown	p = 1.000

[This page is intentionally left blank]

4. DISCUSSION

The main finding for the present study is the significant increase in the beta EEG-EMG $PLV_{PEAK\ AMP}$ and the beta EEG-EMG $coherence_{PEAK\ AMP}$ for the APB muscle and sensorimotor cortex from pre-fatigue to post-fatigue. However, during the fatigue stage, it was observed that the EEG-EMG $coherence_{PEAK\ AMP}$ significantly decreased for the second part of the fatigue stage, whilst the PLV did not.

Since both the beta EEG-EMG $PLV_{PEAK\ AMP}$ and the beta EEG-EMG $coherence_{PEAK\ AMP}$ increased, it could be argued that the change in amplitude from the EMG and/or the EEG, due to fatigue, does not confound the corticomuscular coupling result in pre- and post-fatigue; thus, the EEG-EMG coherence findings appear directly related to the genuine phase synchronisation changes. However, for both the first and second part of the during fatigue stage the beta EEG-EMG $PLV_{PEAK\ AMP}$ and the beta EEG-EMG $coherence_{PEAK\ AMP}$ provided different results, suggesting that during the fatigue stage EEG and EMG amplitude co-variations confound the corticomuscular coupling results. The amplitude co-variations are further supported by the significant increase in EMG amplitude from the first to second part of the fatigue stage.

We further discuss the influence of muscle fatigue on the force, EMG and EEG in Section 4.1, while Section 4.2 discusses the influence that muscle fatigue had on corticomuscular coupling. Section 4.3 explores other possible factors, which could influence corticomuscular coupling during muscle fatigue.

4.1 Muscle fatigue influence on force, EMG and EEG

The $force_{CV}$ increased significantly from pre-fatigue to post-fatigue, which indicated attenuated muscle force steadiness post-fatigue. In addition, the normalised beta $force_{PSD}$ significantly increased post-fatigue as compared to pre-fatigue. This was also shown by Ushiyama et al. (2011), who suggested that an increase in normalised beta $force_{PSD}$ is the sensorimotor cortex's attempt to maintain a stable force by discharging EMG into the beta band. This subsequently gets mimicked in the beta component force driven by the muscle.

In addition, the normalised EMG_{RMS} increased significantly from pre-fatigue to post-fatigue, which was also shown in previous studies (Esposito et al., 1998; Ushiyama et al., 2011). This suggests that the muscle attempts to maintain a stable force by recruiting additional motor units and/or increasing the motor unit firing frequency.

The EMG_{MPF} significantly decreased from pre-fatigue to post-fatigue. This decrease was also observed in a fatigue study done by Barandun et al. (2009) involving the APB muscle, as well as in other studies for different muscles including biceps brachii, vastus medialis, vastus lateralis, rectus femoris and tibilias anterior (Esposito et al., 1998; Georgakis et al., 2003; Ushiyama et al., 2011). A decrease in the EMG_{MPF} suggests an attenuation of the conduction velocity of the action potentials, changes of the motor unit action potential shape and/or the firing rate of motor units (Eberstein & Beattie, 1985; Moritani et al., 1986; Arendt-Nielsen et al., 1989; Merletti & Lo Conte, 1997), suggesting muscle fatigue.

The normalised beta EEG_{RMS} significantly increased from pre-fatigue to post-fatigue in the contra-lateral sensorimotor cortex. This was observed in a previous fatigue study, and it was suggested that an increase in energy was needed by the contra-lateral sensorimotor cortex in order to maintain a stable force (Abdul-latif et al., 2004).

It was also noted that during the fatigue stage (Table 3-5) the beta EEG_{RMS} decreased (i.e., in the contra-lateral sensorimotor region). This decrease in the EEG beta power toward the end of the fatigue stage was also observed in Yang et al. (2010) during a fatigue stage of a finger muscle (flexor digitorum superficialis). Engel and Fries (2010) have suggested that the EEG within the beta band expresses more strongly if 'status quo' is intended (i.e., remain in its current state [in this study, palmar abduct was at 30% of MVC]). Thus, a decrease in EEG power in the beta band could suggest the inability to remain in one state or the need to change state in order to avoid damage to the muscle.

These specific findings are not novel, but match the reported influence of muscle fatigue on force, EMG and EEG from previous studies. Therefore, they provide validation that the experimental protocol in this study is in accordance to previous literature.

4.2 Corticomuscular coupling measures

The present study showed that both the beta EEG-EMG $coherence_{PEAK\ AMP}$ and the beta $PLV_{PEAK\ AMP}$ increased significantly from pre-fatigue to post-fatigue. This result is similar to the findings published by Tecchio et al. (2006) and Ushiyama et al. (2011). However, the other possibility is that during the actual fatigue stage, a different phenomenon could be observed for the corticomuscular coupling (similar to Yang et al., 2009, and Yang et al., 2010) as opposed to pre- and post- fatigue stages. It was found that the beta EEG-EMG $coherence_{PEAK\ AMP}$ decreased, while the beta EEG-EMG $PLV_{PEAK\ AMP}$ did not significantly change from the first to the second

part of the fatigue stage. The normalised beta EMG_{RMS} significantly increased, whilst the normalised beta EEG_{RMS} did not significantly change from the first to the second part of the fatigue stage. Therefore confirming EMG amplitude confound on corticomuscular coupling during fatigue.

This decrease in the corticomuscular coupling using coherence during the fatigue stage matches the findings of Yang et al. (2009) and Yang et al. (2010). But based on the corresponding no-significant change in beta $PLV_{PEAK\ AMP}$, this suggests that the EEG-EMG coherence changes during the fatigue stage are due to amplitude coherence as opposed to phase synchrony and that pre- and post-fatigue changes are due to phase synchrony as opposed to amplitude coherence. Thus, if the phase relationship of corticomuscular coupling needs to be measured, PLV would be the preferred measure as opposed to coherence, particularly during a fatiguing stage.

Section 4.2.1 discusses corticomuscular coupling found within participants pre- and post-fatigue while Section 4.2.2 discusses the confounding effect of amplitude during the fatigue stage.

4.2.1 Corticomuscular coupling measures pre- and post-fatigue

From Appendix H1, it was observed that out of the 15 participants, four participants showed a beta EEG-EMG $coherence_{PEAK\ AMP}$ decrease post-fatigue as compared to pre-fatigue. The beta EEG-EMG $PLV_{PEAK\ AMP}$, shown in Appendix H2, agreed with the EEG-EMG coherence for three out of four participants, but did not agree for participant 2 (whose beta EEG-EMG $PLV_{PEAK\ AMP}$ increased post-fatigue, as compared to pre-fatigue, and whose beta EEG-EMG $coherence_{PEAK\ AMP}$ decreased post-fatigue, as compared to pre-fatigue).

Appendix H3 illustrates the waveforms for EEG-EMG coherence and EEG-EMG PLV. The waveforms during pre-fatigue for participant 2 showed two EEG-EMG coherence and EEG-EMG PLV peaks, one at 28 Hz and the other at 18 Hz. For the EEG-EMG coherence waveform, the EEG-EMG coherence peak, which was around 18 Hz, had a greater pre-fatigue EEG-EMG coherence peak, as compared to the post-fatigue EEG-EMG coherence peak. Conversely, at the same frequency (18 Hz) the EEG-EMG PLV waveform pre-fatigue showed an EEG-EMG PLV peak that was smaller than the post-fatigue EEG-EMG PLV peak. While PLV is only phase-dependent, coherence is both amplitude- and phase-dependent and would suggest that, during the pre-

fatigue stage there was an increase in amplitude coherence at 18 Hz between EMG and EEG, which ultimately increased the EEG-EMG coherence.

Therefore, even if the group data suggests that EEG-EMG coherence follows the phase relationship both pre- and post- fatigue, there are instances where amplitude coherence could play a role.

4.2.2 Corticomuscular coupling measures during fatigue

Furthermore, during the fatigue stage it was found that when the EMG amplitude increased compared to when the EMG amplitude had no change (see Figure 3-6a), the EEG-EMG coherence was smaller (see Figure 3-6f). However, notably, the EEG-EMG PLV (see Figure 3-6g) values remained constant (this effect of amplitude variation on coherence was simulated in Appendix A).

Ushiyama et al. (2011) reported progressive time course changes for a typical participant's EEG-EMG coherence (see Figure 4-1) and observed a similar change (i.e., when EMG amplitude increased compared to when EMG amplitude had no change, EEG-EMG coherence was smaller). The only difference between the present study (and possibly that of Yang et al., 2009) compared to Ushiyama et al.'s (2011) study was the transition to fatigue time at which the EMG amplitude increased. This time point can vary depending on the muscle selection, %MVC and synergistic muscles (mentioned in Section 4.3.1).

Thus, for a corticomuscular coupling study where EMG and/or EEG amplitude fluctuates and the phase coupling is required, PLV is the preferred method.

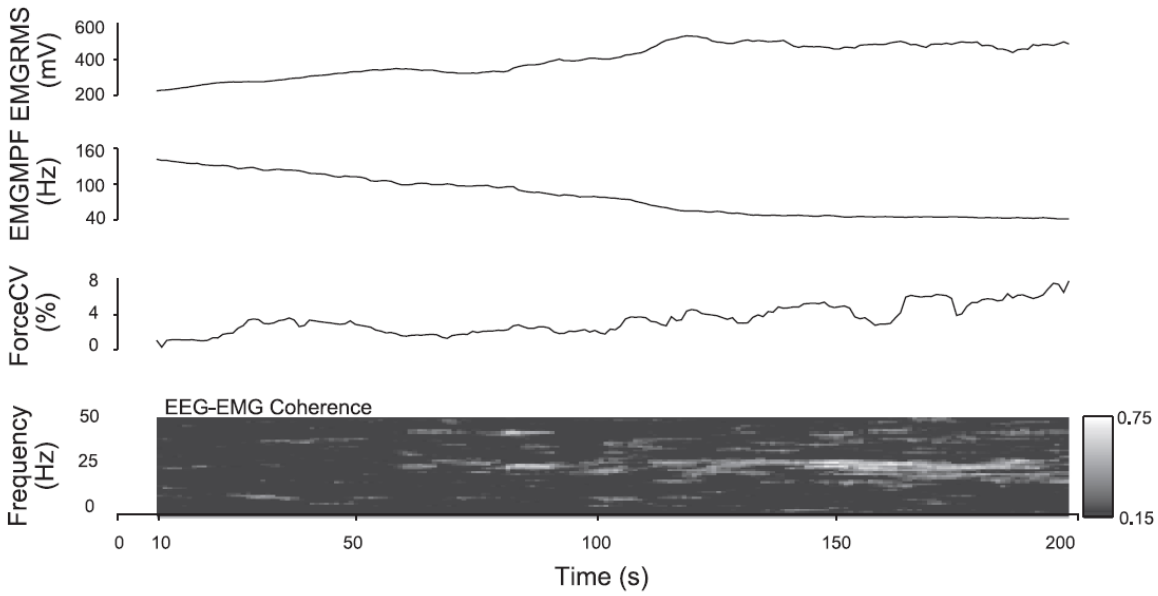

Figure 4-1: Adopted from Ushiyama et al. (2011) showing a 'typical example of progressive changes in EMG RMS, EMG MPF, Force CV, and EEG-EMG coherence during sustained isometric contraction of the tibialis anterior muscle at 50% of MVC until the limit of fatigue. EMG RMS, EMG MPF, Force CV, and EEG-EMG coherence was calculated by sliding the 10-second window along the signal in 1 second steps. As for the time-frequency map of EEG-EMG coherence, the monochrome bar represents the magnitude of EEG-EMG coherence.'

Significant gamma (35–50 Hz) corticomuscular coupling was also found within few participants during the fatigue stage. Gamma corticomuscular coupling has been observed in previous corticomuscular coupling fatigue studies (Tecchio et al., 2006 and Yang et al., 2009, 2010) and suggested to play a function role in regulating the motor performance during strong (Brown, 2000) and dynamic contractions (Omlor et al. ,2007). This may suggest that during the fatigue stage, dynamic and strong voluntary contractions may be required to sustain the required force.

4.3 Potential factors related to phase synchrony and/or fatigue

Various other factors other than the EEG and EMG amplitude can confound the corticomuscular coupling measures, which are explored further in Section 4.3.

4.3.1 Synergistic muscles

When performing a movement in which the major agonist muscle is unable to sustain the force, it is possible that the synergistic muscles increase activity in order to maintain the required force.

Yang et al. (2009) showed a significant decrease in the EEG-EMG coherence (for brachii bicep, brachioradialis and triceps brachii muscle) while performing an isometric elbow contraction. However, Ushiyama et al. (2011) argued based on the earlier findings of Kawakami et al. (1994) that several synergistic muscles contributed to the generation of elbow flexion force (biceps brachii, 34%; brachialis, 47%; and brachioradialis, 19%). Thus, in the study by Yang et al. (2009), it is possible that the sustained force was compensated by the synergistic muscles (Ushiyama et al., 2011) and in particular the brachialis whose EEG-EMG coherence was not measured by Yang et al (2009). In Ushiyama et al.'s (2011) study, the tibilias anterior accounted for approximately 60% of the PCSA (physiological cross-sectional area) of the total dorsiflexors and, therefore, was regarded by him as a major agonist muscle for dorsiflexion.

The APB muscle was chosen for our study, as it was found to be most active during a palmar abduction (van Oudenaarde & Oostendorp, 1995). However, the position of the forearm and hand was not considered for our study. Brandsma et al. (1996) observed that during a palmar abduction, when the forearm is supinated and the hand is in the neutral position, the APB muscle has smaller mean EMG activity compared to the superficial and deep abductor pollicis longus. In this present study, during palmar abduction, the forearm and hand were kept in a neutral position. As a result, the confounding effect of synergistic muscles, such as the superficial and deep abductor pollicis longus could still have had an influence in this study. In this study, the APB EEG-EMG coherence increased post-fatigue as compared to pre-fatigue but the EEG-EMG coherence of the synergistic muscles was not tested. Therefore there is still some uncertainty about the EEG-EMG coherence for the synergists and antagonists before and after the fatigue stage. And is a possible limitation in our study.

4.3.2 Muscles of different fibre composition and function

Since all five experiments (Tecchio et al., 2006; Yang et al., 2009, 2010; Ushiyama et al., 2011; and this study) used different muscles, it is possible that there are different muscle-specific processes, in which case the individual findings may not be generalisable. Furthermore, in corticomuscular coupling studies, ideally the EMG and corticomuscular coupling of all synergists and antagonists should be monitored in addition to that of the main agonist.

One such muscle-specific process possibly suggested by studies, was that in order to sustain a force, an increase or decrease in motor neuron firing plays a more prominent role in the APB and tibialis anterior, while an increase or decrease in the number of motor units plays a more prominent role within the biceps brachii (Kukulka & Clamann, 1981; Seki & Narusawa, 1996; Van Cutsem et al., 1998).

This could imply that the sensorimotor cortex would have to enhance the corticomuscular coupling to the APB muscle and tibialis anterior when compared to the biceps brachii in order to maintain a higher rate of discharge of motor units to sustain the force. Thus, this muscle-specific process could also be the reason for the difference between Ushiyama et al.'s (2011) study using the tibialis anterior muscle and the present study using APB muscle to Yang et al.'s (2009) study using the biceps brachii. In this case, the apparent contradictory corticomuscular coupling results of Yang et al. (2009) may still be valid, but differences may be the result of muscle-specificity.

4.3.3 Influence of EMG electrode placement on corticomuscular coupling measures

The present study has observed that the pre- and post-fatigue result for both the EEG-EMG coherence and the PLV may vary if the IZ is not determined (see Appendix J). Mesin et al. (2009) revealed that placing electrodes without identifying the IZ can cause variations in the amplitude and frequency of the EMG signal. Also, Barandun et al. (2009) observed that when the electrode location was further away from the IZ the mean frequency was lower. This could also explain the varying changes found in the corticomuscular coupling in previous studies, because the IZ was not considered (Ushiyama et al., 2011 ;Yang et al., 2009, 2010). Hence, the IZ should be taken into account for corticomuscular coupling measures.

4.3.4 Isometric and dynamic contractions observed different forms of fatigue

Another notable difference is that the four experiments (Tecchio et al., 2006; Yang et al., 2009; Ushiyama et al., 2011 and this study) performed isometric contractions, while the fifth, Yang et al. (2010) performed dynamic contractions.

Central fatigue forms a larger proportion of attenuated force generation when muscle fatigue is induced by an isometric contraction compared to repetitive MVC dynamic contractions (Søgaard et al., 2006). Therefore, another possible reason for the contradictory results during the fatigue stage could be due to different proportions of induced central fatigue as suggested by Ushiyama et al. (2011).

[This page is intentionally left blank]

5. CONCLUSIONS

This study provides evidence that after muscle fatigue occurs during a sustained isometric submaximal contraction, the corticomuscular coupling in the beta band between the contra-lateral sensorimotor cortex and APB muscle increases significantly, without the confounding effect of amplitude. This suggests that the amplitude changes in the EEG of the sensorimotor cortex and in the EMG of the APB muscle do not affect the conclusions regarding the central nervous system monitoring, either pre- or post-fatigue. This implies an increase in the central nervous system monitoring of muscle activity, post-fatigue. However, during an actual fatiguing contraction, coherence and PLV measures of corticomuscular coupling provide different results, because of the confounding effect of amplitude on the corticomuscular coupling. In such experiments, PLV provides a more reliable measure, resulting in a physiological conclusion that there is no change in corticomuscular phase coupling during a fatiguing contraction.

Whilst the present study is consistent with the confounded findings of Ushiyama et al. (2011) and possibly Yang et al. (2009) for the tibialis anterior muscle and bicep brachii muscle respectively, it is important to note that muscle-specific effects have not been experimentally accounted for. Therefore, these findings are not necessarily generalisable to all muscles without additional experimental and analytical studies.

5.1 Further research

Section 5.1 provides further research to be done.

5.1.1 PLV on larger muscles pre- and post-fatigue

The present study showed that the confounding effect of amplitude between the contracting muscle and sensorimotor cortex does not significantly alter the conclusions regarding the central nervous system monitoring of muscular fatigue in the APB muscle.

However the APB muscle is small muscle required to do only small movements, thus suggesting that amplitude co-variations would be small. However larger muscles could provide higher amplitude co-variations, therefore PLV may still be a useful measure pre- and post-fatigue in larger muscles.

5.1.2 Observation synergist and antagonist muscles during muscle fatigue

As mention in Section 4.3, Yang et al.'s (2009) study observed a decrease in the EEG-EMG coherence from pre- to post-fatigue whereas this study and Ushiyama et al. (2011) study observed an increase. The reason for the difference in the findings as suggested by Ushiyama et al. (2011) was that the main agonist muscle was not observed in Yang et al.'s (2009) study.

Thus, a study measuring the corticomuscular coupling between all synergist and antagonist muscles in addition to the agonist, during muscle fatigue would prove valuable. This would provide a further physiological understanding of how corticomuscular coupling maintains a stable force output.

5.1.3 High–resolution EMG studies during corticomuscular coupling

In the present study, it was shown that the identification of the IZ can change the outcome of corticomuscular coupling measures using coherence or PLV (see Section 4.3.4). Therefore, the method of measuring high-resolution EMG would allow for the identification of IZs and possibly remove any contradictory results.

[This page is intentionally left blank]

6. REFERENCES

Abdul-latif, A. A., Cosic, I., Kumar, D. K., Polus, B., & Da Costa, C. (2004). Power changes of EEG signals associated with muscle fatigue: the root mean square analysis of EEG bands. In Proceedings of the 2004 Intelligent Sensors, Sensor Networks and Information Processing Conference (pp. 531–534). doi:10.1109/ISSNIP.2004.1417517

Al-Mulla, M. R., & Sepulveda, F. (2010). A novel feature assisting in the prediction of sEMG muscle fatigue towards a wearable autonomous system. In 2010 IEEE 16th International Mixed-Signals, Sensors and Systems Test Workshop (IMS3TW) (pp. 1–6). doi:10.1109/IMS3TW.2010.5503001

Al-Mulla, M. R., Sepulveda, F., & Colley, M. (2011). A review of non-invasive techniques to detect and predict localised muscle fatigue. Sensors (Basel, Switzerland), 11(4), 3545–3594. doi:10.3390/s110403545

Baker, S. N. (2007). Oscillatory interactions between sensorimotor cortex and the periphery. Current Opinion in Neurobiology, 17(6), 649–655. doi:10.1016/j.conb.2008.01.007

Barandun, M., von Tscharner, V., Meuli-Simmen, C., Bowen, V., & Valderrabano, V. (2009). Frequency and conduction velocity analysis of the abductor pollicis brevis muscle during early fatigue. Journal of Electromyography and Kinesiology, 19(1), 65–74. doi:10.1016/j.jelekin.2007.07.003

Bigland-Ritchie, B., & Woods, J. J. (1984). Changes in muscle contractile properties and neural control during human muscular fatigue. Muscle & nerve, 7(9), 691-699.

Brandsma, J. W., van Oudenaarde, E., & Oostendorp, R. (1996). The abductores pollicis muscles: Clinical considerations based on electromyographical and anatomical studies. Journal of Hand Therapy, 9(3), 218–222. doi:10.1016/S0894-1130(96)80085-8

Brown, P. (2000). Cortical drives to human muscle: The piper and related rhythms. Progress in Neurobiology, 60(1), 97–108. doi:10.1016/S0301-0082(99)00029-5

Dedrick, G. S., Sizer, P. S., Merkle, J. N., Hounshell, T. R., Robert-McComb, J. J., Sawyer, S. F., … Roger James, C. (2008). Effect of sex hormones on neuromuscular control patterns during landing. Journal of Electromyography and Kinesiology, 18(1), 68–78. doi:10.1016/j.jelekin.2006.09.004

De Luca, C. (1983). Myoelectrical manifestations of localized muscular fatigue in humans. Critical Reviews in Biomedical Engineering, 11(4), 251–279.

Delorme, A., & Makeig, S. (2004). EEGLAB: An open source toolbox for analysis of single-trial EEG dynamics including independent component analysis. Journal of Neuroscience Methods, 134(1), 9–21. doi:10.1016/j.jneumeth.2003.10.009

Dimitrova, N. A., & Dimitrov, G. V. (2003). Interpretation of EMG changes with fatigue: Facts, pitfalls, and fallacies. Journal of Electromyography and Kinesiology, 13(1), 13–36. doi:10.1016/S1050-6411(02)00083-4

Divekar, N. V., & John, L. R. (2012). Neurophysiological, behavioural and perceptual differences between wrist flexion and extension related to sensorimotor monitoring as shown by corticomuscular coherence. Clinical Neurophysiology, (0). Available at: http://www.sciencedirect.com/science/article/pii/S1388245712005494 [Accessed September 7, 2012].

Eberstein, A., & Beattie, B. (1985). Simultaneous measurement of muscle conduction velocity and EMG power spectrum changes during fatigue. Muscle & Nerve, 8(9), 768–773. doi:10.1002/mus.880080905

Edwards, R. H. (1981). Human muscle function and fatigue. Ciba Foundation Symposium, 82, 1–18.

Engel, A. K., & Fries, P. (2010). Beta-band oscillations. Signalling the status quo? Current Opinion in Neurobiology, 20(2), 156–165. doi:10.1016/j.conb.2010.02.015

Enoka, R. M., & Duchateau, J. (2008). Muscle fatigue: What, why and how it influences muscle function. The Journal of Physiology, 586(1), 11–23. doi:10.1113/jphysiol.2007.139477

Esposito, F., Orizio, C., & Veicsteinas, A. (1998). Electromyogram and mechanomyogram changes in fresh and fatigued muscle during sustained contraction in men. European Journal of Applied Physiology and Occupational Physiology, 78(6), 494–501. doi:10.1007/s004210050451

Gandevia, S. C. (2001). Spinal and supraspinal factors in human muscle fatigue. Physiological Reviews, 81(4), 1725–1789.

Georgakis, A., Stergioulas, L. K., & Giakas, G. (2003). Fatigue analysis of the surface EMG signal in isometric constant force contractions using the averaged instantaneous frequency. IEEE Transactions on Biomedical Engineering, 50(2), 262–265. doi:10.1109/TBME.2002.807641

Gerdle, B., Karlsson, S., Day, S., & Djupsjöbacka, M. (1999). Acquisition, Processing and Analysis of the Surface Electromyogram. In P. D. U. Windhorst & P. D. H. Johansson (Eds.), Modern Techniques in Neuroscience Research (pp. 705–755). Springer Berlin Heidelberg. Retrieved from http://link.springer.com/chapter/10.1007/978-3-642-58552-4_26

Gupta, D., & James, C. J. (2007). Narrowband vs. broadband phase synchronization analysis applied to independent components of ictal and interictal EEG. In Proceedings of the. Annual International Conference of the IEEE Engineering in Medicine and Biology Society, pp. 3864–3867. doi:10.1109/IEMBS.2007.4353176

Gwin, J. T., & Ferris, D. P. (2012). Beta- and gamma-range human lower limb corticomuscular coherence. Frontiers in Human Neuroscience, 6, 258. doi:10.3389/fnhum.2012.00258

Halaki, M., & Gi, K. (2012). Normalization of EMG Signals: To Normalize or Not to Normalize and What to Normalize to? In G. R. Naik (Ed.), Computational Intelligence in Electromyography Analysis - A Perspective on Current Applications and Future Challenges. InTech. Retrieved from http://www.intechopen.com/books/computational-intelligence-in-electromyography-analysis-a-perspective-on-current-applications-and-

future-challenges/normalization-of-emg-signals-to-normalize-or-not-to-normalize-and-what-to-normalize-to-

Halliday, D. M., & Farmer, S. F. (2010). On the need for rectification of surface EMG. Journal of Neurophysiology, 103(6), 3547–3547. doi:10.1152/jn.00222.2010

Kattla, S., & Lowery, M. M. (2010). Fatigue related changes in electromyographic coherence between synergistic hand muscles. Experimental Brain Research. Experimentelle Hirnforschung. Expérimentation Cérébrale, 202(1), 89–99. doi:10.1007/s00221-009-2110-0

Kawakami, Y., Nakazawa, K., Fujimoto, T., Nozaki, D., Miyashita, M., &, T. (1994). Specific tension of elbow flexor and extensor muscles based on magnetic resonance imaging. European Journal of Applied Physiology and Occupational Physiology, 68(2), 139–147.

Kayser, J. (2001) Current source density (CSD) interpolation using spherical splines. Retrieved from http://psychophysiology.cpmc.columbia.edu/Software/CSDtoolbox

Keenan, K. G., Collins, J. D., Massey, W. V., Walters, T. J., & Gruszka, H. D. (2011). Coherence between surface electromyograms is influenced by electrode placement in hand muscles. Journal of Neuroscience Methods, 195(1), 10–14. doi:10.1016/j.jneumeth.2010.10.018

Keenan, K. G., Massey, W. V., Walters, T. J., & Collins, J. D. (2012). Sensitivity of EMG-EMG coherence to detect the common oscillatory drive to hand muscles in young and older adults. Journal of Neurophysiology, 107(10), 2866–2875. doi:10.1152/jn.01011.2011

Kukulka, C. G., & Clamann, H. P. (1981). Comparison of the recruitment and discharge properties of motor units in human brachial biceps and adductor pollicis during isometric contractions. Brain Research, 219(1), 45–55. doi:10.1016/0006-8993(81)90266-3

Lachaux, J. P., Rodriguez, E., Martinerie, J., & Varela, F. J. (1999). Measuring phase synchrony in brain signals. Human Brain Mapping, 8(4), 194–208.

Le Van Quyen, M., Foucher, J., Lachaux, J.-P., Rodriguez, E., Lutz, A., Martinerie, J., & Varela, F. J. (2001). Comparison of Hilbert transform and wavelet methods for the analysis of neuronal synchrony. Journal of Neuroscience Methods, 111(2), 83–98. doi:10.1016/S0165-0270(01)00372-7

Liu, J. Z., Shan, Z. Y., Zhang, L. D., Sahgal, V., Brown, R. W., & Yue, G. H. (2003). Human Brain Activation During Sustained and Intermittent Submaximal Fatigue Muscle Contractions: An fMRI Study. Journal of Neurophysiology, 90(1), 300–312. doi:10.1152/jn.00821.2002

Löscher, W. N., & Nordlund, M. M. (2002). Central fatigue and motor cortical excitability during repeated shortening and lengthening actions. Muscle & Nerve, 25(6), 864–872. doi:10.1002/mus.10124

Masuda, K., Masuda, T., Sadoyama, T., Mitsuharu Inaki, & Katsuta, S. (1999). Changes in surface EMG parameters during static and dynamic fatiguing contractions. Journal of Electromyography and Kinesiology, 9(1), 39–46. doi:10.1016/S1050-6411(98)00021-2

Merletti, R., Sabbahi, M., & De Luca, C. (1984). Median frequency of the myoelectric signal. European Journal of Applied Physiology and Occupational Physiology, 52(3), 258–265.

Merletti, R., & Lo Conte, L. R. (1997). Surface EMG signal processing during isometric contractions. Journal of Electromyography and Kinesiology: Official Journal of the International Society of Electrophysiological Kinesiology, 7(4), 241–250.

Mesin, L., Merletti, R., & Rainoldi, A. (2009). Surface EMG: The issue of electrode location. Journal of Electromyography and Kinesiology, 19(5), 719–726. doi:10.1016/j.jelekin.2008.07.006

Moritani, T., Muro, M., & Nagata, A. (1986). Intramuscular and surface electromyogram changes during muscle fatigue. Journal of Applied Physiology, 60(4), 1179–1185.

Motulsky, M. D. H. (1995). Intuitive biostatistics (1st ed.). New York, NY: Oxford University Press.

Nawab, S. H., Chang, S.-S., & De Luca, C. J. (2010). High-yield decomposition of surface EMG signals. Clinical Neurophysiology, 121(10), 1602–1615. doi:10.1016/j.clinph.2009.11.092

Noakes, T. D., & St Clair Gibson, A. (2004). Logical limitations to the “catastrophe” models of fatigue during exercise in humans. British Journal of Sports Medicine, 38(5), 648–649. doi:10.1136/bjsm.2003.009761

Noakes, T., St Clair Gibson, A., & Lambert, E. (2005). From catastrophe to complexity: A novel model of integrative central neural regulation of effort and fatigue during exercise in humans: Summary and conclusions. British Journal of Sports Medicine, 39(2), 120–124. doi:10.1136/bjsm.2003.010330

Omlor, W., Patino, L., Hepp-Reymond, M.-C., & Kristeva, R. (2007). Gamma-range corticomuscular coherence during dynamic force output. NeuroImage, 34(3), 1191–1198. doi:10.1016/j.neuroimage.2006.10.018

Phillips, C. G., & Porter, R. (1964). The pyramidal projection to motoneurones of some muscle groups of the baboon’s forelimb. In J. C. E. and J. P. Schadé (Eds.), Progress in Brain Research (Vol. 12, pp. 222–245). Publisher location: Elsevier. Retrieved from http://www.sciencedirect.com/science/article/pii/S0079612308606251

Respiratory Muscle Fatigue: Report of the Respiratory Muscle Fatigue Workshop Group. (1990). American Review of Respiratory Disease, 142(2), 474–480. doi:10.1164/ajrccm/142.2.47

Rosenberg, J., Amjad, A., Breeze, P., Brillinger, D., & Halliday, D. (1989). The Fourier approach to the identification of functional coupling between neuronal spike trains. Progress in Biophysics and Molecular Biology, 53(1), 1–31.

Sacco, P., Thickbroom, G. W., Thompson, M. L., & Mastaglia, F. L. (1997). Changes in corticomotor excitation and inhibition during prolonged submaximal muscle contractions. Muscle & Nerve, 20(9), 1158–1166. doi:10.1002/(SICI)1097-4598(199709)20:9<1158::AID-MUS11>3.0.CO;2-P

Seki, K., & Narusawa, M. (1996). Firing rate modulation of human motor units in different muscles during isometric contraction with various forces. Brain Research, 719(1–2), 1–7. doi:10.1016/0006-8993(95)01432-2

Schillings, M. L., Hoefsloot, W., Stegeman, D. F., & Zwarts, M. J. (2003). Relative contributions of central and peripheral factors to fatigue during a maximal sustained effort. European Journal of Applied Physiology, 90(5–6), 562–568. doi:10.1007/s00421-003-0913-4

Shibasaki, H., Sadato, N., Lyshkow, H., Yonekura, Y., Honda, M., Nagamine, T., ... & Konishi, J. (1993). Both primary motor cortex and supplementary motor area play an important role in complex finger movement. Brain, 116(6), 1387-1398.

Søgaard, K., Gandevia, S. C., Todd, G., Petersen, N. T., & Taylor, J. L. (2006). The effect of sustained low-intensity contractions on supraspinal fatigue in human elbow flexor muscles. Journal of Physiology, 573(2), 511–523. doi:10.1113/jphysiol.2005.103598

Srinath, R., & Ray, S. (2014). Effect of amplitude correlations on coherence in the local field potential. Journal of Neurophysiology, jn.00851.2013. doi:10.1152/jn.00851.2013

Taylor, J. L., & Gandevia, S. C. (2008). A comparison of central aspects of fatigue in submaximal and maximal voluntary contractions. Journal of Applied Physiology, 104(2), 542–550. doi:10.1152/japplphysiol.01053.2007

Tecchio, F., Porcaro, C., Zappasodi, F., Pesenti, A., Ercolani, M., & Rossini, P. M. (2006). Cortical short-term fatigue effects assessed via rhythmic brain-muscle coherence. Experimental Brain Research, 174(1), 144–151.

Ushiyama, J., Takahashi, Y., & Ushiba, J. (2010). Muscle dependency of corticomuscular coherence in upper and lower limb muscles and training-related alterations in ballet dancers and weightlifters. Journal of Applied Physiology, 109(4), 1086-1095.

Ushiyama, J., Katsu, M., Masakado, Y., Kimura, A., Liu, M., & Ushiba, J. (2011). Muscle fatigue-induced enhancement of corticomuscular coherence following sustained submaximal isometric contraction of the tibialis anterior muscle. Journal of Applied Physiology 110(5), 1233–1240. doi:10.1152/japplphysiol.01194.2010

Van Cutsem, M., Duchateau, J., & Hainaut, K. (1998). Changes in single motor unit behaviour contribute to the increase in contraction speed after dynamic training in humans. The Journal of Physiology, 513(Pt 1), 295–305. doi:10.1111/j.1469-7793.1998.295by.x

Van Duinen, H., Renken, R., Maurits, N., & Zijdewind, I. (2007). Effects of motor fatigue on human brain activity, an fMRI study. NeuroImage, 35(4), 1438–1449. doi:10.1016/j.neuroimage.2007.02.008

Van Oudenaarde, E., & Oostendorp, R. A. (1995). Functional relationship between the abductor pollicis longus and abductor pollicis brevis muscles: An EMG analysis. Journal of Anatomy, 186(Pt 3), 509–515.

Viitasalo, J. H. T., & Komi, P. V. (1977). Signal characteristics of EMG during fatigue. European Journal of Applied Physiology and Occupational Physiology, 37(2), 111–121. doi:10.1007/BF00421697

Weir, J. P., Beck, T. W., Cramer, J. T., & Housh, T. J. (2006). Is fatigue all in your head? A critical review of the central governor model. British Journal of Sports Medicine, 40(7), 573–586. doi:10.1136/bjsm.2005.023028

Yang, Q., Fang, Y., Sun, C.-K., Siemionow, V., Ranganathan, V. K., Khoshknabi, D., Yue, G. H. (2009). Weakening of functional corticomuscular coupling during muscle fatigue. Brain Research, 1250, 101–112. doi:10.1016/j.brainres.2008.10.074

Yang Q, Siemionow, V., Wanxiang Yao, Sahgal, V., & Yue, G. H. (2010). Single-trial EEG-EMG Coherence analysis reveals muscle fatigue-related progressive alterations in corticomuscular coupling. IEEE Transactions on Neural Systems and Rehabilitation Engineering, 18(2), 97–106. doi:10.1109/TNSRE.2010.2047173

Zijdewind, I., Zwarts, M. J., & Kernell, D. (1998). Influence of a voluntary fatigue test on the contralateral homologous muscle in humans? Neuroscience Letters, 253(1), 41–44.

Appendix A SIMULATED AND SAMPLE DATA FOR PHASE LOCK VALUE (PLV) VS. COHERENCE

A.1 Simulated Data

Studies have shown that coherence is dependent on both phase and amplitude (Lachaux et al., 1999; Srinath & Ray, 2014), while PLV is only dependent on phase.

To prove this was, in fact, the case, the author generated three cases.

A.1.1 Both signals have a phase lock at 30 Hz with noise.

A.1.2. Both signals have a phase lock at 30 Hz, but one signal has a random increasing amplitude gain.

A.1.3 Both signals have a phase lock at 30 Hz, but one signal has a random decreasing amplitude gain.

These cases are presented below:

A.1.1 No Noise

The two signal $s_x(t)$ and $s_y(t)$ are generated with a phase lock at 30 Hz and shown in Figure A-1:

$$s_x(t) = \cos(2\pi * 5t) + \sin(2\pi * 50t) + \sin(2\pi * 30(t+2))$$

$$s_y(t) = \cos(2\pi * 30(t+2)) + \sin(2\pi * 20t) + \sin(2\pi * 10t)$$

Coherence and PLV (refer to Section 2.3.4 and Section 2.3.5) were then applied to $s_x(t)$ and $s_y(t)$ to show that both measures show a phase lock at 30 Hz (shown in Figure A-2 and Figure A-3).

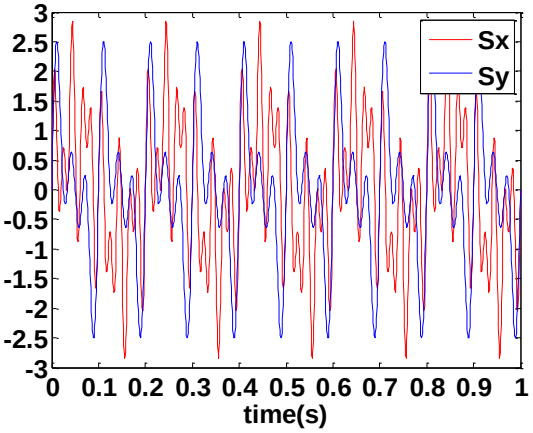

Figure A-1: Section of the two signals $s_x(t)$ and $s_y(t)$ in blue and red, respectively. The signals are phase lock at 30 Hz with no noise added.

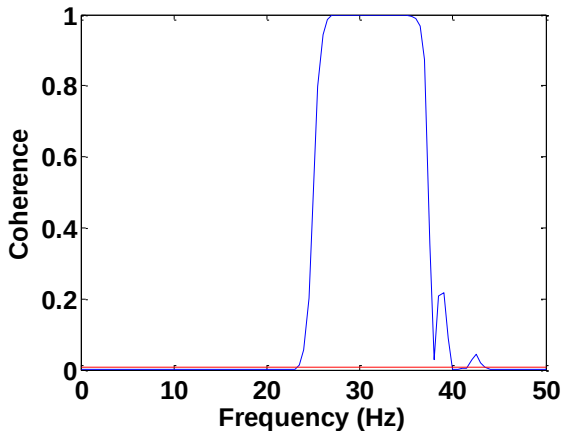

Figure A-2: Coherence amplitude vs. frequency when applied to simulated signals $s_x(t)$ and $s_y(t)$ with a phase lock at 30 Hz. There is a clear peak at 30 Hz. The waveform in blue is EEG-EMG coherence and the waveform in red is the 95% confidence level (CL).

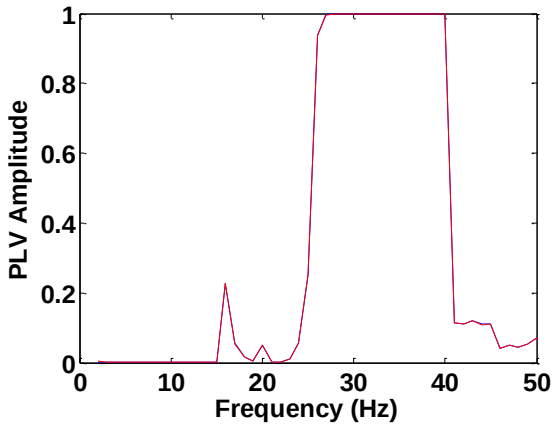

Figure A-3: PLV amplitude vs. frequency when applied to simulated signals $s_x(t)$ and $s_y(t)$ with a phase lock at 30 Hz. There is a clear peak at 30 Hz. The waveform in blue is PLV, and the waveform in red is the 95% confidence level (PLS).

From this, we can observe that both PLV and coherence provide an accurate phase lock at 30 Hz.

A.1.2 Increasing Gain

The two signals $s_x(t)$ and $s_y(t)$ are generated with a phase lock at 30 Hz, but a random increasing gain (ζ(t)) was added to the amplitude of $s_y(t)$

$$s_x(t) = \cos(2\pi * 5t) + \sin(2\pi * 50t) + \sin(2\pi * 30(t+2))$$

$$s_y(t) = \big(\zeta(t)\big) * t * \cos\big(2\pi * 30(t+2)\big) + \big(\zeta(t)\big) * t * \sin(2\pi * 20t) + \big(\zeta(t)\big) * t * \sin(2\pi * 10t)$$

Coherence and PLV (refer to Section 2.3.4 and Section 2.3.5) were then applied to $s_x(t)$ and $s_y(t)$ to demonstrate that both measures show a phase lock at 30 Hz (shown in Figure A-5 and Figure A-6).

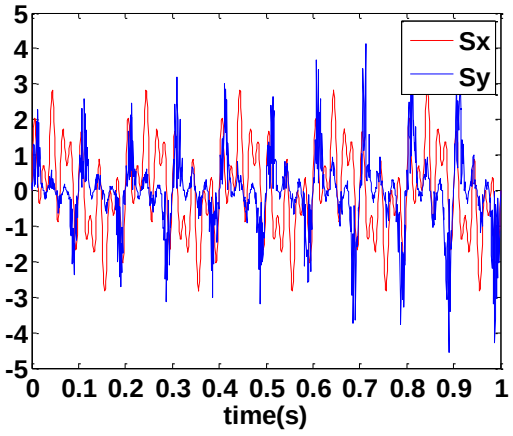

Figure A-4: Section of the two signals $\boldsymbol{s_x(t)}$ and $\boldsymbol{s_y(t)}$ in blue and red, respectively. The signals are phase lock at 30 Hz with a random increasing gain on $\boldsymbol{s_y(t)}$.

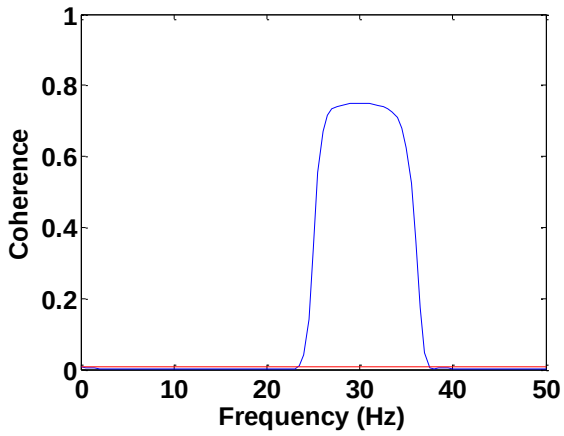

Figure A-5: Coherence amplitude vs. frequency when applied to simulated signals $\boldsymbol{s_x(t)}$ and $\boldsymbol{s_y(t)}$ with a phase lock at 30 Hz. There is a clear peak at 30 Hz. The waveform in blue is EEG-EMG coherence, and the waveform in red is the 95% confidence level (CL).

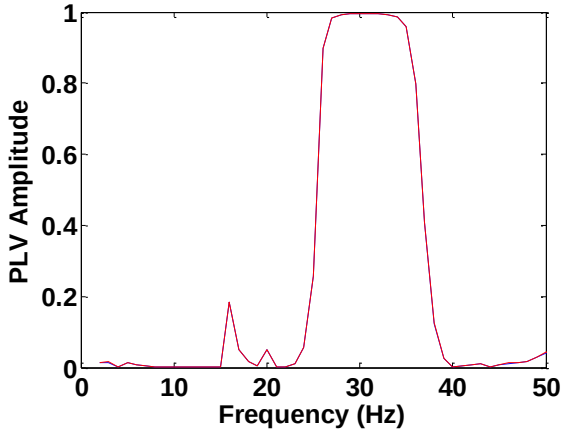

Figure A-6: PLV amplitude vs. frequency when applied to simulated signals $\boldsymbol{s_x(t)}$ and $\boldsymbol{s_y(t)}$ with a phase lock at 30 Hz. There is a clear peak at 30 Hz. The waveform in blue is PLV, and the waveform in red is the 95% confidence level (PLS).

From this, we can observe that both the PLV and coherence provide an accurate phase lock at 30 Hz, but the coherence seems to have decreased from an amplitude of 1 to an amplitude of 0.7, while the PLV remains with a peak of 1 at 30 Hz. Thus, the PLV is more amplitude noise robust compared to coherence.

A.1.3 Decreasing Gain

The two signals $s_x(t)$ and $s_y(t)$ are generated with a phase lock at 30 Hz, but a random decreasing gain ($\zeta(t)$) was added to the amplitude of $s_y(t)$

$$s_x(t) = \cos(2\pi * 5t) + \sin(2\pi * 50t) + \sin\big(2\pi * 30(t+2)\big)$$

$$s_y(t) = \big(\zeta(t)\big) * \frac{1}{t} * \cos\big(2\pi * 30(t+2)\big) + \big(\zeta(t)\big) * \frac{1}{t} * \sin(2\pi * 20t) + \big(\zeta(t)\big) * \frac{1}{t} * \sin(2\pi * 10t)$$

Coherence and PLV (refer to Section 3.6.10 and Section2.3.5) were then applied to $s_x(t)$ and $s_y(t)$ to demonstrate that both measures show a phase lock at 30 Hz (shown in Figure A-8 and Figure A-9).

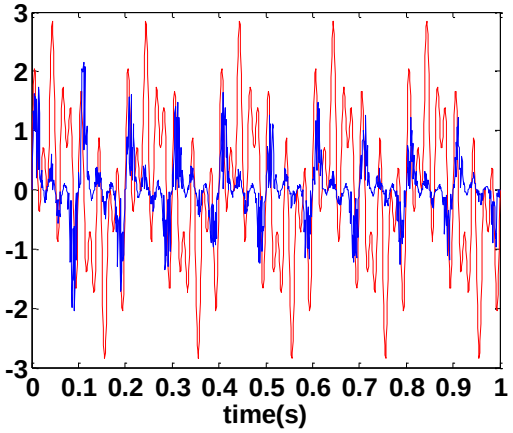

Figure A-7: Section of the two signals $s_x(t)$ and $s_y(t)$ in blue and red, respectively. The signals are phase lock at 30 Hz with a random decreasing gain applied to $s_y(t)$.

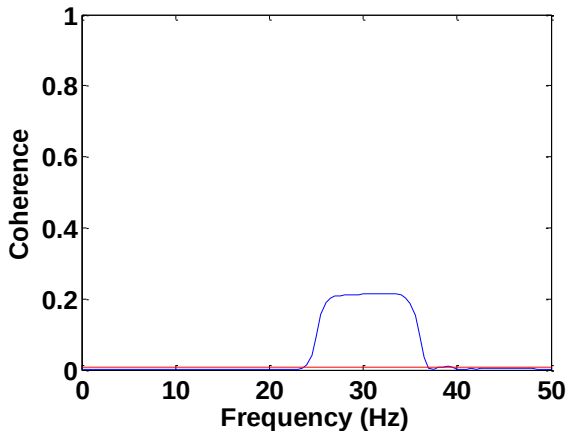

Figure A-8: Coherence amplitude vs. frequency when applied to simulated signals $s_x(t)$ and $s_y(t)$ with a phase lock at 30 Hz. There is a clear peak at 30 Hz. The waveform in blue is EEG-EMG coherence, and the waveform in red is the 95% confidence level (CL).

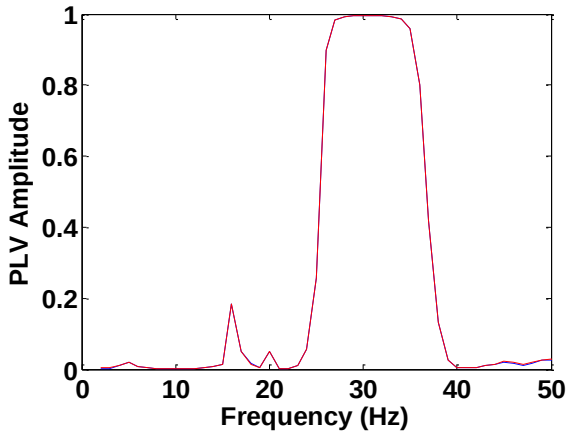

Figure A-9: PLV amplitude vs. frequency when applied to simulated signals $s_x(t)$ and $s_y(t)$ with a phase lock at 30 Hz. There is a clear peak at 30 Hz. The waveform in blue is EEG-EMG coherence, and the waveform in red is the 95% confidence level (PLS).

From this, we can observe that both the PLV and coherence provide an accurate phase lock at 30 Hz, but the coherence seems to have decreased from an amplitude of 1 to an amplitude of 0.3, while the PLV remains with a peak of 1 at 30 Hz. Thus, the PLV is more noise robust compared to coherence.

A.2 Sample Data

Divekar and John's (2012) study provided sample data for the present study in order to validate the consistency of the EEG-EMG PLV method. The sample data contained information regarding the EMG from the extensor carpi radialis longus and the EEG from C5, while a participant extended his wrist for 45 seconds. Figure A-10 shows the EEG-EMG coherence waveform generated from the sample data, and Figure A-11 shows the PLV waveform generated from the sample data.

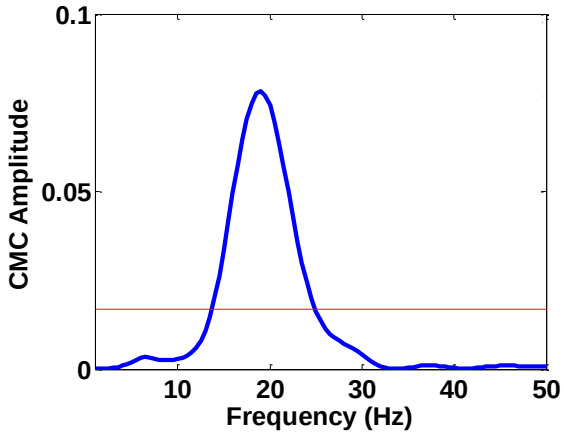

Figure A-10: EEG-EMG coherence amplitude vs. frequency when applied to sample data signals. The sample data were the EMG from the extensor carpi radialis longus and the EEG from C5 while a participant extended his wrist for 45 seconds. The waveform in blue is the EEG-EMG coherence, and the waveform in red is the 95% confidence level (CL).

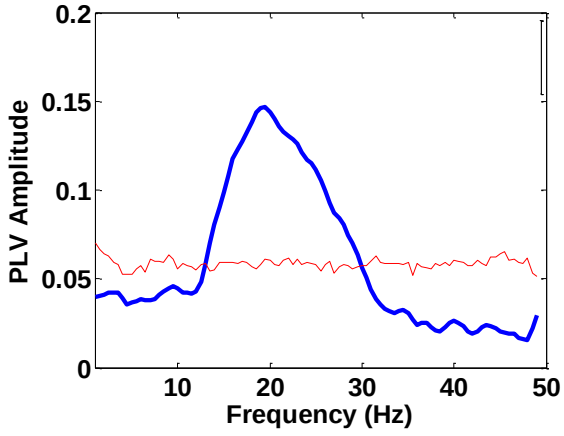

Figure A-11: The EEG-EMG PLV amplitude vs. frequency when applied to sample data signals. The sample data contained EMG data from the extensor carpi radialis longus and EEG data from C5 while a participant extended his wrist for 45 seconds. The waveform in blue is EEG-EMG PLV, and the waveform in red is the 95% confidence level (PLS).

Figure A-10 and Figure A-11 both show similar waveforms with peaks at 20 Hz. This corresponds to the data found in Divekar and John (2012), which reveals that EEG-EMG PLV can be used for EEG-EMG coherence studies.

Appendix B SAMPLE SIZE ESTIMATION

Since this study is concerned with comparing PLV as a corticomuscular coupling measure to EEG-EMG coherence, the sample size was estimated by comparing the effect of two independent variables (IVs, e.g., pre-fatigue vs. post-fatigue) on dependent variables (DVs, e.g., EMG-EEG EEG-EMG coherence, EMG-EEG PLV), with the null hypothesis being that the IVs have an identical effect on each DV. In order to confirm an alternate hypothesis (i.e., the IVs do not have an identical effect on each DV), the hypothesis test must have significant statistical power$(1-\beta)$. That is, there must be sufficient probability that the test will be able to reject a false null hypothesis. β is the probability of accepting a false null hypothesis (Type II error). Statistical power can therefore also be seen as the probability that a false null hypothesis will not be accepted. In order to achieve sufficient statistical power, the sample size of the test must be large enough to ensure that random sampling error does not influence the results or inaccurately represent the population. A typical value for power is 80% or $\beta = 0.2$ (Motulsky, 1995).

The test result is said to be statistically significant if the p-value is below a certain significance level (α), where α is the probability of an accepting a false alternative hypothesis (Type I error). The lower the p-value, the less likely that the null hypothesis is true, and thus, the more significant the result is. A typical value for the significance level is 5% or $\alpha = 0.05$ (Motulsky, 1995).

This study aims to detect a significant difference in the EEG-EMG coherence and PLV peak amplitude in participants before and after fatigue. During the hypothesis testing, when comparing two means (EEG-EMG coherence or PLV peak amplitude pre- and post-fatigue), the following formula was used to estimate the sample size:

$$N \approx \frac{2(SD)^2(z_\alpha + z_\beta)^2}{\Delta^2} \qquad \textbf{Equation B-1}$$

where SD is the standard deviation, $(z_\alpha + z_\beta)^2$ is the power index and Δ is the minimum distance between population means that is detected as significant. Using a one-tailed distribution and choosing typical values of $\alpha = 0.05$ and $\beta = 0.2$, the power index $(z_\alpha + z_\beta)^2$ is found to be 6.2, as noted in Table 22.1 in Motulsky (1995).

The standard deviation and mean difference for this study was adopted from a similar study (Ushiyama et al., 2011) for pre- and post-fatigue coherence where $SD \approx 0.5$ and $\Delta \approx 0.5$.

From Equation B-1, the appropriate sample size is 12.4 ($N \approx 13$). Thus, in this study, 15 participants were used to ensure significant statistical power.

Appendix C SUBJECT CONSENT FORM

Definitions:

Electrodes: Small metal caps placed on the skin to measure bio-electrical signals.

Surface Electromyography (EMG): Study of bio-electrical signals which can be measured with electrodes on the skin surface near a muscle and which represent the muscle's activity.

Electroencephalography (EEG): Study of bio-electrical signals which can be measured on the scalp by electrodes and which are representative of cortical activity.

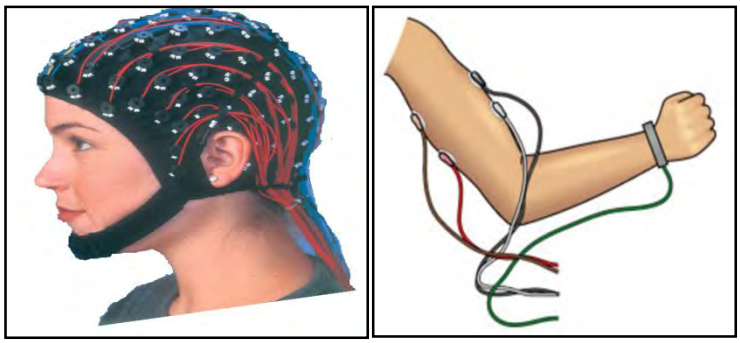

Figure C-1: High-resolution EEG cap (left), EMG recording from muscles (right).

Informed Consent

Researchers at the Medical Research Center (MRC) /University of Cape Town (UCT) Medical Imaging Research Unit are developing an accurate method of determining muscle fatigue using EMG and EEG. Brain and muscle function would be measured by recording EEG and EMG waveforms from participants whilst they are required to perform a fatiguing contraction. Both EEG and EMG are safe, non-invasive recording techniques that require the placement of electrodes on the head of a participant for EEG, and the placement of electrodes on the palm of the hand for EMG. Each test will last approximately 1 hour, and 15 participants are required for the trial.

Testing Procedure

All testing will be carried out at the UCT Faculty of Health Sciences and has been pre-approved by the Human Ethics Committee. You will be required to wash your hair with shampoo prior to testing. For good electrical conductivity, the skin above the palm of your hand will be abraded and cleaned with alcohol; this causes miniscule discomfort, if any. Electrodes will be covered with conducting gel; this causes no discomfort. You will be seated in a chair facing a computer monitor and will be fitted with a 16-channel EEG cap (see Figure 1, left) and EMG electrodes on

the palm of your hand (similar to Figure 1, right). A series of instructions for movements will be presented on a computer screen. The movements will require you to abduct your thumb and try to maintain it at a particular force until task failure. There will be no direct benefit to you, but the results of the research will be used to further the understanding of muscle fatigue. The trial is voluntary, and you may refuse to participate or withdraw from the trial, at any time, without penalty or loss of benefits to which you are otherwise entitled.

Possible Risks Associated with Participation

The EEG and EMG equipment is inherently safe. Temporary mild skin sensitivity may result from the conducting gel. In the unlikely case that you experience discomfort, you should alert the investigator. UCT has a public liability cover (a no-fault insurance policy) should some unforeseen event occur whilst you are participating in this study.

UCT No-Fault Insurance Policy

UCT undertakes that, in the event of your suffering any significant deterioration in health or well-being, from any unexpected sensitivity or toxicity, that is caused by your participation in the study, it will provide immediate medical care. UCT has appropriate insurance cover to provide prompt payment of compensation for any trial-related injury, according to the guidelines outlined by the Association of the British Pharmaceutical Industry (ABPI, 1991). Broadly speaking, the ABPI guidelines recommend that the insured organisation (UCT), without legal commitment, should compensate you without your having to prove that UCT is at fault. An injury is considered trial-related if, and to the extent that, it is caused by study activities. You must notify the study doctor immediately of any side effects and/or injuries during the trial, whether they are research-related or other related complications.

UCT reserves the right not to provide compensation if, and to the extent that, your injury came about because you chose not to follow the instructions that you were given while you were taking part in the study. Your right in law to claim compensation for injury where you prove negligence is not affected. Copies of these guidelines are available on request.

Statement of Understanding and Consent

I confirm that I am over 18 years of age and that the exact procedure and techniques and the possible complications of the above tests have been thoroughly explained to me. I am free to withdraw from the study at any time should I choose to do so. I understand that I may not go through with the testing procedure if I suffer from any kind of neuromuscular or muscular

disorder and may ask questions at any time during the testing procedure. I know that the personal information required by the researchers and derived from the testing procedure will remain strictly confidential and will only be revealed as a number in classification analysis. I have carefully read this form and understand the nature, purpose and procedures of this study. I agree to participate in this research project conducted by the MRC/UCT Medical Imaging Research Unit.

Subject Information Sheet

Name of volunteer / guardian (if necessary):_____

Signature:_____

Name of investigator:_____

Signature:_____

Date:_____

Research Team

Principal Investigator: Dr LR John (Lecturer, UCT)

Co-Investigators: Mr J Joseph (MSc (Med) (BME) student, UCT)

Contact details:

Principal Investigator contact:	Research Ethics Committee contact:
Lester John, BScEng, PhD Electronic & Biomedical Engineer MRC/UCT Medical Imaging Research Unit Department of Human Biology Faculty of Health Sciences University of Cape Town Observatory 7925 South Africa Tel: +27 21 406-6548 Fax: +27 21 448-7226 Lester.John@uct.ac.za	Mrs Lamees Emjedi Research Ethics Committee E 52 Room 24, Old Main Building, Groote Schuur Hospital, Observatory Telephone: 27 21 406 6338 Fax: 27 21 406 6411 Email: nosi.tsama@uct.ac.za shuretta.thomas@uct.ac.za

Appendix D STRAIN GAUGE AMPLIFIER DATASHEET

RS Components, Stock no. 435-692

GB **RS Stock No.**

435-692

A printed circuit board to accept the RS Strain Gauge Amplifier and associated components to make an amplifier decoder for resistive bridge type sensors.

Assembly

All components positions are marked on the PCB, shorting links are indicated by solid lines.The components list below includes PCB mounting screw terminals for ease of connection, however these need not be used as wires can be directly soldered to the board. The values of R1 and R2 given below set the gain to 1000. The gain can be set to other values and is defined by the equation.

$$\text{Gain} = 1+\frac{R_1}{R_2}$$

C5, C6 and C7 are for reduction of noise and considerably slow the output response. In some applications these components are best removed.

RS Components shall not be liable for any liability or loss of any nature (howsoever caused and whether or not due to RS Components' negligence) which may result from the use of any information provided in **RS** technical literature.

D **RS Best-Nr.**

435-692

Die Leiterplatte dient zur Aufnahme des RS DMS-Verstärkers und der zugehörigen Bauteile, so daß ein Verstärker/Dekoder für Sensoren mit ohmscher Brücken-Konfiguration erstellt wird.

Montage

Alle Bauteilpositionen sind auf der Leiterplatte aufgedruckt, Kurzschlußverbindungen sind durch durchgehende Linien gekennzeichnet. Die Liste der Bauteile (siehe unten) umfaßt u.a. eine Schraubklemme zur einfachen Leiterplattenmontage, die Drähte können jedoch auch direkt mit der Platte verlötet werden. Die unten genannten Werte von R1 und R2 ergeben eine Verstärkung von 1000. Eine andere Einstellung de Verstärkung ist anhand der folgenden Formel möglich:

$$\text{Verstärkung} = 1+\frac{R_1}{R_2}$$

C5, C6 und C7 dienen der Rauschverminderung, verlangsamen die Ausgabegeschwindigkeit jedoch erheblich. Bei manchen Anwendungen empfiehlt es sich daher, diese Bauteile wegzulassen.

RS Components haftet nicht für Verbindlichkeiten oder Schäden jedweder Art (ob auf Fahrlässigkeit von RS Components zurückzuführen oder nicht), die sich aus der Nutzung irgendwelcher der in den technischen Veröffentlichungen von **RS** enthaltenen Informationen ergeben.

E **Código RS.**

435-692

Se trata de una tarjeta de circuito impreso que acepta el amplificador RS para galga extensométrica y los componentes correspondientes, lo que le convierte en un decodificador amplificador para sensores del tipo de puente de resistencias.

Conjunto

En la tarjeta de circuito impreso están marcadas las posiciones de todos los componentes; los puentes de enlace están indicados por trazos continuos. La siguiente lista de componentes incluye los terminales de tornillo para montaje de la tarjeta con el fin de facilitar su conexión, aunque no es necesario utilizarlos, ya que se pueden soldar directamente los holos a la tarjeta.

Los valores de R1 y R2 que se indican a continuación dan una ganancia de 1.000. La ganancia se puede ajustar a otros valores y viene definida por la ecuación.

$$\text{Ganancia} = 1+\frac{R_1}{R_2}$$

Los condensadores C5, C6 y C7 están destinados a reducir el ruido y ralentizar considerablemente la respuesta de salida. En determinadas aplicaciones conviene quitar estos componentes.

RS Components no será responsable de ningún daño o responsabilidad de cualquier naturaleza (cualquiera que fuese su causa y tanto si hubiese mediado negligencia de RS Componentscomo si no) que pudiese derivar del uso de cualquier información incluida en la documentación técnica de **RS**.

F **Code commande RS.**

435-692

Carte de circuits imprimés recevant l'amplificateur de la jauge extensométrique RS et les composants correspondants, pour offrir un décodeur d'amplificateur pour les capteurs de type pont résistif.

Assemblage

Toutes les positions des composants sont indiquées sur la carte de circuits imprimés, les liaisons de court-circuitage sont indiquées par une ligne continue. La liste des composants ci-dessous comprend les bornes de montage à vis de la carte de circuits imprimés pour faciliter les connexions; cependant, celles-ci ne sont pas nécessaires, car on peut souder directement les fils à la carte.
Les valeurs R1 et R2 ci-dessous établissent le gain à 1 000. On peut régler le gain à un autre chiffre et le définir par l'équation.

$$\text{Gain} = 1+\frac{R_1}{R_2}$$

C5, C6 et C7 sont pour la réduction du bruit et ralentissent considérablement la réponse de sortie. Dans certains cas, il vaut mieux enlever ces composants.

La société RS Components n'est pas responsable des dettes ou pertes de quelle que nature que ce soit (quelle qu'en soit la cause ou qu'elle soit due ou non à la négligence de la société RS Components) pouvant résulter de l'utilisation des informations données dans la documentation technique de **RS**.

I **RS Codici.**

435-692

Un circuito stampato accoglie l'amplificatore per estensimetri RS ed altri componenti ad esso associati, per realizzare un amplificatore/decodificatore per sensori con configurazione a ponte resistivo.

Complessivo

La posizione di ogni componente è contrassegnata sulla scheda, ed i collegamenti di corto circuito sono indicati da delle linee solide. I componenti elencati qui di seguito sono compresi dei terminali con vite di montaggio su scheda per un facile collegamento. Non è tuttavia necessario utilizzare tali viti, in quanto è possibile saldare i fili direttamente sulla scheda. I valori R1 ed R2 riportati qui di seguito, impostano il guadagno a 1000. Il guadagno può essere impostato ad altri valori e viene definito in base alla seguente equazione:

$$\text{Guadagno} = 1+\frac{R_1}{R_2}$$

C5, C6 e C7 servono per ridurre il disturbo e rallentare in modo considerevole la risposta di uscita. In alcune applicazioni è meglio eliminare questi componenti.

La RS Components non si assume alcuna responsabilità in merito a perdite di qualsiasi natura (di qualunque causa e indipendentemente dal fatto che siano dovute alla negligenza della RS Components), che possono risultare dall'uso delle informazioni fornite nella documentazione tecnica.

Instruction Leaflet
Bedienungsanleitung
Hojas de instrucciones
Feuille d'instructions
Foglio d'instruzioni

Strain Gauge Amplifier PCB (GB)

Leiterplatte für Dehnungsmeßstreifen -Verstärker (D)

PCB de amplificación para galga extensométrica (E)

Carte de circuits imprimés de l'amplificateur de jauge extensométrique (F)

Scheda circuito stampato per amlificatore di estensimetri (I)

Figures / Figures / Figura

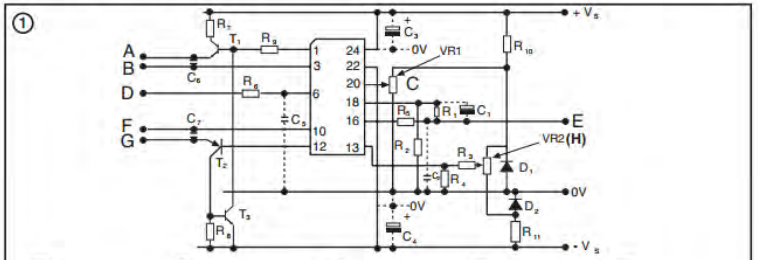

GB **Circuit diagram**
A. + Bridge supply
B. Compensation
C. Set bridge supply
D. + Input
E. Output
F. - Input
G. - Bridge supply
H. Set zero

D **Schaltplan**
A. pos. Brückenspeisung
B. Kompensation
C. Eingestellte Brückenspeisung
D. pos. Eingang
E. Ausgang
F. neg. Eingang
G. neg. Brückenspeisung
H. Nullstellung

E **Esquema del circuito**
A. Alimentación positiva del puente
B. Compensación
C. Alimentación fija del puente
D. Entrada positiva
E. Salisa
F. Entrada negativa
G. Alimentación negativa del puente
H. Cero ajustado

F **Schéma du circuit**
A. Alimentation positive de pont
B. Compensation
C. Alimentation établie de pont
D. Entrée positive
E. Sortie
F. Entrée négative
G. Alimentation négative de pont
H. Réglage à zéro

I **Diagramma circuito**
A. Alimentazione poitiva del ponte
B. Compensazione
C. Alimentazione fissa del ponte
D. Ingresso positiva
E. Uscita
F. Ingresso negativo
G. Alimentazione negativo del ponte
H. Zero fisso

Components List / Liste der Bauteile / Lista de componentes / Liste des componants / Elenco componeti

Component / Bauteile / Componentes / Componsant / Componente	Value / Wert / Valor / Valeur / Valore	RS Stock no. / RS Best.-Nr / Código RS / Code Commande RS / Codice	Quantity Required / Benötigte Anzahl / Cantidad necesaria / Quantité necessaire / Quantità
R1 & R3	100 KΩ	148-972	1
R2 & R6	100 Ω	148-269	1
R4	68Ω	148-219	1
R5 & R8	10Ω	148-017	1
R7	47Ω	148-174	1
R9	1KΩ	148-506	1
R10 & R11	680Ω	148-461	1
VR1 & VR2	10K	186-520	2
C1, C6 & C7	100nF	312-1469	1
C2 & C5	10nF	312-1431	1
C3 & C4	10µF	103-957	1
T1	BD135	299-323	1
T2	BD136	299-339	1
T3	BC108	293-533	1
4-Way Connector/ 4poliger Stecker/ Conector de 4 vias/ 4-point Connecteurs/ Connettore a 4 vie		425-847	1
3-Way Connector/ 3poliger Stecker/ Conector de 3vias/ 3-point Connecteurs/ Connettore a 3 vie		424-686	1
Strain Gauge Amp/ Dehnungsmeß-Sensor/ Amplificador para galga extensométrica/ l'amplificateur de la jauge extensométrique/ Amplificatore de estensimetrii		846-171	1
Diode / Diodo / Diodi D1 & D2	LM4040DIZ-5.0	168-9351 / 299-187	2

Appendix E DATA ACQUISITION

The following section further explains how the user interface application was generating in LABVIEW.

Figure E-1 shows the switches used to activate the different sections of the experiment. The participants had 17 stages to complete.

- Eyes closed and eyes open: Two stages of eyes open and eyes closed, where the participant just relaxed.
- Pre-fatigue stage: Six stages of pressing the thumb at 10% of MVC for 10 seconds.
- Fatigue stage: One stage of pressing the thumb at 30% of MVC until task failure.
- Post-fatigue Stage: Six stages of pressing this thumb at 10% of MVC for 10 seconds.
- Eyes closed and eyes open: Two stages of eyes open and eyes closed, where the participant just relaxed.

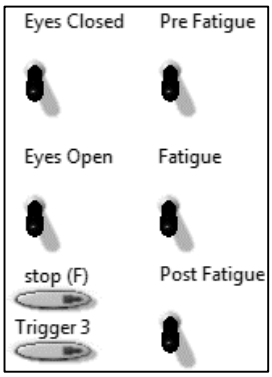

Figure E-1: Start/stop switches for the experiment

The switches controlled the recording of data. They were only activated by the invigilator, once the participant reached his targeted %MVC, and were then deactivated when each stage was completed.

Each stage, except for the fatigue stage, was deactivated using 'if' statements as shown in Figure E-2 and Figure E-3. The switches were checked every 100 milliseconds.

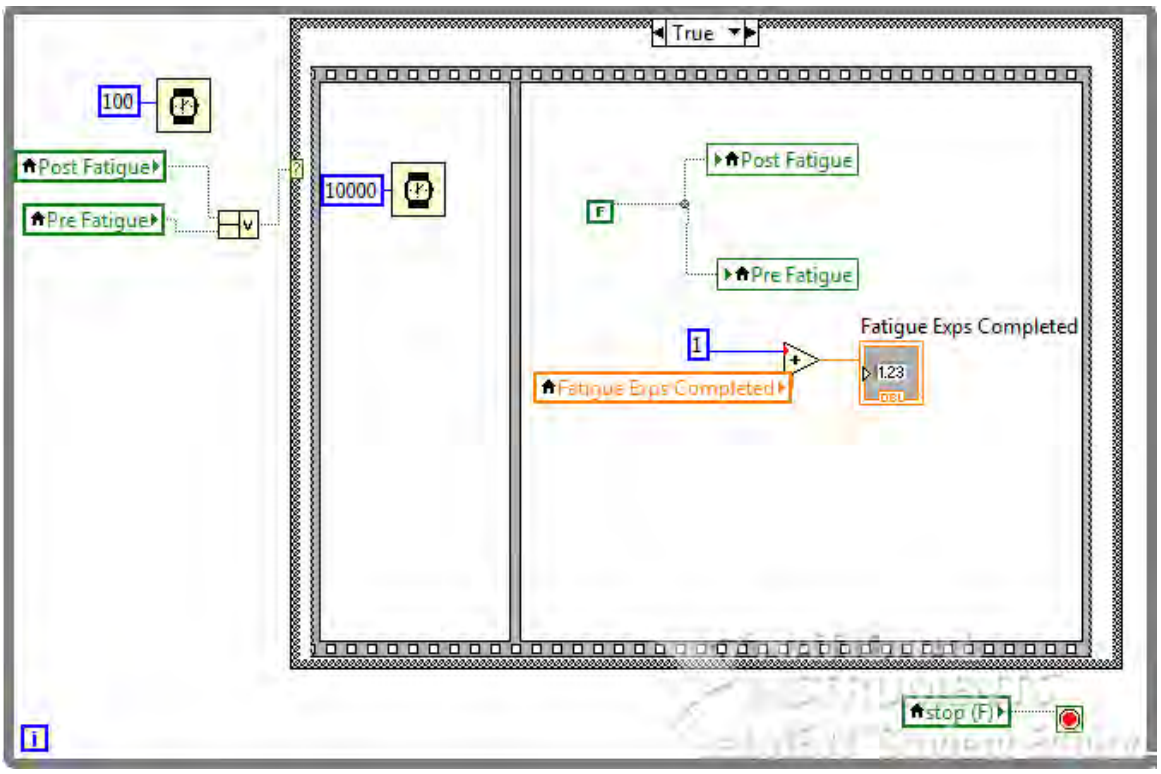

Figure E-2: If statement to deactivate pre- and post-fatigue stages after 10 seconds.

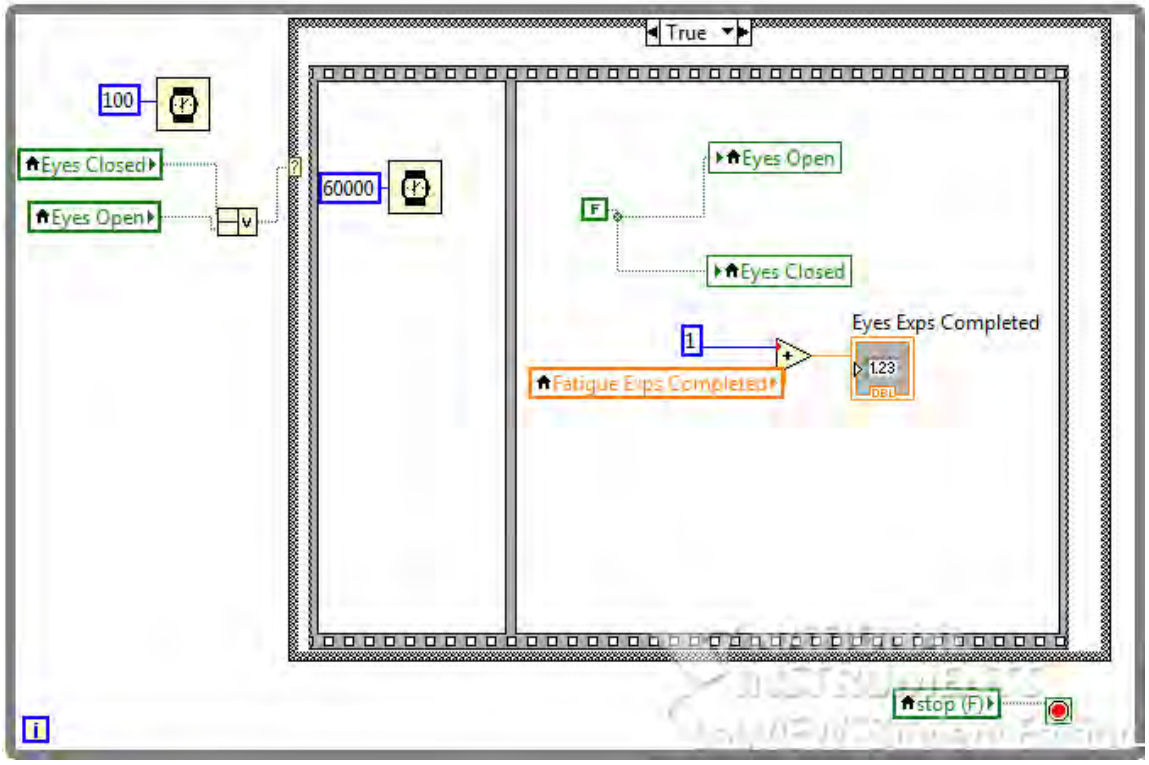

Figure E-3: If statement to deactivate eyes open and eyes closed stages after 60 seconds.

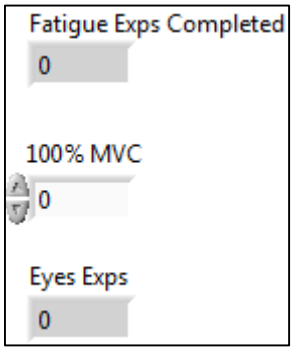

Figure E-4: Illustrates the number of stages completed

Figure E-4 gave the invigilator the number of stages completed as well as the input of the participant's %MVC in volts. Each stage was incremented by 1, when a switch was deactivated. This can be seen in Figure E-3 and Figure E-2.

The %MVC was calculated using a MATLAB script as shown in Figure E-5.

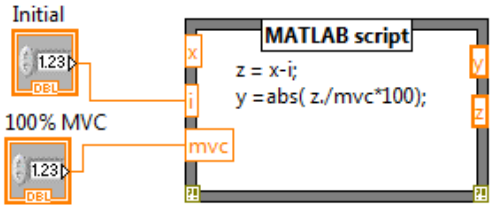

Figure E-5: MATLAB script converting the voltage strain gauge value into a percentage MVC, where *x* is the current strain gauge value, *i* is the initial value to bring the strain to 0, *mvc* is the 100% of MVC entered by the invigilator, *y* is the current %MCV and *z* is the real value of the strain gauge.

As shown in Figure E-6, the fatigue stage switch was deactivated, which stopped the recording of data, using a MATLAB script and circular buffer. The MATLAB script was used to deactivate recording once the participant was thought to be fatigued. A participant was considered fatigued when his %MCV was below 10% of the target %MVC for longer than 2 seconds.

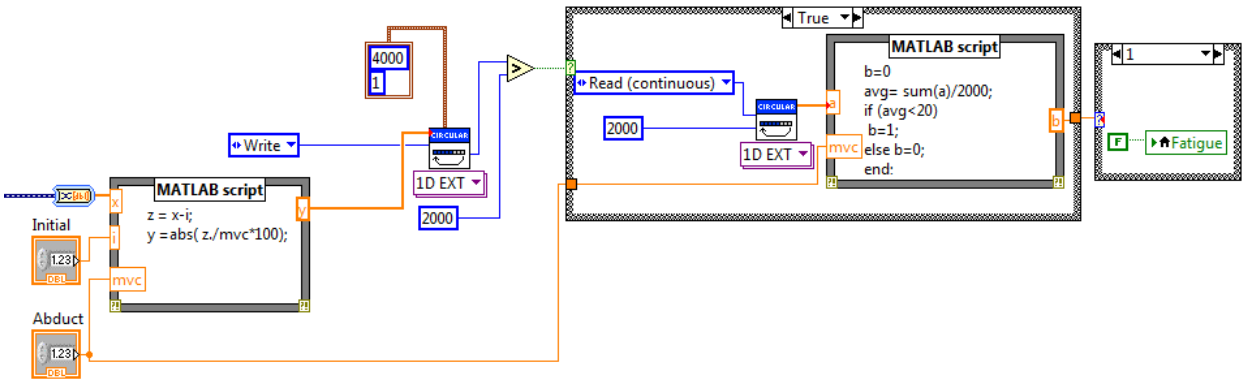

Figure E-6: LabVIEW block diagram of invigilator's screen. Deactivation of the fatigue switch stopped the recording of data once the participant was below 20% of MVC for longer than 2 seconds. The %MCV was calculated in the initial MATLAB script (refer to Figure E-5), and 2000 samples (i.e., 2 seconds of data) were then stored in the circular buffer. Once the buffer was full, the data were extracted and checked to see whether the average value was below 20% of

the participant's MVC. In the diagram, *a* is the array containing the 2000 samples, *mvc* is 100% of MCV of the participant entered by the invigilator and *b* indicates whether the participant's %MVC was below 20%. The second 'if' statement (third block) activated the fatigue switch if the average was below 20%.

The timers shown in Figure 2-12 were controlled by the switches shown in Figure E-7. Once the switch was deactivated, the timers would reset. These timers allowed the invigilator to view the amount of time that had elapsed per stage.

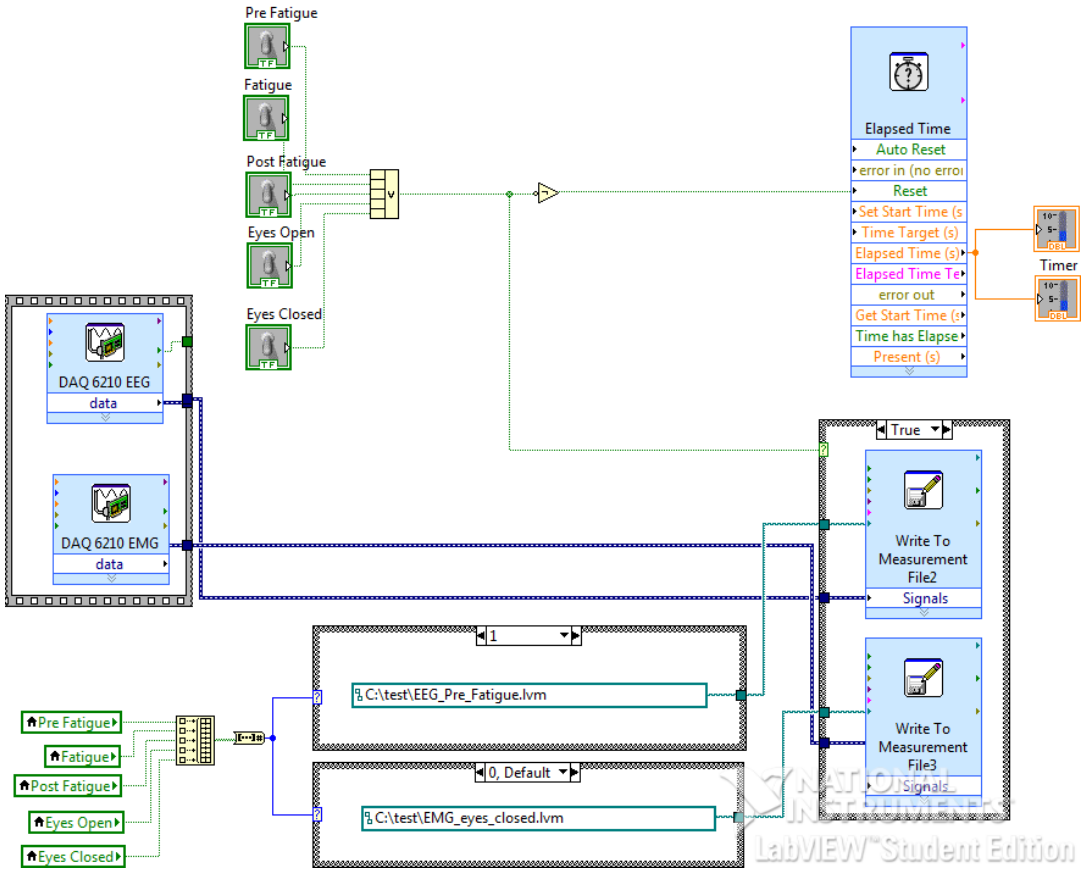

Figure E-7: The top of the figure shows the five switches that controlled when the timers reset and started in addition to when data needed to be recorded into files. The data were extracted from the DAQ 6210 EEG for the 16-channel EEG and from the DAQ 6210 EMG for the eight-channel EMG, two-channel EOG and one-channel strain gauge voltage. The different stages were saved into different files that were controlled by the switches.

Appendix F EMG AVERAGE INSTANTANEOUS FREQUENCY (AIF)

F.1 Method

The average instantaneous frequency (AIF) has been shown to be a more robust method for the EMG fatigue analysis as opposed to the EMG_{MNF}, since it is not sensitive to different window sizes (Georgakis et al., 2003). The EMG_{AIF} was applied by the following method (refer to Code G-9 for MATLAB code):

1. Using Hilbert transform ($H[s(t)]$) to find the instantaneous phase ($\theta(t)$).

$$\theta(t) = (\frac{H[s(t)]}{s(t)}) \qquad \textbf{Equation F-1}$$

2. The instantaneous frequency $\omega(t)$ is estimated as the first derivative of the phase (implemented with first-order finite differences).

$$\omega(t) = \theta'(t) \qquad \textbf{Equation F-2}$$

3. The instantaneous frequency values are then averaged over consecutive non-overlapping windows of a fixed length to provide the required AIF values.

$$EMG_{AIF} = \frac{1}{t_a - t_b}\int_{t_b}^{t_a} \omega(t)\ dt \qquad \textbf{Equation F-3}$$

F.2 Result

Figure F-1 illustrates a typical example of EMG_{AIF}, pre- and post-fatigue.

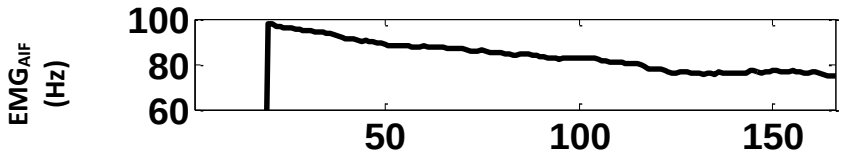

Figure F-1: Typical example of a participant showing progressive changes in their EMG_{AIF} during sustained isometric contraction of the APB muscle at 30% of MVC until task failure. The EMG_{AIF} was calculated by sliding the 20-second window along the signal in 1-second increments.

F.3 Statistical Analysis: EMG_{AIF} comparisons between pre- and post-fatigue

The EMG_{AIF} decreased significantly from pre-fatigue to post-fatigue (116.072 ± 15.698 to 97.366 ± 15.055 Hz, p =0.000).

Testing for assumptions, through the presence of outliers, is shown in Figure F-2, and Table F-1 shows the testing of normality. The box plot, shown in Figure F-2, shows no outliers. Table F-1, which presents the results of the Shapiro-Wilk test, shows a $p > 0.05$, which indicates that the data are approximately normally distributed.

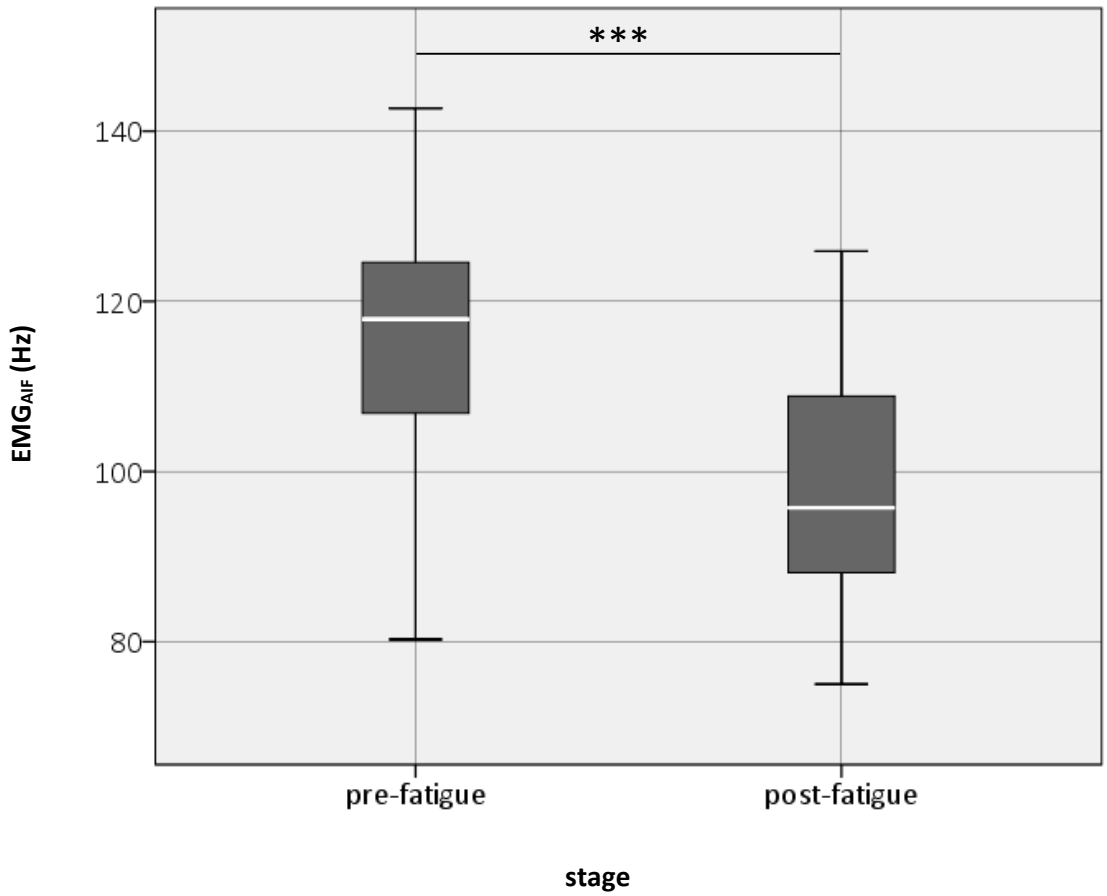

Figure F-2: Box plot of the EMG_{AIF} between pre- and post-fatigue. Significant differences denoted by: * ($p < 0.05$), ** ($p < 0.01$) and *** ($p < 0.001$).

Table F-1: Shapiro-Wilk test of normality for the EMG_{AIF} pre- and post-fatigue using SPSS.

Stage		Shapiro-Wilk		
		Statistic	**df**	**Sig.**
EMG_{AIF}	Pre-fatigue	.920	15	.190
	Post-fatigue	.961	15	.715

Appendix G CODE SNIPPETS

The following section contains code snippets used in this study for data analysis.

Code G-1: Extract data from LabVIEW into MATLAB

```
eeg_exp1 = dlmread('EEG_Pre_Fatigue.lvm','',23,0);
emg_exp1 = dlmread('EMG_Pre_Faigue.lvm','',23,0);

eeg_exp2 = dlmread('EEG_Fatigue.lvm','',23,0);
emg_exp2 = dlmread('EMG_Fatigue.lvm','',23,0);

eeg_exp3 = dlmread('EEG_Post_Fatigue.lvm','',23,0);
emg_exp3 = dlmread('EMG_Post_Fatigue.lvm','',23,0);


EEG_1=eeg_exp1(:, 2:17)';
EEG_2=eeg_exp2(:, 2:17)';
EEG_3=eeg_exp3(:, 2:17)';



EMG_1=emg_exp1(:,2:9)';
EMG_2=emg_exp2(:,2:9)';
EMG_3=emg_exp3(:,2:9)';
```

Code G-2: EEG and EMG filtering

```
[b,a] = butter(4,[10/500 200/500],'bandpass');
[f,e] = butter(4,[0.5/500 100/500],'bandpass');

for emg_elec=1:8
    EMG_1(emg_elec,:)  = filtfilt(b,a,EMG_1(emg_elec,:) );
    EMG_2(emg_elec,:)  = filtfilt(b,a,EMG_2(emg_elec,:) );
    EMG_3(emg_elec,:)  = filtfilt(b,a,EMG_3(emg_elec,:) );
    EMG_1(emg_elec,:)  = filtfilt(d,c,EMG_1(emg_elec,:) );
    EMG_2(emg_elec,:)  = filtfilt(d,c,EMG_2(emg_elec,:) );
    EMG_3(emg_elec,:)  = filtfilt(d,c,EMG_3(emg_elec,:) );
end;

for eeg_elec=1:16
    EEG_1(eeg_elec,:)  = filtfilt(f,e,EEG_1(eeg_elec,:) );
    EEG_2(eeg_elec,:)  = filtfilt(f,e,EEG_2(eeg_elec,:) );
    EEG_3(eeg_elec,:)  = filtfilt(f,e,EEG_3(eeg_elec,:) );
    EEG_1(eeg_elec,:)  = filtfilt(d,c,EEG_1(eeg_elec,:) );
    EEG_2(eeg_elec,:)  = filtfilt(d,c,EEG_2(eeg_elec,:) );
    EEG_3(eeg_elec,:)  = filtfilt(d,c,EEG_3(eeg_elec,:) );
end;
```

Code G-3: Remove gain from EMG and EEG data

```
EEG_1=EEG_1./5000;
EEG_2=EEG_2./5000;
EEG_3=EEG_3./5000;
EMG_1=(EMG_1)./1800;
EMG_2=(EMG_2)./1800;
EMG_3=(EMG_3)./1800;
```

Code G-4: La placian of EEG and rectification of EMG

```
%--------------- la placian of eeg-----------------------------------------
E =
{'CP3';'C6';'FCZ';'CPZ';'C1';'FC4';'F2';'C3';'CZ';'CP4';'C5';'FC3';'FZ';'C2';'C
4';'F1'};
M = ExtractMontage('10-5-System_Mastoids_EGI129.csd',E);
[G,H] = GetGH(M);
head=15;
lamda=1.0e-5;

EEG_2=eeg_exp2(:, 2:17);
EEG_2=detrend(EEG_2,'linear');
EEG_2=EEG_2';
EEG_2= CSD (EEG_2, G, H,lamda,head);
EEG_2=EEG_2';

%-------------------- recify emg-----------------------------------------
EMG_2=emg_exp2(:,2:9);
EMG_2=detrend(EMG_2,'linear');
EMG_2=abs(EMG_2);
```

Code G-5: Power Spectral Density

```
Psd=pwelch(data,1024,0,2000,1000);
```

The function consisted of five attributes:

1. Input signal.
2. Window size attribute/number of samples to use for each window. The smaller the sample size, the greater the amount of windows.
3. Number of samples by which the sections overlapped, which was selected to be zero.
4. FFT length, which determined the frequencies at which the coherence was estimated. This study chose a frequency resolution of 0.5 Hz.
5. Sampling frequency, which was 1000 Hz.

Code G-6: $Force_{CV}$

```
force_CV=abs(std(force)/mean(force) *100;
```

Code G-7: Normalised EMG_{RMS}

```
normalised_emg_rms=(sum((emg/emg_peak).^2)/length(emg)).^0.5;
```

Code G-8: EMG_{MNF}

```
PEMG,freq]= pwelch(emg,1024,0,2000,1000));

MPF=sum(PEMG.*freq)/sum(PEMG)
```

The function consisted of five attributes:

1. Input signal.
2. Window size attribute/number of samples to use for each window. The smaller the sample size, the greater the amount of windows to be averaged.
3. Number of samples by which the sections overlapped, which was selected to be zero.
4. FFT length, which determined the frequencies at which the coherence was estimated, which allowed a frequency resolution of 0.5 Hz.
5. Sampling frequency, which was 1000 Hz.

Code G-9: EMG_{AIF}

```
Hx=hilbert(emg);
Phi_emg = atan2(imag(Hx),emg);
freq_emg=abs(diff(Phi_emg)/(1/1000));
FAIF=sum(freq_emg)/(length(freq_emg));
```

Code G-10: Normalised beta force PSD

```
[b,a] = butter(2,[15/500 35/500],'bandpass');
Force  = filtfilt(b,a, Force)
[data, freq]=pwelch(Force,1024,0,2000,1000);
sd_force_beta(subject,2)=sum(data(30:70).*freq(30:70))/sum(data.*freq);
```

The function consisting of pwelch expected five attributes:

1. Input signal.
2. Window size attribute/number of samples to use for each window. The smaller the sample size, the greater the amount of windows. This was selected to be 1024 samples in order to pick up very low frequencies.
3. Number of samples by which the sections overlapped, which was selected to be zero.
4. FFT length, which determined the frequencies at which the coherence was estimated. This study chose a frequency resolution of 0.5 Hz.
5. Sampling frequency, which was 1000 Hz.

Code G-11: Beta EEG_{RMS}

```
[b,a] = butter(4,[15/500 35/500],'bandpass');
Eeg_beta  = filtfilt(b,a,eeg(:,2:17))'
beta_eeg_rms=(sum((eeg_beta).^2)/length(eeg_eeg_beta)).^0.5;
```

Code G-12: Coherence between two signals

```
Coh_before(eeg_elec,:)=mscohere(EEG,EMG,256,0,2000,1000);
```

Each stage for each participant was a 2D matrix, which comprised the first dimension for the EEG channel used and the last dimension containing the EEG-EMG coherence values respective to their frequency.

The function required six attributes:

1. The first signal, which was an EEG channel.
2. The second signal, which was the EMG channel.
3. Window size/number of samples to use for each section. The smaller the sample size, the greater the amount of windows to be averaged for the EEG-EMG coherence value. This was selected to be 256 Hz, allowing the lowest beta band signal (i.e., 15 Hz) to be picked up at least three times (sampling rate 1000 Hz).
4. Number of samples by which the sections overlapped, which was selected to be zero.
5. FFT length, which determined the frequencies at which the coherence was estimated, which allowed a frequency resolution of 0.5 Hz.
6. Sampling frequency, which was 1000 Hz.

Code G-13: Phase lock value between two signals

```
window=ceil((6*srate)/lowerfreq);

freqdiff=0.5;

%filter signals
filtSpec.range = [lowerfreq-freqdiff upperfreq+freqdiff];
filtSpec.order = 200;
filtPts = fir1(filtSpec.order, 2/srate*filtSpec.range);
sx = filter(filtPts, 1, sx);
sy = filter(filtPts, 1, sy);

%Hilbert tranform
Hx=hilbert(sx);
Hy=hilbert(sy);

%Instantaneous Phase
Phi_Gx = atan2(imag(Hx),sx);
Phi_Gy = atan2(imag(Hy),sy);

%% PLV
expon_plv=(exp(1i.*(unwrap(Phi_Gx-(Phi_Gy)))));
plv=abs(mean(expon_plv)));
```

Code G-14: Phase lock value significance between two signals

```
%% PLV Sig
parfor shift=1:100

       Phi_Gx_shift=circshift(Phi_Gx,[ceil(((length(sx)/100)*shift)*rand(1))
       0]);
       expon_plv_sig_shift=(exp(1i.*(unwrap(Phi_Gx_shift-(Phi_Gy)))));
       expon_plv_sig_surrogate(shift)=abs(mean(mean(expon_plv_sig_shift)));

end;

plv_sig=squeeze(prctile(expon_plv_sig_surrogate,95));
```

Code G-15: 1D spectro

EMG_{POWER}:

```
[data,freq]=pwelch(EMG,1024,128,2000,1000);
EMG_Power=sum(data.*freq)
```

EMG_{MNF}:

```
[data, freq]=pwelch(EMG),1024,128,2000,1000);
        for point=11:499
                  temp(point)=abs((sum(data(point:500).*freq(point:500)
                  ))-(sum(freq(10:point).*data(10:point))));
        end;
[~,MNF(count)]= min(temp(11:499));
```

1D spectro:

```
oneDspectro=normalise(EMG_Power)-normalise(MNF);
```

Appendix H CORTICOMUSCULAR COUPLING RESULTS FOR ALL 15 PARTICIPANTS DURING PRE- AND POST-FATIGUE

The following section provides the corticomuscular coupling results for all 15 participants pre- and post-fatigue.

H.1 Beta EEG-EMG coherence$_{PEAK\ AMP}$

Participant	**Pre-Fatigue beta EEG-EMG coherence$_{PEAK\ AMP}$**	**Post-Fatigue beta EEG-EMG coherence$_{PEAK\ AMP}$**	**Decrease(↓)or Increase(↑)**
1	0.0183629717536934	0.0609836696794722	↑
2	0.0331842319037816	0.0312433296048990	↓
3	0.0321651152491742	0.0202478475756662	↓
4	0.0157468602046451	0.0238549549400445	↑
5	0.0233762144459524	0.0629043567283901	↑
6	0.0137496300937412	0.0297720933818294	↑
7	0.0327403541191855	0.0397166919356443	↑
8	0.0236315332652836	0.0162752257284659	↓
9	0.0224265174473097	0.0344548758946102	↑
10	0.0298976727827585	0.0276243918237810	↓
11	0.0122452782616103	0.0156622527293475	↑
12	0.0293205416472235	0.0508640843044285	↑
13	0.0224692930070013	0.0251859879491958	↑
14	0.0216399718859184	0.0371458461535892	↑
15	0.0177939818521451	0.0406366950520167	↑

H.2 Beta EEG-EMG PLV $_{PEAK\ AMP}$

Participant	**Pre-Fatigue beta EEG-EMG PLV $_{PEAK\ AMP}$**	**Post-Fatigue beta EEG-EMG PLV $_{PEAK\ AMP}$**	**Decrease(↓)or Increase(↑)**
1	0.0931124706446549	0.172843327929132	↑
2	0.126358769308164	0.133789600211654	↑
3	0.117449547960637	0.0931338851179774	↓
4	0.109680293834906	0.110812580995039	↑
5	0.0908576213232329	0.181183226852361	↑
6	0.113626944735515	0.137949902211405	↑
7	0.0768013270210087	0.132532752357386	↑
8	0.105540755526864	0.0892700599950594	↓
9	0.0908117620071869	0.139186781042359	↑
10	0.0977317870007614	0.0765789778134839	↓
11	0.110706327658335	0.115211951737522	↑
12	0.119766324784115	0.143881462790900	↑
13	0.0868084186408449	0.0993445340396393	↑
14	0.0868503404140767	0.111693699624352	↑
15	0.106079830280569	0.135217693379313	↑

H.3 EEG-EMG PLV and EEG-EMG Coherence Pre- and Post-fatigue Waveforms

---- CL ---pre-fatigue ----post-fatigue --- pre-fatigue significance ---post-fatigue significance

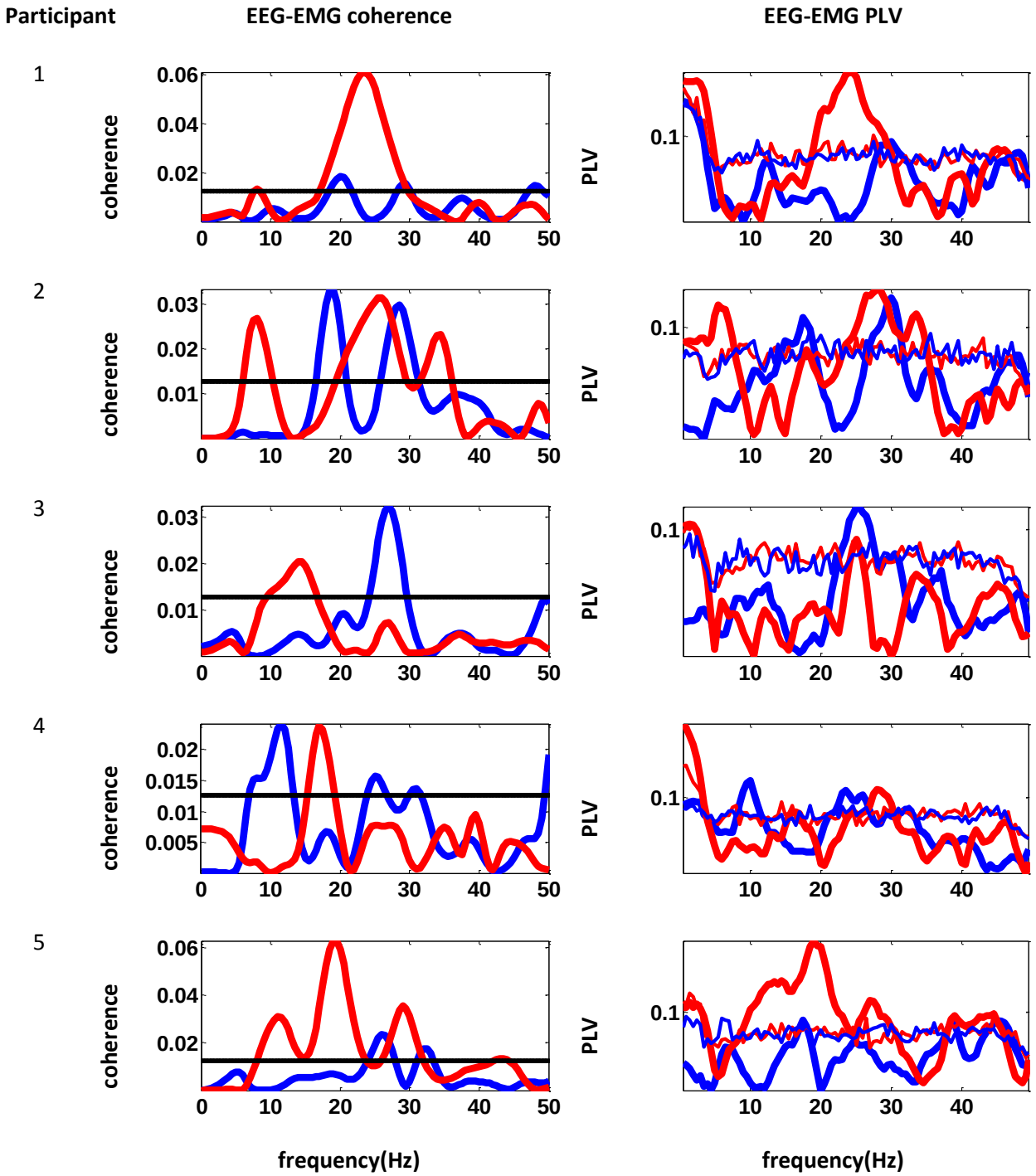

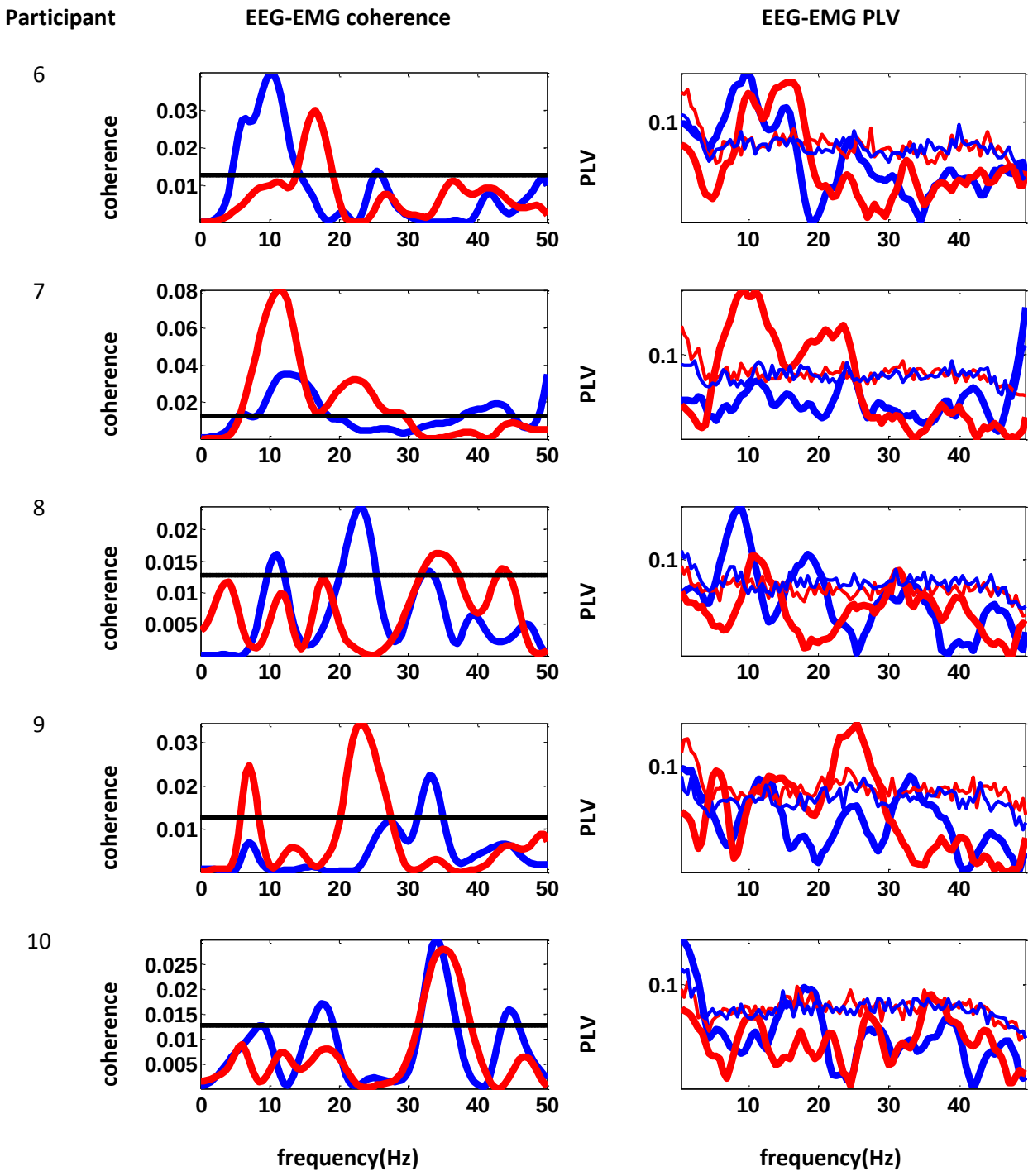
Participant
EEG-EMG coherence
EEG-EMG PLV
6
7
8
9
10
coherence
PLV
0.03
0.02
0.01
0.08
0.06
0.04
0.02
0.015
0.005
0.025
0.1
0
10
20
30
40
50
frequency(Hz)

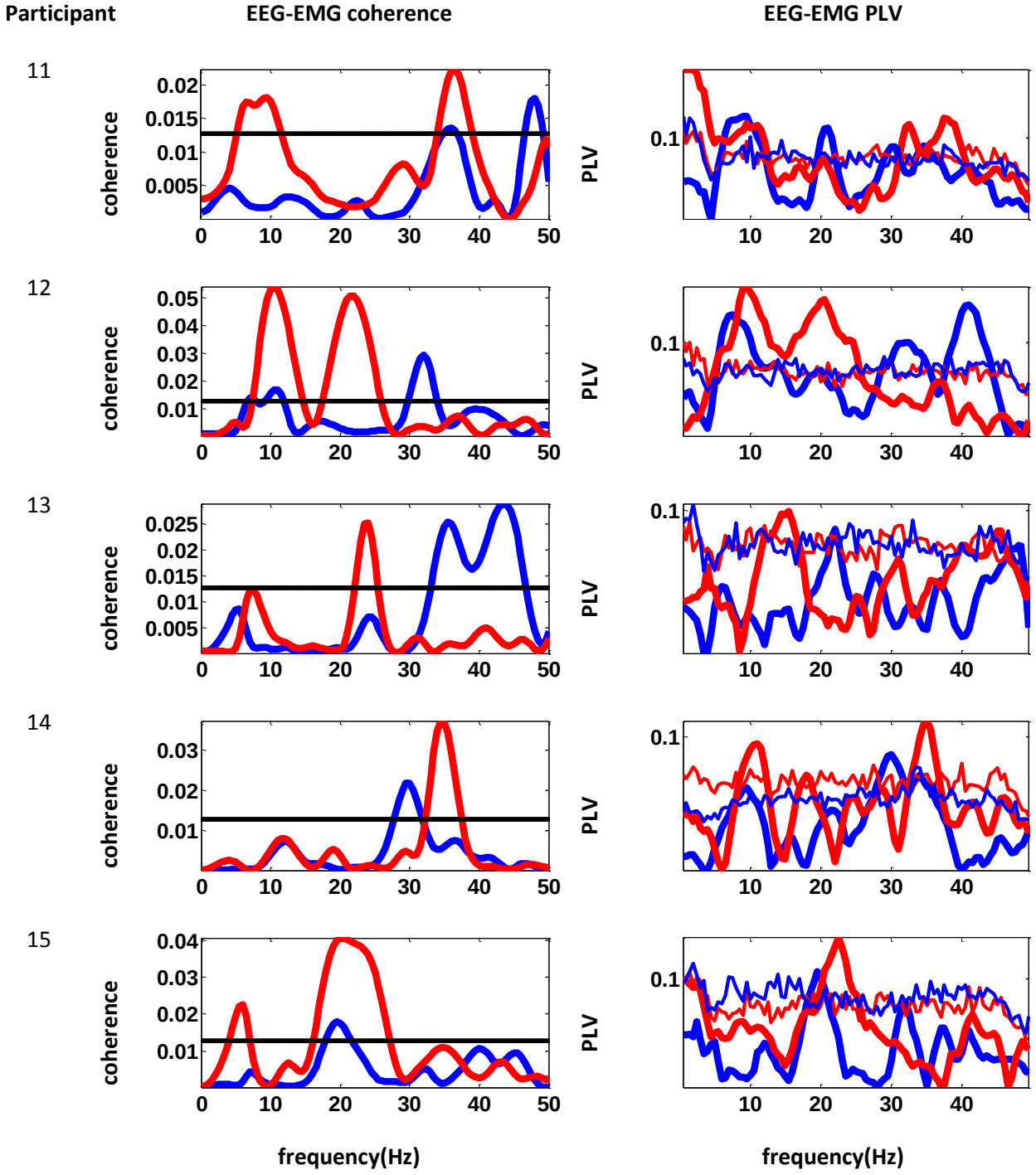
Participant
EEG-EMG coherence
EEG-EMG PLV
11
12
13
14
15
coherence
PLV
frequency(Hz)
frequency(Hz)

Appendix I CORTICOMUSCULAR COUPLING RESULTS FOR ALL 15 PARTICIPANTS DURING THE FIRST AND SECOND PART OF THE FATIGUE STAGE

The following section provides the corticomuscular coupling results for all 15 participants during the first and second fatigue stage.

I.1 beta EEG-EMG coherence$_{PEAK\ AMP}$

Participant	First part of the fatigue stage beta EEG-EMG coherence$_{PEAK\ AMP}$	Second part of the fatigue stage beta EEG-EMG coherence$_{PEAK\ AMP}$	Decrease(↓)or Increase(↑)
1	0.0644897469361312	0.0361004408282405	↓
2	0.0489997087618671	0.0334889901961487	↓
3	0.0396260076007534	0.0270491863364569	↓
4	0.0588389270528980	0.0392330773108138	↓
5	0.0923641140131857	0.0832587521636676	↓
6	0.0515979284588585	0.0367338546390713	↓
7	0.0570734413996620	0.0804151383008023	↑
8	0.0624438015702863	0.0415229241971975	↓
9	0.0596052123463371	0.0366588446045059	↓
10	0.0483457945120075	0.0347416379317567	↓
11	0.0688759170183508	0.0372479705412022	↓
12	0.0350541423500456	0.0261938015901441	↓
13	0.0430388682818212	0.0361477667474020	↓
14	0.0794176761205572	0.0515376864645929	↓
15	0.0779480320668481	0.0270927106470108	↓

I.2 beta EEG-EMG PLV $_{PEAK\ AMP}$

Participant	First part of the fatigue stage beta EEG-EMG PLV $_{PEAK\ AMP}$	Second part of the fatigue stage beta EEG-EMG PLV $_{PEAK\ AMP}$	Decrease(↓)or Increase(↑)
1	0.129303855500476	0.113379173730370	↓
2	0.128960310418971	0.163137595566550	↑
3	0.138390474084314	0.122871956833493	↓
4	0.141463007475027	0.170013063631083	↑
5	0.240654256884577	0.267478811772516	↑
6	0.136529383933236	0.136242986513911	↓
7	0.143291974531524	0.210705736259326	↑
8	0.124084785172180	0.143676674051873	↑
9	0.137277588461526	0.151426593947092	↑
10	0.120331108051706	0.160588204259055	↑
11	0.158807268263484	0.153206879094984	↓
12	0.175515078172112	0.119185461410642	↓
13	0.113242152336277	0.132415176885495	↓
14	0.216992475238212	0.186052618754417	↑
15	0.209305457192911	0.161777919016205	↓

I.3 EEG-EMG PLV and EEG-EMG coherence pre- and post-fatigue waveforms

---- CL ---pre-fatigue ----post-fatigue --- pre-fatigue significance ---post-fatigue significance

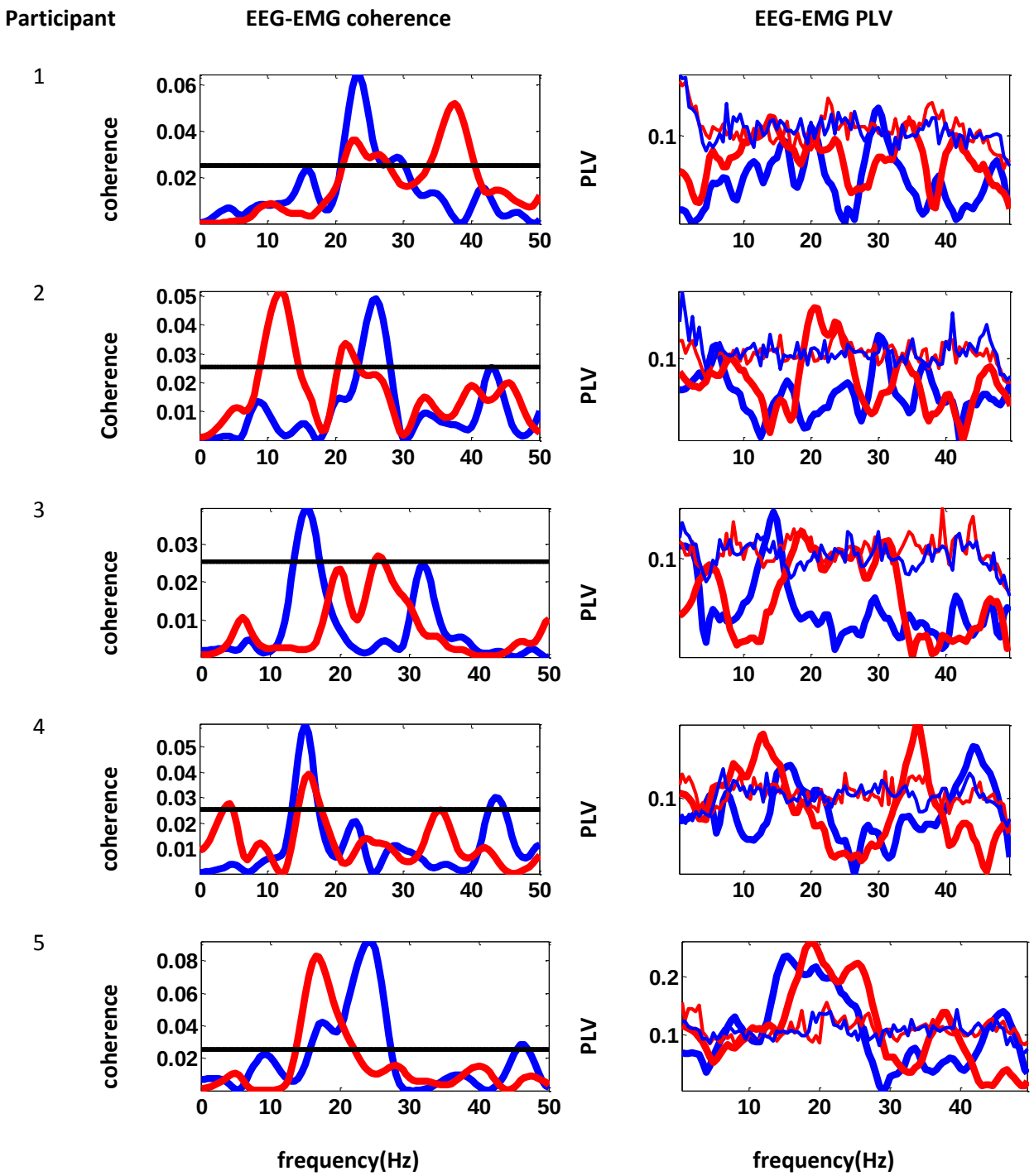

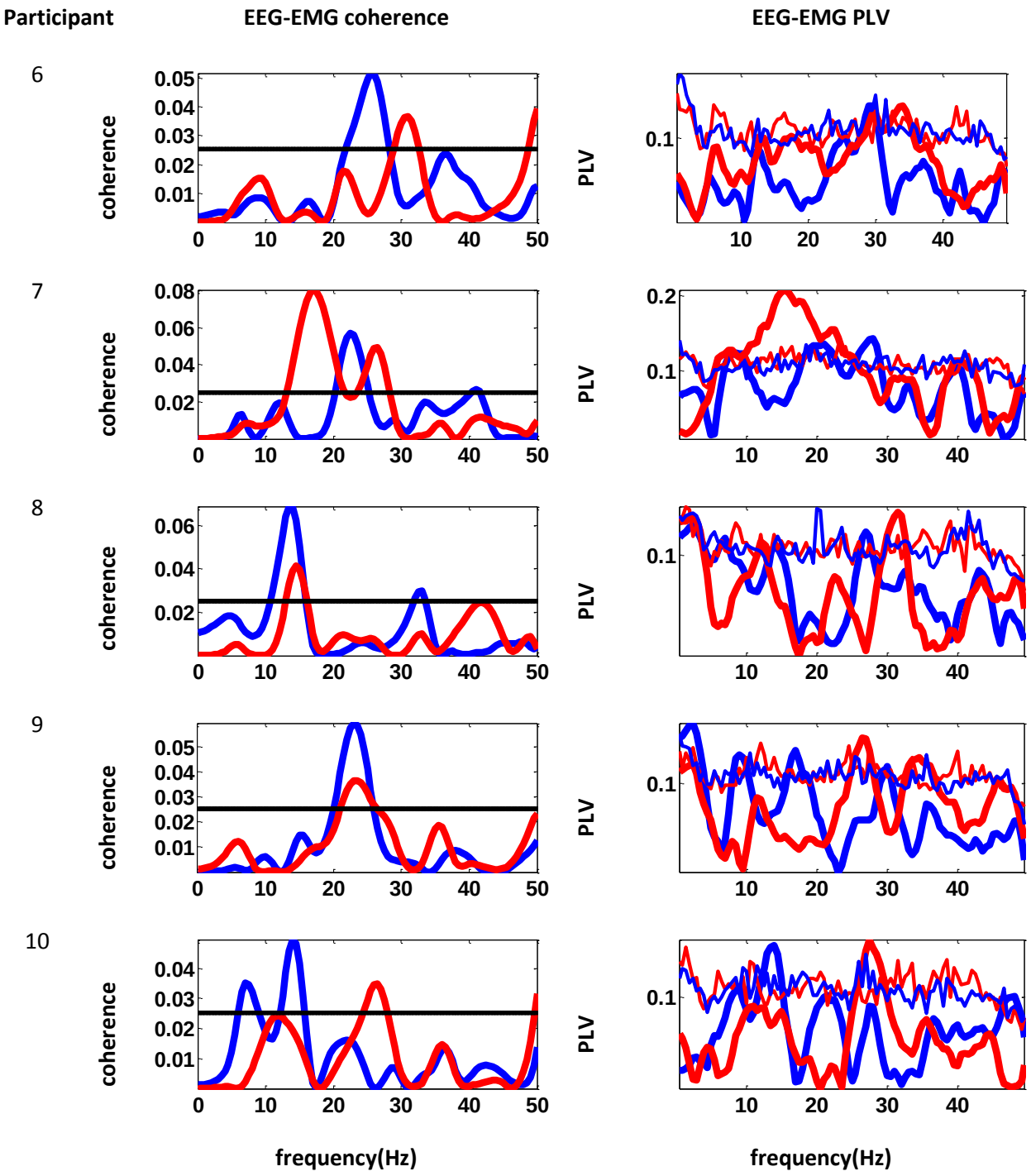
Participant
EEG-EMG coherence
EEG-EMG PLV
6
7
8
9
10
coherence
PLV
frequency(Hz)
frequency(Hz)

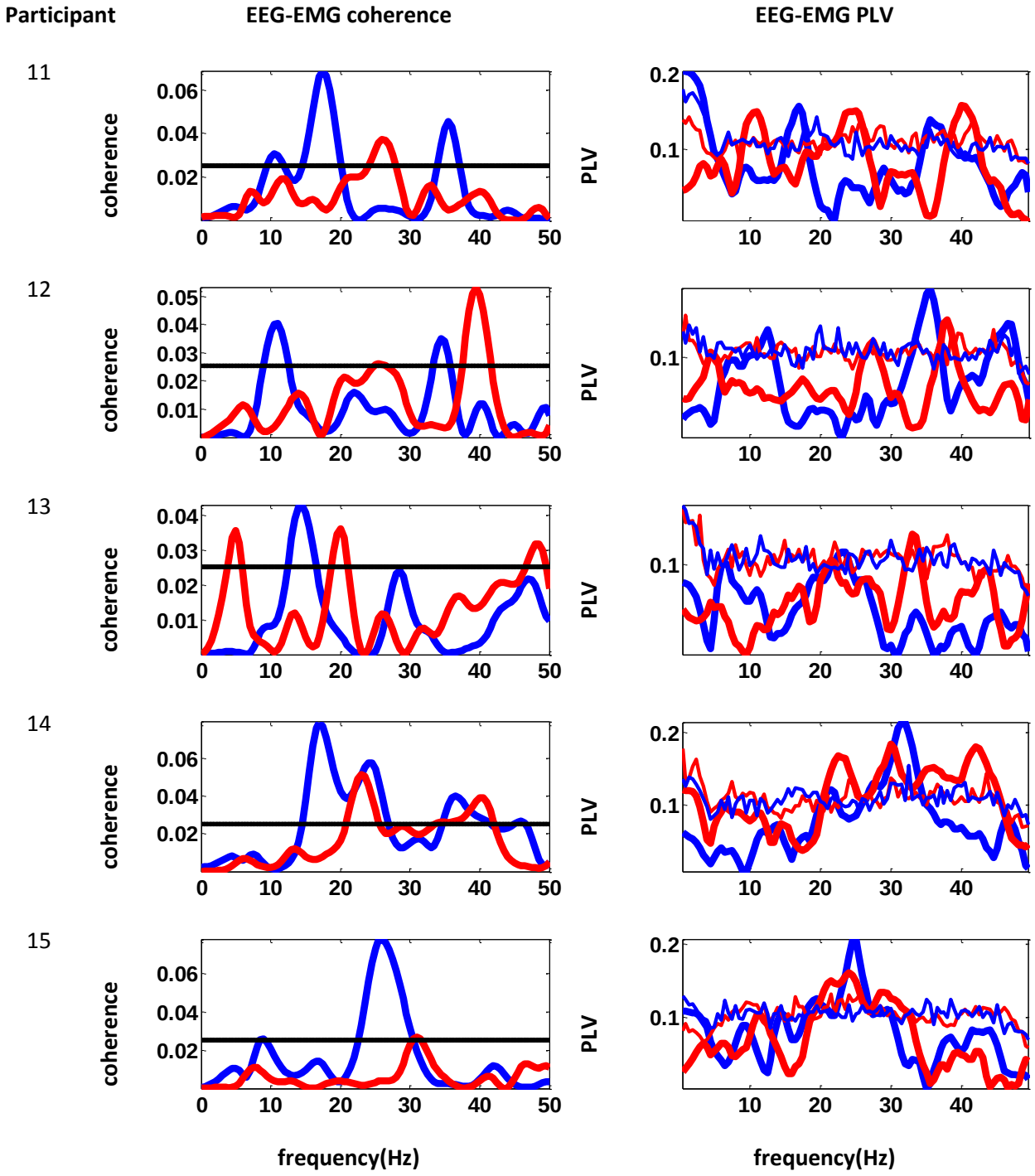
Participant
EEG-EMG coherence
EEG-EMG PLV
11
12
13
14
15
coherence
PLV
frequency(Hz)
frequency(Hz)

Appendix J DETAILED QUANTITATIVE RESULTS

Appendix J contains the results of the statistical comparisons of the neurophysiological variables, which were noted in Section 3.1. All data are represented as (means (M) ± standard deviation (SD)), and significance of a factor conforms to $p < 0.05$.

J.1 Muscle fatigue influence on force, EMG and EEG pre- and post-fatigue

Section J.1 follows from Section 3.1.2 and provides the quantitative statistics as mentioned in Section 2.2.7 for all 15 participants for the observed measures pre- and post-fatigue:

1. $force_{CV}$
2. normalised beta $force_{PSD}$
3. normalised EMG_{RMS}
4. EMG_{MPF}
5. normalised beta EEG_{RMS}

As mentioned in Section 2.2.7, testing for assumptions was done for each measure. The observation of outliers was shown in the box-plots below each measure. The tests for normality were shown in the tables below each measure. Box plots for all measures, showed no outliers, and the results of all Shapiro-Wilk tests of normality, showed a $p > 0.05$, indicating an approximate normal distribution in each respective measure.

J.1.1 Force$_{CV}$ comparisons between pre- and post-fatigue (see also Figure 3-2d)

The force$_{CV}$ significantly increased from pre-fatigue to post-fatigue (3.473 ± 2.269 to 7.873 ± 5.568%, p = 0.001).

See Figure J-1 for the box plot and Table J-1 for the normality test.

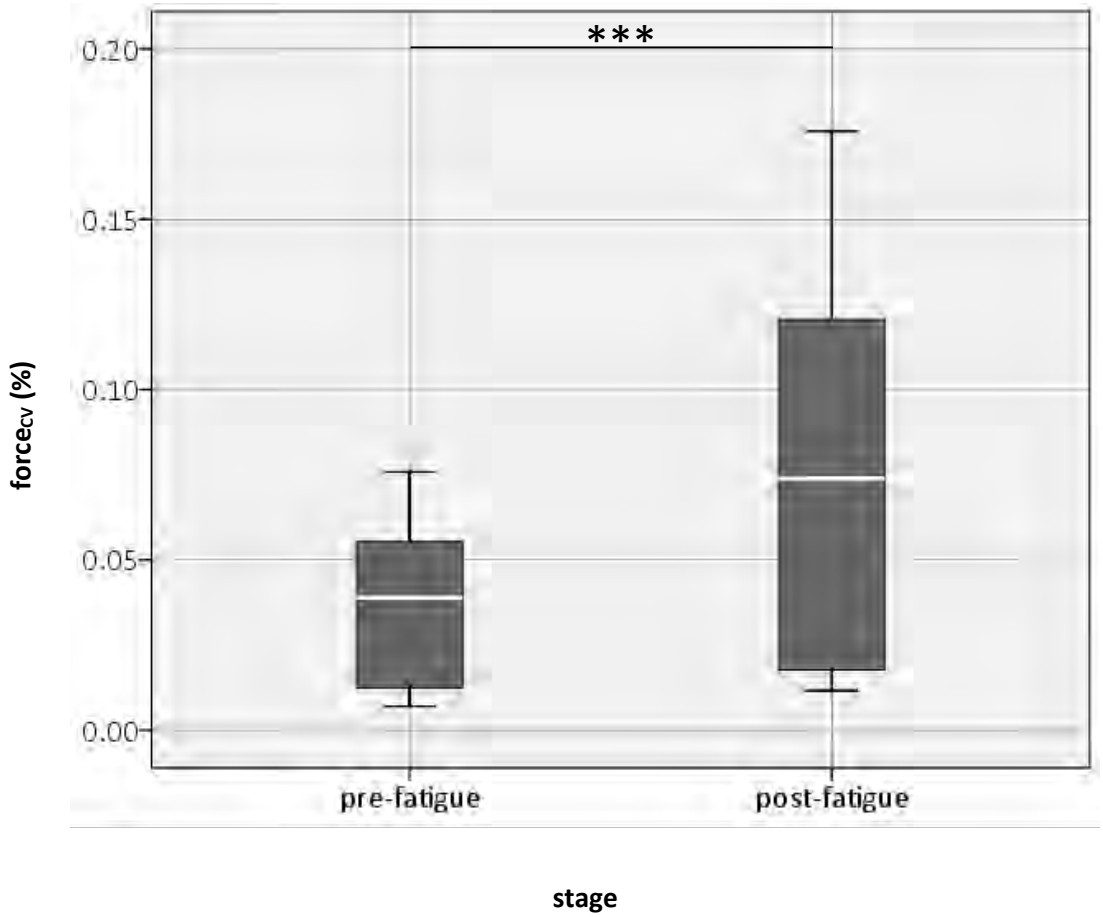

Figure J-1: Box plot of the force$_{CV}$ between pre- and post-fatigue. Significant differences are denoted by: * (p < 0.05), ** (p < 0.01) and *** (p < 0.001).

Table J-1: Shapiro-Wilk test of normality for the force$_{CV}$, pre- and post-fatigue using SPSS.

Stage		Shapiro-Wilk		
		Statistic	df	Sig.
Force$_{CV}$	Pre-fatigue	.924	15	.221
	Post-fatigue	.919	15	.187

J.1.2 Normalised beta force$_{PSD}$ comparisons between pre- and post-fatigue (see also Figure 3-2e)

The normalised beta force$_{PSD}$ significantly increased from pre-fatigue to post-fatigue (0.004 ± 0.001 to 0.005 ± 0.001, p = 0.014).

See Figure J-2 for the box plot and Table J-2 for the normality test.

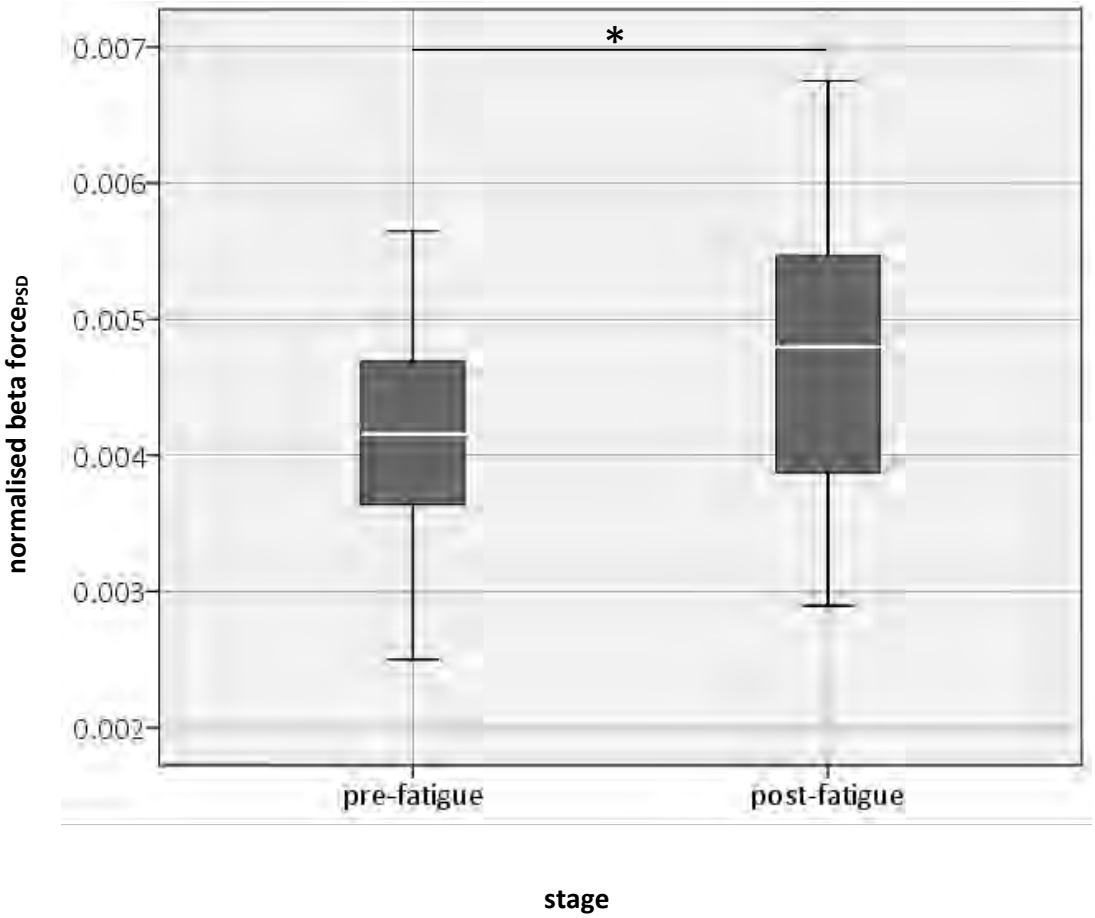

Figure J-2: Box plot of beta the force$_{PSD}$ between pre- and post-fatigue. Significant differences are denoted by: * (p < 0.05), ** (p < 0.01) and *** (p < 0.001).

Table J-2: Shapiro-Wilk test of normality for the normalised beta force$_{PSD}$ pre- and post-fatigue using SPSS.

Stage		Shapiro-Wilk		
		Statistic	df	Sig.
Normalised beta force$_{PSD}$	Pre-fatigue	.973	15	.905
	Post-fatigue	.951	15	.545

J.1.3 Normalised EMG_{RMS} comparisons between pre- and post-fatigue (see also Figure 3-2f)

The normalised EMG_{RMS} significantly increased from pre-fatigue to post-fatigue (0.037 ± 0.022 to 0.051 ± 0.033, p = 0.017).

See Figure J-3 for the box plot and Table J-3 for the normality test.

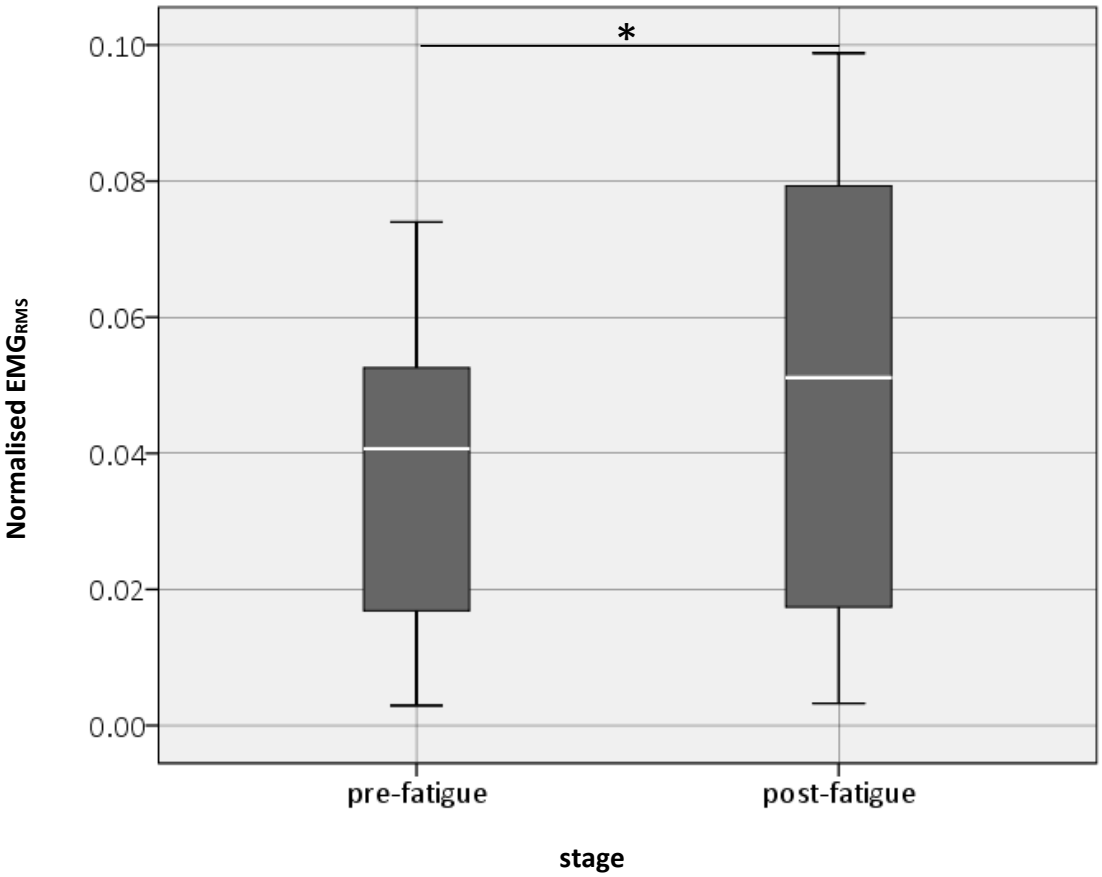

Figure J-3: Box plot of the normalised EMG_{RMS} between pre- and post-fatigue. Significant differences are denoted by: * (p < 0.05), ** (p < 0.01) and *** (p < 0.001).

Table J-3: Shapiro-Wilk test of normality for the normalised EMG_{RMS} pre- and post-fatigue using SPSS.

Stage		Shapiro-Wilk		
		Statistic	df	Sig.
Normalised EMG_{RMS}	Pre-fatigue	.925	15	.233
	Post-fatigue	.929	15	.266

J.1.4 EMG_{MPF} comparisons between pre- and post-fatigue (see also Figure 3-2g)

The EMG_{MPF} decreased significantly from pre-fatigue to post-fatigue (100.589 ± 17.366 to 86.948 ± 19.814 Hz, p = 0.001).

See Figure J-4 for the box plot and Table J-4 for the normality test.

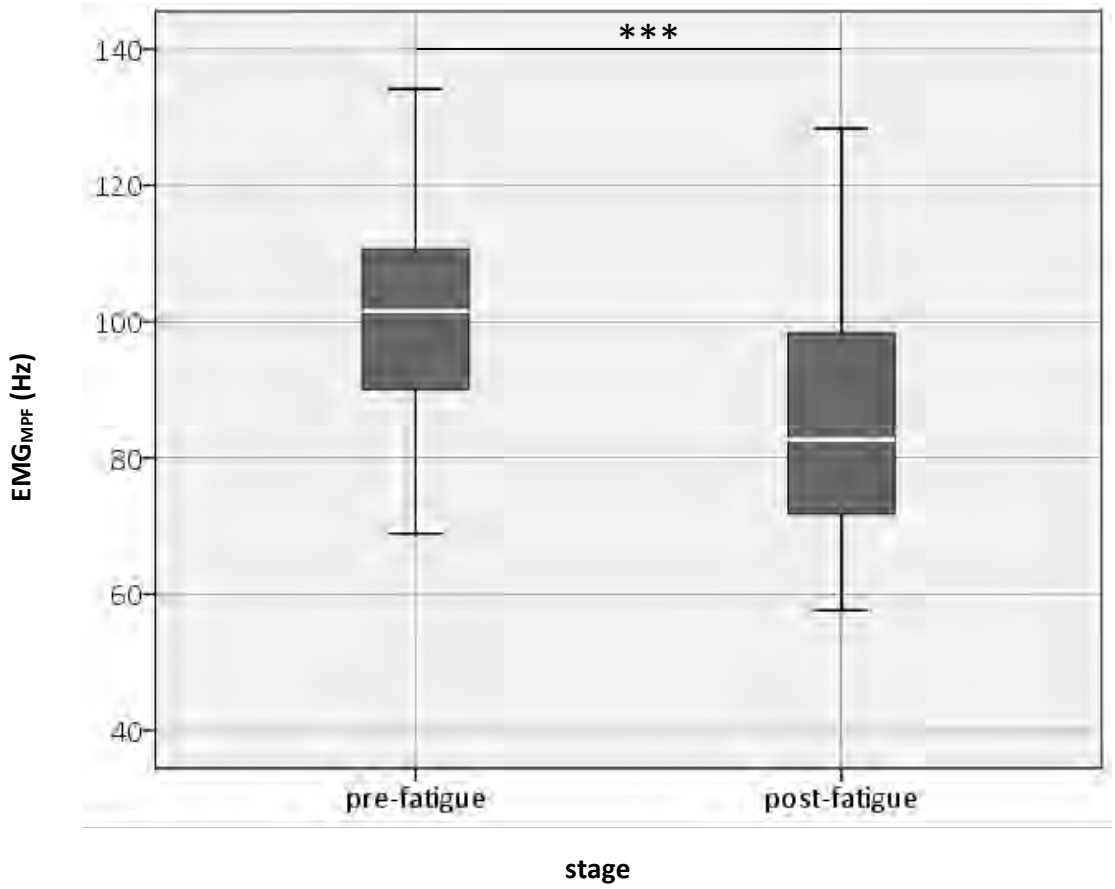

Figure J-4: Box plot of the EMG_{MPF} between pre- and post-fatigue where ˚ (number) indicates a participant who is a mild outlier. Significant differences denoted by: * (p < 0.05), ** (p < 0.01) and *** (p < 0.001).

Table J-4: Shapiro-Wilk test of normality for the EMG_{MPF} pre- and post-fatigue using SPSS.

Stage		Shapiro-Wilk		
		Statistic	df	Sig.
EMG_{MPF}	Pre-fatigue	.985	15	.993
	Post-fatigue	.965	15	.779

J.1.5 Normalised beta EEG_{RMS} comparisons between pre- and post-fatigue (see also Figure 3-2h)

The normalised beta EEG_{RMS} significantly increased from pre-fatigue to post-fatigue (0.043 ± 0.017 to 0.048 ± 0.021, p=0.025).

See Figure J-5 for the box plot and Table J-5 for the normality test.

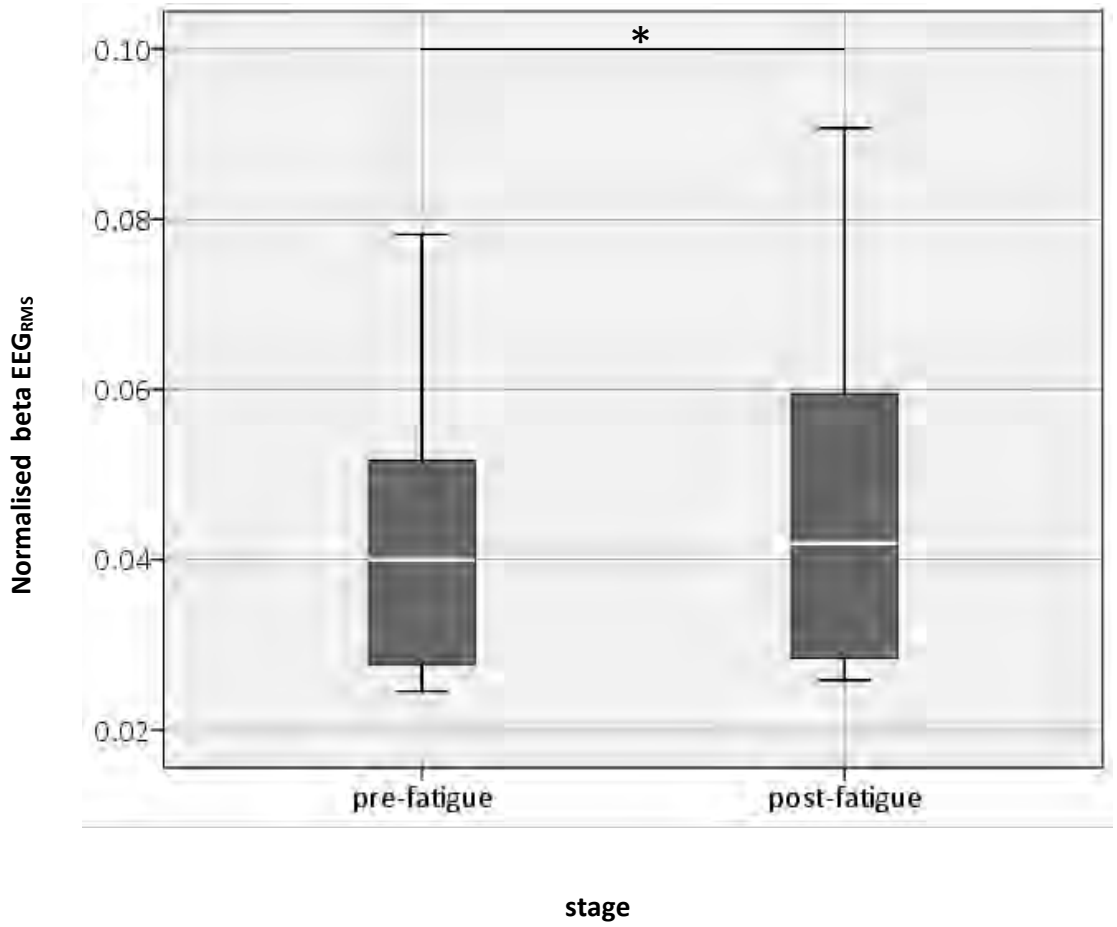

Figure J-5: Box plot of the normalised beta EEG_{RMS} between pre- and post-fatigue. Significant differences are denoted by: * ($p < 0.05$), ** ($p < 0.01$) and *** ($p < 0.001$).

Table J-5: Shapiro-Wilk test of normality for the normalised beta EEG_{RMS} pre- and post-fatigue using SPSS.

Stage		Shapiro-Wilk		
		Statistic	df	Sig.
Normalised beta EEG_{RMS}	Pre-fatigue	.903	15	.106
	Post-fatigue	.898	15	.090

J.2 Corticomuscular coupling measures pre- and post-fatigue

Section J.2 follows Section 3.1.3.3 and provides the quantitative statistics as mentioned in Section 2.3.6 for all 15 participants for the observed measures pre- and post-fatigue:

1. beta EEG-EMG coherence $_{PEAK\ AMP}$
2. beta EEG-EMG coherence $_{PEAK\ FREQ}$
3. beta EEG-EMG $PLV_{PEAK\ AMP}$
4. beta EEG-EMG $PLV_{PEAK\ FREQ}$

As mentioned in Section 2.3.6, testing for assumptions was done for each measure. The observation of outliers was shown in the box-plots below each measure. The tests for normality were shown in the tables below each measure. Box plots for all measures, showed no outliers, and the results of all Shapiro-Wilk tests of normality, showed a $p > 0.05$, indicating an approximate normal distribution in each respective measure.

J.2.1 Beta EEG-EMG coherence $_{PEAK\ AMP}$ comparisons between pre- and post-fatigue (See also Figure 3-5a)

The beta EEG-EMG coherence $_{PEAK\ AMP}$ significantly increased from pre-fatigue to post-fatigue (0.023 ± 0.007 to 0.034 ± 0.017, p = 0.008).

See Figure J-6 for the box plot and Table J-6 for the normality test.

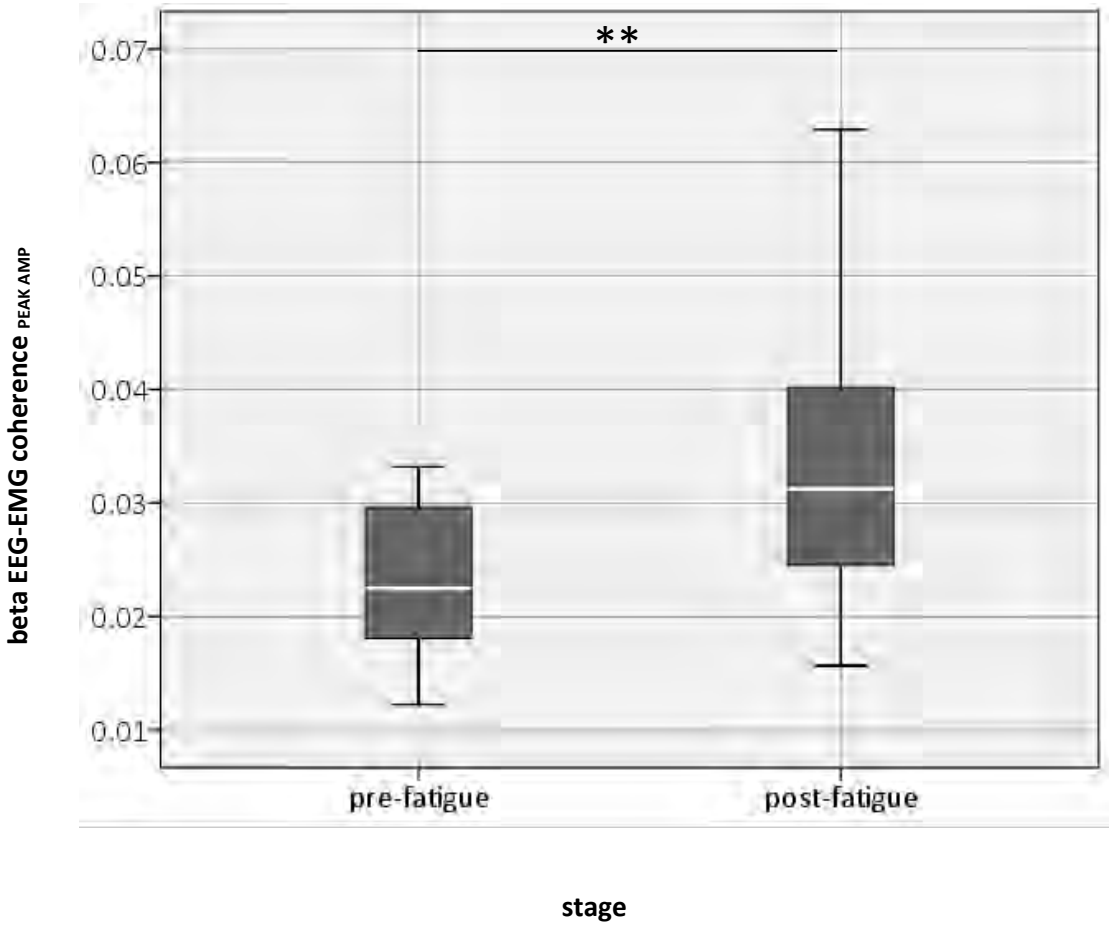

Figure J-6: Box plot of the beta EEG-EMG coherence $_{PEAK\ AMP}$ between pre- and post-fatigue. Significant differences denoted by: * (p < 0.05), ** (p < 0.01) and *** (p < 0.001).

Table J-6: Shapiro-Wilk test of normality for the beta EEG-EMG coherence $_{PEAK\ AMP}$ pre- and post-fatigue using SPSS.

Stage		Shapiro-Wilk		
		Statistic	df	Sig.
Beta EEG-EMG coherence$_{PEAK\ AMP}$	Pre-fatigue	.936	15	.336
	Post-fatigue	.928	15	.251

J.2.2 Beta EEG-EMG coherence $_{PEAK\ FREQ}$ between pre- and post-fatigue (see also Figure 3-5a)

The beta EEG-EMG coherence $_{PEAK\ FREQ}$ did not differ significantly from pre-fatigue to post-fatigue (26.967± 6.399 to 24.33 ± 7.459 Hz, p = 0.195).

See Figure J-7 for the box plot and Table J-7 for the normality test.

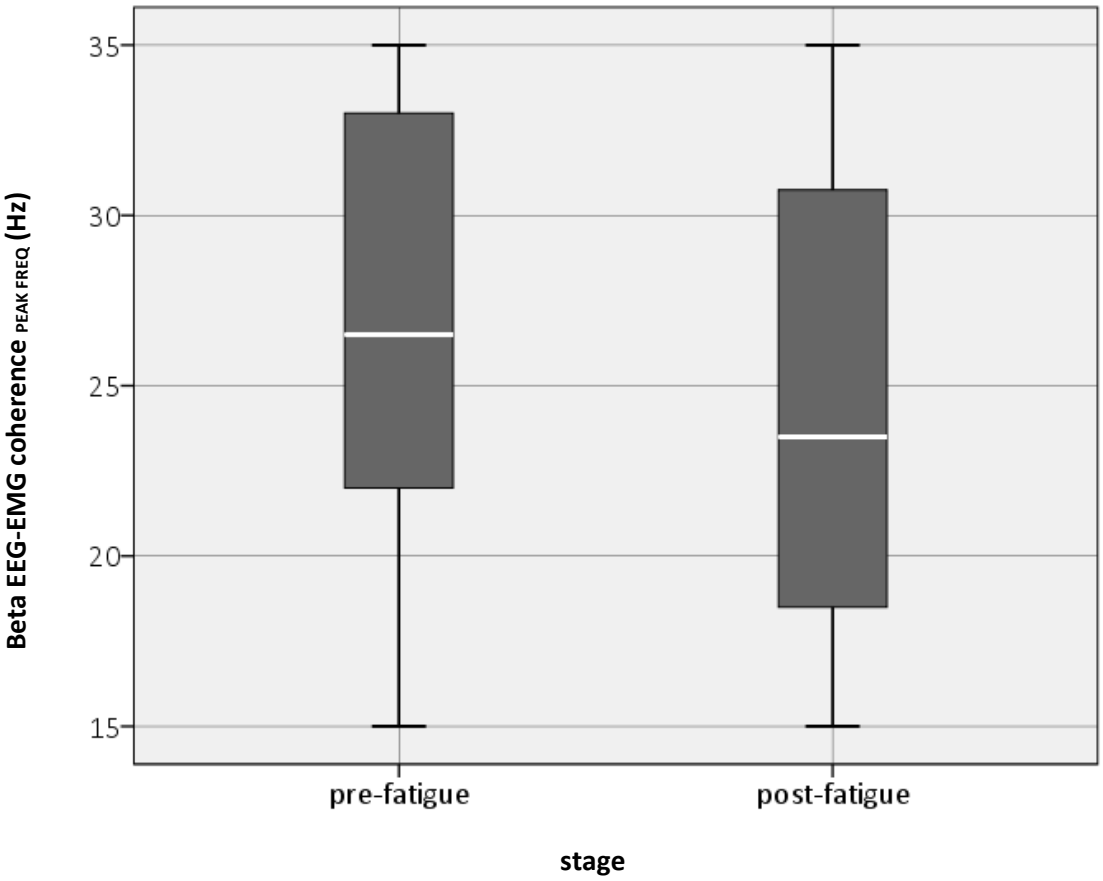

Figure J-7: Box plot of the beta EEG-EMG coherence $_{PEAK\ FREQ}$ between pre- and post-fatigue.

Table J-7: Shapiro-Wilk test of normality for the beta EEG-EMG coherence $_{PEAK\ FREQ}$ pre- and post-fatigue using SPSS.

Stage		Shapiro-Wilk		
		Statistic	df	Sig.
Beta EEG-EMG coherence $_{PEAK\ FREQ}$	Pre-fatigue	.936	15	.336
	Post-fatigue	.928	15	.251

J.2.3 Beta EEG-EMG $PLV_{PEAK\ AMP}$ comparisons between pre and post fatigue (see also Figure 3-5b)

The beta EEG-EMG $PLV_{PEAK\ AMP}$ significantly increased from pre-fatigue to post-fatigue (0.102 ± 0.014 to 0.125 ± 0.029, p = 0.011).

See Figure J-8 for the box plot and Table J-8 for the normality test.

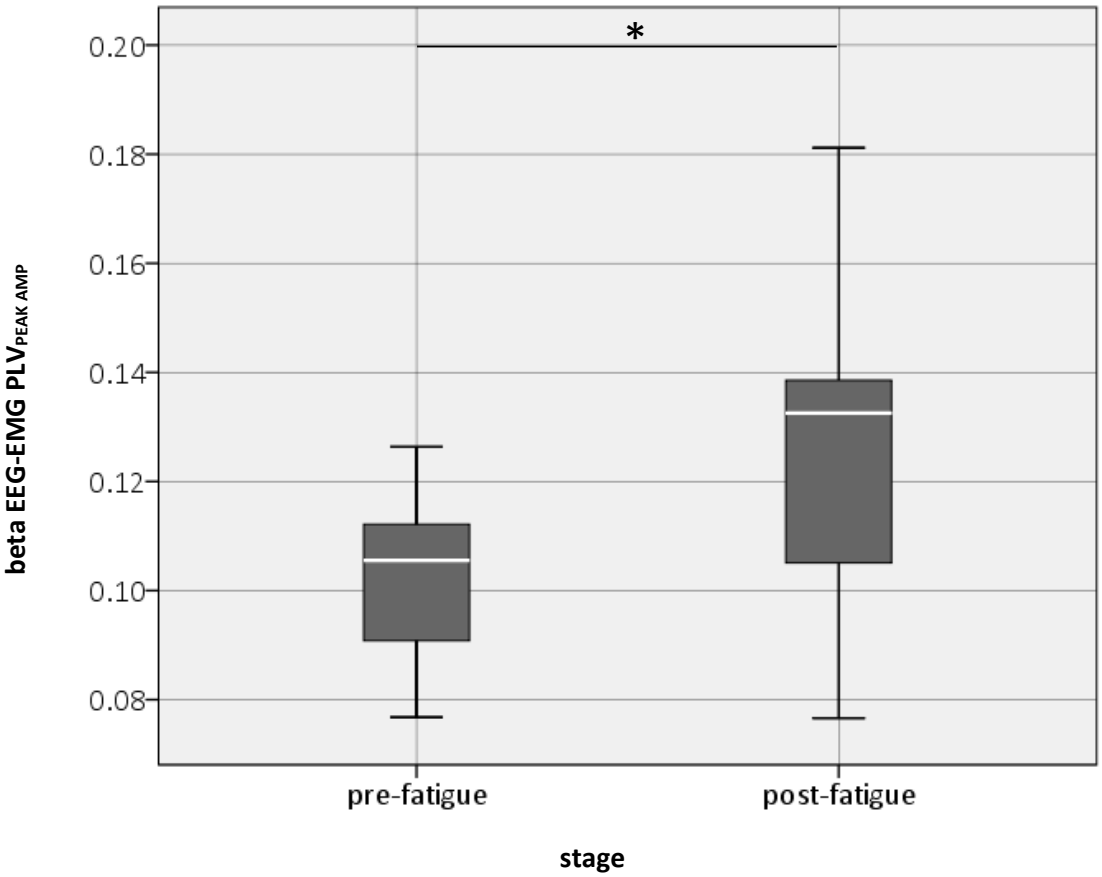

Figure J-8: Box plot of the beta EEG-EMG $PLV_{PEAK\ AMP}$ between pre- and post-fatigue. Significant differences denoted by: * (p < 0.05), ** (p < 0.01) and *** (p < 0.001).

Table J-8: Shapiro-Wilk test of normality for the beta EEG-EMG $PLV_{PEAK\ AMP}$ pre- and post-fatigue using SPSS.

Stage		Shapiro-Wilk		
		Statistic	df	Sig.
Beta EEG-EMG $PLV_{PEAK\ AMP}$	Pre-fatigue	.967	15	.809
	Post-fatigue	.961	15	.716

J.2.4 Beta EEG-EMG $PLV_{PEAK\ FREQ}$ between pre- and post-fatigue (see also Figure 3-5b)

The beta EEG-EMG $PLV_{PEAK\ FREQ}$ did not differ significantly from pre-fatigue to post-fatigue (23.967± 5.835 Hz to 24.8 ± 5.64 Hz, p = 0.686).

See Figure J-9 for the box plot and Table J-9 for the normality test.

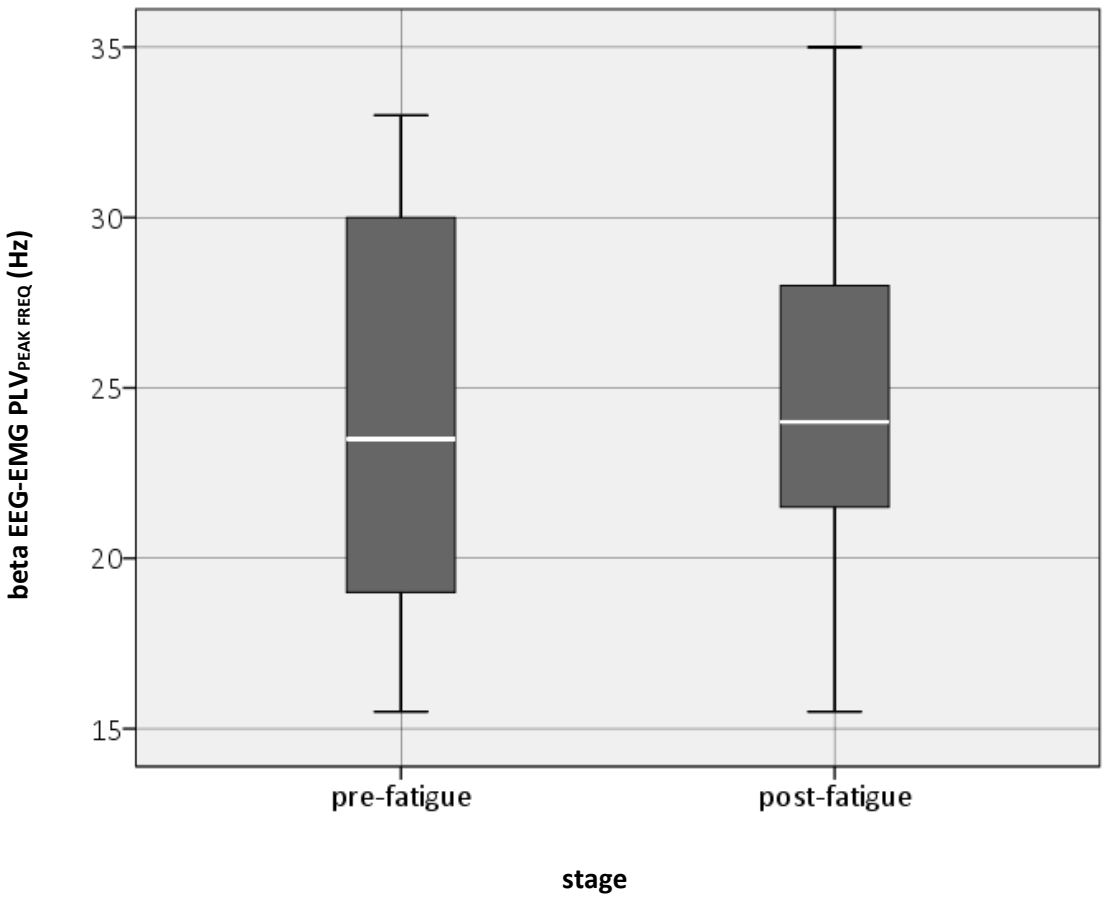

Figure J-9: Box plot of the beta EEG-EMG $PLV_{PEAK\ FREQ}$ between pre- and post-fatigue.

Table J-9: Shapiro-Wilk test of normality for the beta EEG-EMG $PLV_{PEAK\ FREQ}$ pre- and post-fatigue using SPSS.

Stage		Shapiro-Wilk		
		Statistic	df	Sig.
Beta EEG-EMG $PLV_{PEAK\ FREQ}$	Pre-fatigue	.922	15	.206
	Post-fatigue	.974	15	.917

J.3 Measures during the first and second part of the fatigue stage

Section J.3 follows from Section 3.1.3.4 and Section 3.1.3.4 and provides the quantitative statistics, as mentioned in Section 2.3.7, for all 15 participants for the observed measures during the first and second part of the fatigue stage:

1. normalised beta EMG_{RMS}
2. normalised beta EEG_{RMS}
3. beta EEG-EMG coherence $_{PEAK\ AMP}$
4. beta EEG-EMG $PLV_{PEAK\ AMP}$

As mentioned in Section 2.3.7, testing for assumptions was done for normalised beta EMG_{RMS} and normalised beta EEG_{RMS}. The observation of outliers was shown in the box-plots below each measure. The tests for normality were shown in the tables below each measure. Box plots for all measures, showed no outliers, and the results of all Shapiro-Wilk tests of normality, showed a $p > 0.05$, indicating an approximate normal distribution in each respective measure.

J.3.1 Normalised beta EMG_{RMS} comparisons during the first and second part of the fatigue stage (see also Figure 3-6d)

The normalised beta EMG_{RMS} significantly increased from the first to the second part of the fatigue stage (0.096 ± 0.081 to 0.122 ± 0.081, p = 0.004).

See Figure J-10 for the box plot and Table J-10 for the normality test.

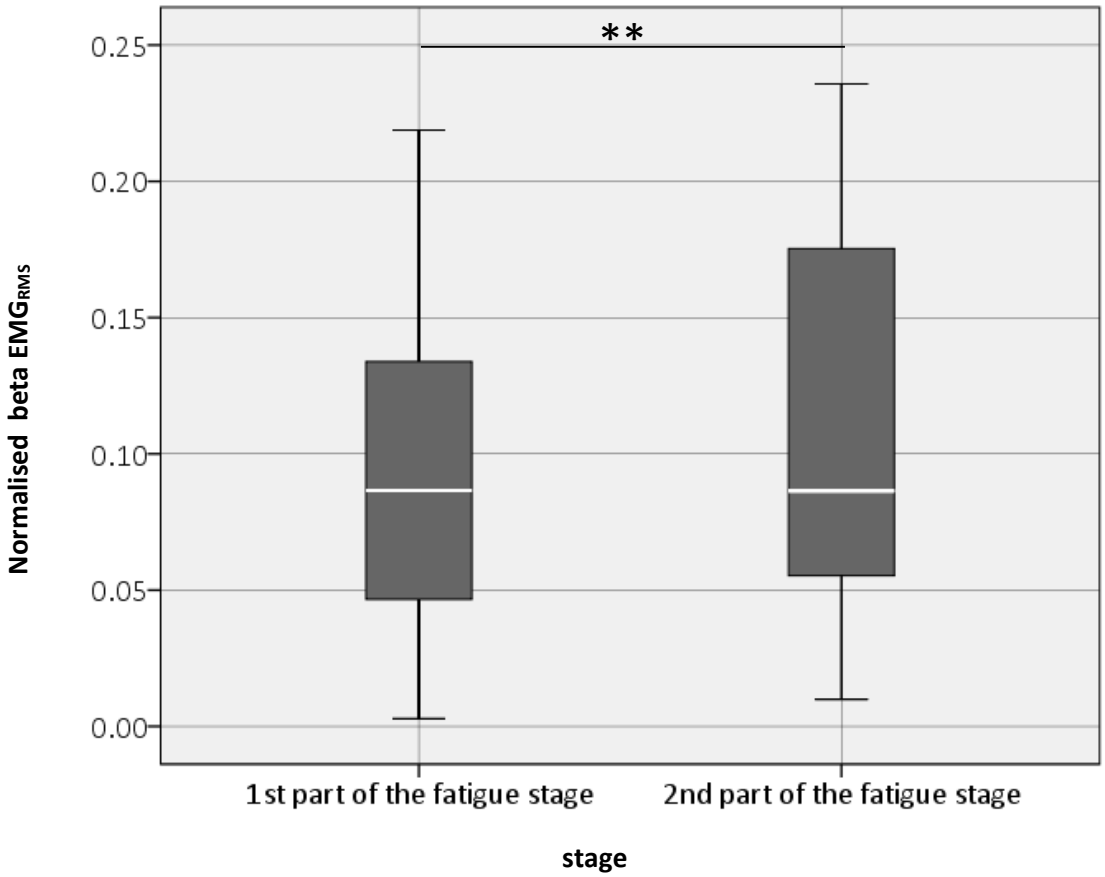

Figure J-10: Box plot of the normalised beta EMG_{RMS} during the first and second part of the fatigue stage. Significant differences are denoted by: * (p < 0.05), ** (p < 0.01) and *** (p < 0.001).

Table J-10: Shapiro-Wilk test of normality for the normalised beta EMG_{RMS} during the first and second part of the fatigue stage.

Stage		Shapiro-Wilk		
		Statistic	df	Sig.
Normalised beta EMG_{RMS}	first part of the fatigue stage	.949	15	.511
	second part of the fatigue stage	.902	15	.102

J.3.2 Normalised beta EEG_{RMS} comparisons during the first and second part of the fatigue stage (see also Figure 3-6e)

The normalised beta EEG_{RMS} did not differ from the first to the second part of the fatigue stage (0.089 ± 0.061 to 0.095 ± 0.055, p = 0.135).

See Figure J-11 for the box plot and Table J-11 for the normality test.

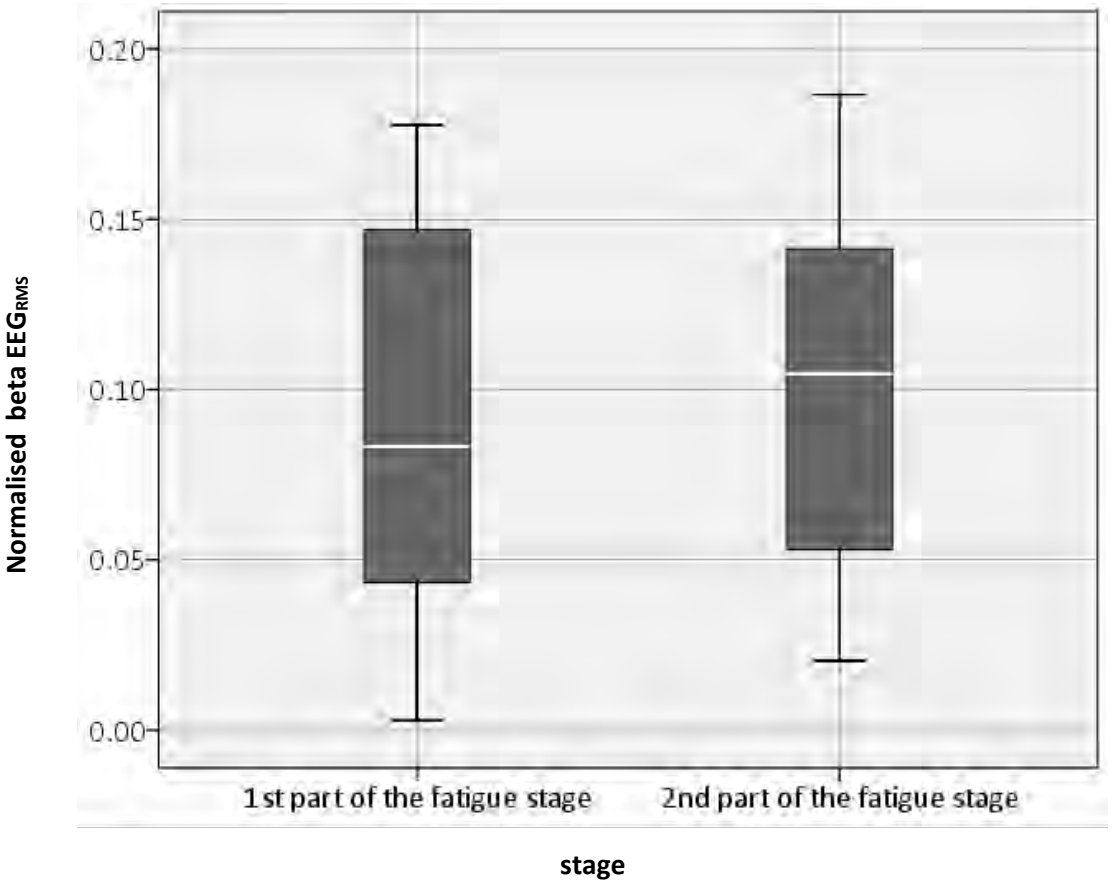

Figure J-11: Box plot of the normalised beta EEG_{RMS} during the first and second part of the fatigue stage.

Table J-11: Shapiro-Wilk test of normality for the normalised beta EEG_{RMS} during the first and second part of the fatigue stage.

Stage		Shapiro-Wilk		
		Statistic	df	Sig.
Normalised beta EEG_{RMS}	first part of the fatigue stage	.915	15	.184
	second part of the fatigue stage	.908	15	.149

J.3.3 Beta EEG-EMG coherence $_{PEAK\ AMP}$ comparisons during the first and second part of the fatigue stage (see also Figure 3-7a)

The beta EEG-EMG coherence$_{PEAK\ AMP}$ significantly decreased from the first to the second part of the fatigue stage (0.059 ± 0.016 to 0.042 ± 0.017, p = 0.001). See Table J-12 for the non-parametric signed test results.

Table J-12: Non-parametric signed test of the beta EEG-EMG coherence$_{PEAK\ AMP}$ for the first part of the fatigue stage compared to the second part of the fatigue stage using SPSS.

Comparisons from the first to the second part of the fatigue stage	Number of participants
decreased	14
increased	1

J.3.4 Beta EEG-EMG PLV $_{PEAK\ AMP}$ comparisons during the first and second part of the fatigue stage (see also Figure 3-7b)

The beta EEG-EMG PLV $_{PEAK\ AMP}$ did not differ from the first to the second part of the fatigue stage (0.154 ± 0.039 to 0.16 ± 0.04, p = 1.000). See Table J-13 for the non-parametric signed test results.

Table J-13: Non-parametric signed test of the beta EEG-EMG PLV$_{PEAK\ AMP}$ for the first part of the fatigue stage compared to the second part of the fatigue stage using SPSS.

Comparisons from the first to the second part of the fatigue stage	Number of participants
decreased	8
increased	7

Appendix K CORTICOMUSCULAR COUPLING OVER INNERVATION ZONE AND AWAY FROM INNERVATION ZONE

This section shows the vulnerability of performing EEG-EMG coherence and PLV without considering the IZ. Figure K-1 is an example of a participant's EEG-EMG coherence and PLV pre- and post-fatigue when choosing EMG electrodes located over the IZ and away from the IZ.

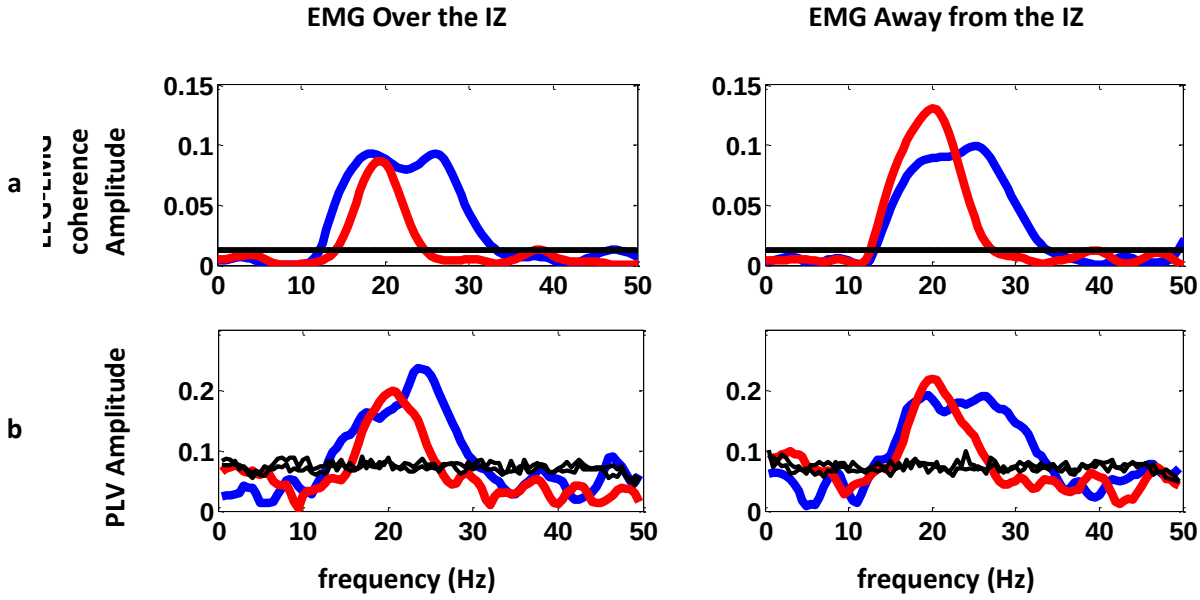

Figure K-1: Pre- (blue) and post-fatigue (red) comparisons of a) EEG-EMG coherence and b) EEG-EMG PLV while performing a sustained isometric contraction at 10% of MVC. The estimated confidence level for PLV and EEG-EMG coherence is shown by the black lines within the respective graph.

From Figure K-1, it is apparent that EEG-EMG coherence and PLV decrease post- fatigue compared to pre-fatigue over the IZ, while the contradictory result is found when placed away from the IZ.

From Figure K-1a, the EEG-EMG coherence amplitude peak is also higher away from the IZ as denoted in an EMG-EMG coherence study done by Keenan et al. (2011). In addition, the increase in the EEG-EMG coherence amplitude could be attributed to the increase in the EMG amplitude away from the IZ.

From Figure K-1b, the PLV amplitude seems to increase with an electrode placed away from the innervation post-fatigue and to decrease pre-fatigue. However, the PLV is not amplitude-sensitive but is frequency-dependent; thus, the result could be attributed to the spectral estimates of the frequency content having been altered by electrode location relative to the IZ (Mesin et al., 2009).